Performance Analysis of Shadowed Fading model for Indoor Wireless Communication

A thesis submitted

in fulfillment of the requirement for the award of degree

of

Doctor of Philosophy

Submitted by

Hari Shankar

Registration Number: 901606013

Under the Supervision of

Dr. Ankush Kansal

Associate Professor, ECED

DEPARTMENT OF ELECTRONICS AND COMMUNICATION ENGINEERING
THAPAR INSTITUTE OF ENGINEERING AND TECHNOLOGY,
PATIALA-147004

February 2021

CERTIFICATE

I hereby certify that the work which is being presented in the thesis entitled, "**Performance Analysis of Shadowed Fading model for Indoor Wireless Communication**", for the award of degree of **Doctor of Philosophy** in the department of Electronics and Communication Engineering (ECED), Thapar Institute of Engineering and Technology, Patiala, is an authentic record of my own work carried out under the supervision and guidance of Dr. Ankush Kansal, Associate Professor, ECED, Thapar Institute of Engineering and Technology, Patiala.

The results presented in this thesis have not been submitted in part or in full to any other University or Institute for the award of any degree or diploma.

Hari Shankar

Hari Shankar

This is to certify that the above statement made by the candidate is correct to the best of my knowledge and belief.

16/9/12

Dr. Ankush Kansal

Associate Professor, ECED

Thapar Institute of Engineering and Technology,

Patiala, Punjab, India

ACKNOWLEDGEMENTS

First and foremost, I would like to express my sincere, humble and deep sense of gratitude to my supervisor **Dr. Ankush Kansal**, Associate Professor, Department of Electronics and Communication Engineering, Thapar Institute of Engineering and Technology (TIET), Patiala, for his support and motivation throughout the course of this research work. His enthusiastic supervision and beneficial remarks during inspiring discussions helped a lot to the accomplishment of this thesis.

I am highly grateful to **Dr. Alpana Agarwal**, Head of Electronics and Communication Engineering Department (ECED), TIET, Patiala for her continuous support and encouragement in my research work. I am also grateful to my doctoral committee members **Dr. Ashutosh Kumar Singh**, Associate Professor, **Dr. Amit Mishra**, Assistant Professor in ECED, TIET, Patiala and **Dr. M. D. Singh**, Associate Professor in Electrical and Instrumentation Engineering Department, TIET, Patiala for their valuable suggestions during my entire research. I am also immensely thankful to my fellow researchers Dr. Gitali Dhingra, Mr. Amit Kumar, Ms. Kanwarpreet Kaur, and Ms. Navneet Kaur at Thapar Institute of Engineering and Technology, Patiala for helping me throughout my research.

Finally, I would like to thanks my parents for their continuous support and encouragement throughout my life and the course of Ph.D.

Hari Shankar

ABSTRACT

In this thesis, the performance of the shadowed fading model over indoor wireless communication channels is presented. Three shadowed fading models namely; κ-μ/gamma, Fisher Snedecor ($\mathcal{F}$) and Rayleigh/TWDP are considered for obtaining the performance measures such as Average Bit Error Rate (ABER), Outage Probability and Channel Capacity. The analyses have been performed under different scenarios like single channel, multiple channel, and OFDM systems.

In order to analyze the performance of shadowed fading for single-channel; κ-μ/gamma and Rayleigh/TWDP models have been considered. The expressions of Probability Density Function (PDF), Cumulative Distribution Function (CDF), Moment Generating Function (MGF), Moments, Outage Probability, Amount of Fading (AF), ABER for different modulations schemes and Channel Capacity over various adaptive transmissions protocols for κ-μ/gamma shadowed fading model have been derived. As special case, the numerical results have been presented for different parameters of the κ-μ/gamma model and compared with previous reported results. Further, the expressions of PDF, CDF, MGF, Outage Probability, and ABER for different modulation schemes for Rayleigh/TWDP shadowed fading model have also been presented. The numerical results have been presented for different parameter values of Rayleigh/TWDP model. The improvement in system performance is observed by varying the shadowing parameter.

Fading has a significant role to degrade the performance of wireless communication systems. This fading effect can be mitigated by employing the diversity combining techniques at the receiver. MRC diversity is the best method to improve the SNR at the output of the receiver. Therefore, the performance of $\mathcal{F}$ shadowed fading model with MRC diversity for i.i.d. branches have been analyzed in this thesis work. Primarily, the expressions of MGF, Moments, AF, ABER and Channel Capacity for $\mathcal{F}$ shadowed fading model have been derived. Also, the numerical results for different multipath fading and shadowing parameter values of $\mathcal{F}$ shadowed fading model have been presented. In light shadowing environment, the new results converge to

existing results of Nakagami-m and Rayleigh distribution. Additionally, the Monte Carlo simulations are provided to cross verify the derived expressions.

In multipath propagation, generally, the time period of signal (symbol duration) becomes smaller than the delay time of the channel and that introduces inter-symbol interference (ISI). To remove the ISI effect, the OFDM technique is widely used which increases the symbol duration by converting the serial data stream into the parallel data stream. Also, in the real environment, the channel is not always stationary (transmitter and/or receiver also) and therefore inter-carrier interference (ICI) introduces in the received signal. The Fractional Fourier transform (FrFT) based OFDM technique can easily deal with this type of impairment. Thus, the performances of the OFDM system with Fast Fourier transform (FFT) and FrFT over $\mathcal{F}$ and κ-μ/gamma shadowed fading channels have also been analyzed in this research work. Particularly, the exact and approximate expressions of ABER for uncoded OFDM with FFT and FrFT have been derived. Both MQAM and MPSK signaling schemes have been considered to derive these expressions. Moreover, the ABER expressions for space-frequency block coded (SFBC)-OFDM with FFT and FrFT have also been derived to improve the quality and reliability of the received signal. Both exact and approximate BER results closely matched to each other. The derived expressions have been validated through Monte Carlo simulation results and previous existing results.

Acronyms and Abbreviations

Abbreviation	Description
3 GPP	3rd generation partnership project
ABER	Average BER
ACC	Average channel capacity
ADC	Analog to digital converter
AF	Amount of fading
AFD	Average fade duration
AM	Amplitude modulation
AMC	Automatic modulation classification
AoA	Angle of arrival
APER	Average packet error rate
ASER	Average SER
AWGGN	Additive white generalized Gaussian noise
AWGN	Additive white Gaussian noise
BAN	Body area network
BDPSK	Binary differential phase shifting keying
BER	Bit error rate
BFSK	Binary FSK
BPSK	Binary phase shifting keying
CDF	Cumulative distribution function
CEP	Conditional error probability
CFO	Carrier frequency offset
CIFR	Channel inversion with fixed-rate
CP	Cyclic prefix
CSI	Channel state information

D2D	Device-to-device
DAB	Digital audio broadcasting
DAC	Digital to analog converter
DQPSK	Differential quadrature PSK
DVB	Digital video broadcasting
EGC	Equal gain combining
FDM	Frequency division multiplexing
FFT	Fast Fourier transform
FrFT	Fractional Fourier transform
FSK	Frequency shift keying
FSO	Free space optical
GSC	Generalized SC
GTR	Generalized two ray
i.i.d.	Independent identically distributed
i.n.i.d.	Independent but not identically distributed
ICI	Inter-carrier interference
IEEE	Institute of Electrical and Electronics Engineers
IFFT	Inverse FFT
IFrFT	Inverse FrFT
IMGF	Incomplete MGF
ISI	Inter-symbol interference
JFTS	Joint fading and two path shadowing
LCR	Level crossing rate
LMS	Land mobile satellite
LOS	Line of sight
LPF	Low pass filter
MAM	M-ary AM
MDPSK	M-ary differential PSK
MGF	Moment generating function
MIMO	Multiple-input and multiple-output

mm-wave	Milli metre wave
MPSK	M-ary PSK
MQAM	M-ary QAM
MRC	Maximum ratio combining
MSK	Minimum shift keying
mW	mili watt
NCFSK	Non-coherent FSK
NCMFSK	Non-coherent M-ary FSK
NLOS	Non-LOS
OFDM	Orthogonal frequency division multiplexing
OPRA	Optimal power and rate adaption
ORA	Optimal rate adaption
PDA	Personal digital assistant
PDF	Probability density function
PDP	Power delay profile
PSK	Phase shift keying
QAM	Quadrature amplitude modulation
QPSK	Quadrature phase shift keying
RF	Radio frequency
RMS	Root mean square
SAR	Synthetic aperture radar
SC	Selection combining
SER	Symbol error rate
SISO	Single-input and single-output
SNR	Signal-to-noise ratio
SIR	Signal-to-interference ratio (SIR)
SINR	Signal-to-interference plus noise ratio (SINR)
SSC	Switch-and-stay combining
STO	Symbol timing offset
TIFR	Truncated CIFR
TWDP	Two-wave with diffuse power

UAC	Underwater acoustic communication
UAV	Unmanned arial vehicle
UE	User equipment
UWB	Ultra wide band
WBAN	Wireless body area network
WLAN	Wireless local area network
WMAN	Wireless metropolitan area network
WPAN	Wireless personal area network

List of Symbols

$\exp(\cdot)$	Exponential function
$I_0(\cdot)$	Modified Bessel function of first kind with zero order
$\Gamma(\cdot)$	Gamma function
Ω	Mean power
σ^2	Variance
V_1	Peak amplitude of dominant signal
m	Fading severity parameter
Δ	Shape parameter of TWDP fading
q	A Fading parameter of Nakagami-q Channel
K	A Rician factor
κ	A fading parameter of κ-μ channel
μ	A fading parameter of κ-μ channel
η	A fading parameter of η-μ channel
α	A shape parameter of Gamma model
β	A scale parameter of Gamma model
δ^2	Total power of dominant component
m_s	A shadowing parameter of Fisher Snedecor model
S_h	A shadowing parameter of Rayleigh/TWDP model
$\mathcal{F}$	Fisher Snedecor shadowed fading model
P_1	Mean power of Rayleigh model
P_2	Mean power of TWDP shadowing
E_s	Energy signal
m'	Median value
$I_v(\cdot)$	Modified Bessel function of first kind with order v
$\ln(\cdot)$	Natural log

$\log_{10}(\cdot)$	Log with base 10
$\mathrm{Max}(\cdot)$	Maximum
$\sum_{i=0}^{n}$	Summation
$\prod_{i=0}^{n}$	Product
$\mathrm{B}(\cdot,\cdot)$	Beta function
γ	Instantaneous SNR
$\bar{\gamma}$	Average SNR or mean SNR
$\mathrm{K_v}(\cdot)$	Modified Bessel function of second kind with order v
$\mathrm{g_k}$	Gain factor
$\mathrm{F_p}[\cdot]$	FrFT operator with order p
$\mathrm{K_p}(\cdot,\cdot)$	FrFT Kernel
ϕ	Angle of rotation
$\mathrm{E_i}(\cdot)$	Exponential integral
$G_{p,q}^{m,n}[\cdot\,|\,\cdot]$	Meijer G function
${}_2F_1(\cdot,\cdot;\cdot;\cdot)$	Gauss hypergeometric function
$\mathrm{W_{a,b}}(\cdot)$	Whittaker function
$\mathrm{Erfc}(\cdot)$	Complementary error function
$\mathrm{Q}(\cdot,\cdot)$	Marcum Q function
γ_{MRC}	Output SNR of MRC receiver
γ_{SC}	Output SNR of SC receiver
γ_0	Threshold SNR
L	Number of diversity branch
${}_3F_1(\cdot,\cdot,\cdot;\cdot;\cdot)$	Gauss hypergeometric function
$\lvert\cdot\rvert$	Absolute value
$\mathrm{E}[\cdot]$	Expectation operator
M	Modulation index
A	Modulated data signal
t	Symbol duration

V_a	Number of subband
V	Number of subchannel
R_c	Code rate of SFBC encoder
H	Frequency response of the channel
B	Received signal
C	Additive white Gaussian noise (AWGN)
$diag(\cdot)$	Diagonal matrix
M_{T}	Number of transmitting antenna
M_{R}	Number of receiving antenna

List of Figures

List of Tables

Table of Contents

Chapter 1

Introduction

1.1 Indoor Communication System

The technology in wireless communication is improving every day. This technology has covered huge areas of application such as medical, military, education, entertainment, sport, and communications. The wireless communication system has more enormous advantages over wired communication systems because of its easy installation, system reliability, mobility, and low cost [1]. The transmitted signals are reflected, refracted and/or diffracted through the surrounding objects, and only some part of the signals is received at the receiver.

In indoor wireless communication, the transmission of information may be possible between two or more users within a maximum of 100 meters. In this type of system, communication is possible among the users in building-to-building, multi-floor buildings, office areas, conference room, hall, laboratory, airport, railway stations, shopping complex, etc. [1]. In the indoor scenarios, the signal covers a small distance but has high channel variation in comparison with the outdoor environment. In this type of environment, the obstruction in signal occurs due to walls partition, multi-floor buildings, doors, chairs, humans, tables, etc. Various statistical measurements and modeling of the channel for indoor scenarios have been proposed in reported literature [2-4]. Generally, channel measurements have been taken in the office building, laboratory, multi-floor buildings, and corridors only.

The Wireless Local Area Network (WLAN) provides considerably good coverage over the local area and has a range of up to 100 meters. The WLAN has been extremely popular today since it provides not only wireless connectivity but also a high data rate, minimum maintenance cost, easy installation, and simple operation. The WLAN standards IEEE 802.11 series, HiperLAN1, and HyperLAN2 are used for establishing the connection among users.

WLAN is popular in residential as well as the commercial application which includes:

- Alternative to wired LAN
- Extension of existing LAN

- Nomadic access
- Interconnection between buildings
- Adhoc Networking.

The Wireless Personal Area Network (WPAN) technologies are used for short-distance communications, and it provides coverage within 10 meters. This technology requires minimum cost and low power wireless devices [5]. The most common devices that support short-range communication are laptops, computer peripherals, wearable devices, PDAs, sensors, mobile phones, etc.

The Wireless Body Area Network (WBAN) technologies are used for very short distance communication, and it provides coverage up to 1 meter. In WBAN, sensors are used as communication devices which may be positioned on or around the human body. It requires low power devices (maximum radiated power is 1mW) [6, 7]. IEEE 802.15.6 standard is used for WBAN. In WBAN, the attenuation or fluctuations in the signal depends on the position of transmitter (Tx) and receiver (Rx) on the human body, nearby scattering objects, and posture of the human body. Three different types of links are possible in the body-centric communication system. This includes body-to-body, off-body, and on-body communication [6]. In off-body communication, the sensor nodes are placed on the body surface which can directly communicate with the nearest base station. In on-body communication, two or more sensor nodes are placed on the body surface so the shadowing occurs due to body parts. In body-to-body communication, the sensor nodes are positioned on different human bodies.

The signal propagation structure into and inside the building is more complex in comparison with outdoor environment because of building structure, layout of the room and type of material used to construct the buildings. In the indoor environment, the signal propagation depends on various factors like thickness of wall partition, the position of transmitting and receiving antenna, closed or open doors, etc. Therefore, practically, it is difficult to develop a generic channel model for indoor wireless communication. Indoor radio propagation accounts various losses such as free space transmission loss, and penetration loss. The penetration loss includes both wall partition loss and floor partition loss. In addition to noise and interference, the propagated signal may also influence by multipath fading and shadowing that degrade the system performance.

Thus, a low quality of received signal introduces higher error rate. The limitations of indoor wireless communication can be summarized as:

- Unreliability
- Limited frequency
- Low data rate
- Security
- Interference
- Health hazard

1.2 Shadowed Fading Model

The random variation in received signal strength is called fading. With the effect of multipath and Doppler shift, a signal component with some distortion is obtained at Rx, which is different from the originally transmitted signal [8]. There are two classes of fading: small-scale fading and large-scale fading. The short-term fluctuation in the received signal amplitude is called small-scale fading [9]. This type of fading is the cause of the multipath effect. The small-scale fading models include κ-μ, Nakagami-m, Hoyt, Two-wave with diffuse power (TWDP), Weibull, Rayleigh, Beckmann, and Rician distribution.

The large-scale fading occurs when the receiver moves over a large area. Large scale fading depends on the presence of obstacles in the signal path, the position of the receiver, and its distance from the transmitter [9]. When the receiver travels over a large distance, some losses occur that depend on the Tx and Rx distance, known as path loss (n^{th}-power law). Also, since the receiver moves in the shadow region of objects (like buildings, trees, mountains, etc.), the shadowing occurs [1]. Hence, the term large-scale fading corresponds to the combined effects of path-loss and shadowing loss. This type of fading is commonly characterized by lognormal distribution [1]. Due to the complexity of lognormal distribution, it has rarely used for further analysis. The gamma distribution is the better replacement of the lognormal distribution since its statistical behavior is similar to the lognormal model [9].

In real environment, the received signal at the receiver characterizes both multipath fading and shadowing effects simultaneously by considering the shadowed fading model (or composite fading model). This type of fading is found in indoor scenarios, urban areas where the pedestrians and vehicles move with slow speed, and in Land Mobile Satellite (LMS) systems,

where the vehicles have high speed [8]. The different shadowed models are available in the reported literature that found suitable in cellular communication, optical wireless communication, LMS communication, body-centric communication, vehicular communication, etc. [10-20]. Based on obstructions in the signal path, the shadowed fading model can be classified into two types: multiplicative shadowed fading model and Line of Sight (LOS) shadowed fading model. The LOS shadowed fading occurs only when the dominant LOS signal component is obscured by surrounding objects like trees, buildings, chairs, and the human body [10-14].

On the other hand, the multiplicative shadowed fading occurs when both dominant and multipath signal components are obscured by surrounding objects (including the human body) which causes variations in net power of the received signal component [15-19]. The experimental results have shown that the multiplicative model shows the better characterization of the wireless channel environment in comparison to the LOS shadowed fading model [19]. Because in LOS shadowed fading, only the LOS component is obscured by surrounding objects; however, in multiplicative shadowed fading, both LOS and diffuse power signal components are obscured by surrounding objects.

1.3 Thesis Contributions

This research investigates the performance of the shadowed fading model which can help the researcher/scientist to design an optimal indoor wireless communication system. The performance analysis parameters such as Average Bit Error Rate (ABER), Channel Capacity, Average Signal-to-Noise Ratio (SNR), and Outage Probability measure the quality and reliability of distorted received signal at the receiver. The choice of modulation/detection scheme is the primary interest for system designer that helps to reconstruct the distorted signal with minimum error. The implementation of Maximum Ratio Combining (MRC) diversity at the receiver provides the maximum SNR that helps to strengthen the received signal. The design of the OFDM system at the transmitter and receiver section provides high data transmission over a given bandwidth. Also, the OFDM system with FrFT can efficiently perform over doubly dispersive channels. The κ-μ/gamma, Fisher Snedecor ($\mathcal{F}$), and Rayleigh/TWDP shadowed fading models have specified indoor applications and these are adequate for indoor off-body

communication, indoor device-to-device communication, and indoor WLAN system, respectively.

The main contributions of research work based on objectives are summarized as follows:

1. The aim of the first objective is to study and analyze various composite fading model for indoor communication. Shadowed fading models such as κ-μ/gamma, Generalized K, Fisher Snedecor ($\mathcal{F}$), Rician/TWDP (JFTS), and Rayleigh/TWDP are adequate for indoor wireless communication. In this research work, three shadowed fading models: κ-μ/gamma, Fisher Snedecor ($\mathcal{F}$), and Rayleigh/TWDP are presented to evaluate the performances over indoor wireless channels. The κ-μ/gamma model has seven special cases. Therefore, by setting the several κ-μ/gamma parameters, the newly obtained results converge to existing results of special cases. Also, the new results of $\mathcal{F}$ model converge to existing results of classical multipath fading models by putting the several parameter values. The analysis of $\mathcal{F}$ model with maximum ratio combining (MRC) coding has shown improvement in system performance.

2. The second objective aims to analyze the performance of composite fading model over single channel for indoor scenarios. To achieve the second objective, the performance of κ-μ/gamma model is investigated. In this context, the statistical parameters such as Probability Density Function (PDF), Moment Generating Function (MGF), Cumulative Distribution Function (CDF), and Moments in the term of instantaneous Signal-to-Noise Ratio (SNR) for this generalized fading distribution model are computed mathematically. Further, the exact novel analytical expressions of Outage Probability and Error Probability using several signaling techniques are derived. Also, the novel analytical expressions for several capacities are obtained. The numerical results are presented for various κ-μ/gamma parameters. Moreover, the newly achieved results converge to existing results of shadowed and multipath fading models, as special cases.

   Thereafter, the performance of Rayleigh/TWDP shadowed fading model is evaluated. In this context, the novel mathematical expressions of PDF, CDF, and MGF over Rayleigh/TWDP channels are derived. Further, the expressions of different Average Error Probabilities and Outage Probability are derived. Using several shadowing and

shape factors, the analytical results are illustrated. Moreover, the results of ABER for Rayleigh/TWDP model are compared with the corresponding results of Rayleigh/gamma model. The higher value of shadowing parameter for both shadowed fading models shows better performance. In single channel, the ABER and outage probability has shown the improvement in system performance as compared to existing models.

3. The third objective aims to analyze the performance of composite fading model using diversity combining technique for indoor scenario. Therefore, the performance of *L*-branch Maximum Ratio Combining (MRC) receiver for $\mathcal{F}$ model is evaluated. In this context, novel mathematical expressions for MGF, Amount of Fading (AF), Moments, and ABER for various modulation techniques are derived. Also, the several capacities expressions over this generalized shadowed fading channel are computed mathematically. As an illustration, the results are plotted for fading severity parameter, shadowing parameter, and for different number of branches. Further, in light shadowing environment, the numerical results are reduced to corresponding existing results. Both simulation and numerical results showing the perfect match. The performance improvement is seen as the number of diversity branches varies.

4. The fourth objective aims to analyze the performance of composite fading model using OFDM and FrFT OFDM schemes. To achieve the fourth objective, the novel mathematical ABER expressions using M-ary signaling technique of uncoded and SFBC coded OFDM system for κ-μ/gamma and $\mathcal{F}$ models are derived. Both FrFT and FFT domain are considered to derive these expressions. With the condition of no shadowing, the newly obtained results converge to results of multipath fading models, as special cases. The Monte Carlo simulations are carried out for validation purposes. The Error Probability reduction depends on the mean SNR, modulation index, code rate, number of Rx and Tx antennas, and type of signaling schemes. The error rate of FrFT based OFDM shows better performance than FFT based OFDM. For example, (at 40dB average SNR) the error probability of 4-PSK signaling for uncoded OFDM with FrFT and FFT are 3.12×10^{-3} and 7.77×10^{-3}, respectively.

1.4 Thesis Outline

The organizations of thesis are as follows

Chapter 2 introduces the literature survey that covers some important topics used in thesis work. This Chapter starts with a brief survey on the measurement and modeling of indoor wireless channels. After that, previously proposed various shadowed fading models are reviewed which includes applications such as LMS, urban environment, (device-to-device) D2D, wearable communication, vehicular communication, and medical imaging. The performance parameters such as ABER, Channel Capacity, Outage Probabilities, and AF have an important role to implement any wireless systems. Therefore, the survey on the performance of various shadowed fading models over a single channel is discussed. The performance on the several diversity combining techniques is also reviewed in this Chapter which is frequently used to improve the SNR at the receiver output. Chapter 2 also reviewed the literature on the performance of the OFDM systems in several fading channels. On the basis of literature survey, some problems are formulated. With the help of the formulated problem, the objectives, and methodology of the research work are decided.

Chapter 3 starts with the mathematical modeling of some important multipath fading, shadowing, and shadowed fading, which is related to the shadowed fading models used in this thesis for performance analysis. This Chapter also introduces the basics of diversity combining techniques, mathematical models, and types. After that, the basics of the OFDM system, its block diagram, applications, advantages, and disadvantages are discussed. Further, the definition of FrFT, its mathematical model, and applications are discussed. Finally, the definition and mathematical formulas of performance parameters, for example, AF, Average Error Probability of several signaling techniques, Outage Probabilities, and different capacities are presented. To this extent, the formulas of BER for different modulation techniques and Channel Capacity for different power adaptive methods using both PDF and MGF based approaches are discussed.

The performance analysis of two shadowed fading models, namely κ-μ/gamma and Rayleigh/TWDP, are investigated in Chapter 4. Initially, in this Chapter, the statistical parameters such as CDF, PDF, MGF, and moments for κ-μ/gamma model are proposed. Correspondingly, the performance in the term of ABER for various modulation techniques, Channel Capacity for several policies and Outage Probability are obtained. Further, the

numerical results are demonstrated and their conversions to special cases are presented by setting several factors. This Chapter also proposed the PDF, CDF, and MGF of Rayleigh/TWDP model. To this end, the performances in the term of Outage Probabilities, and Error Probabilities for some signaling technique are presented.

Chapter 5 presents the performance of the diversity combining technique for $\mathcal{F}$ shadowed fading model. The MRC receiver algorithm has been used to obtain performance measures such as Moments, AF, ABER, and Channel Capacity. Correspondingly, the numerical results are plotted for several shadowing and fading factors. The improvement in performance depends on the signaling schemes used, modulation index, number of diversity branches, and average SNR. Further, the generalized results reduce to previous existing results, as special cases. Moreover, the simulations and new proposed results show good agreement.

The performance of uncoded OFDM and SFBC-OFDM systems for two shadowed fading models i.e. κ-μ/gamma, and $\mathcal{F}$ is evaluated in Chapter 6. Both FFT and FrFT algorithms are considered for such analysis. In this context, Average Error Probability expressions are derived using several M-ary signaling techniques. Further, the newly obtained results converge to reported existing results that show the generality of both shadowed model. The simulation results show a good match with new results.

Chapter 2

Literature Review

In this Chapter, a brief survey on indoor channel modeling and measurements is presented. Throughout study on the various shadowed fading models and their performance analysis over single-channel are also presented in this Chapter. The diversity mechanism in wireless communication combat the effect of fading and provide a good quality signal at the receiver output; therefore, the survey on performance analysis using diversity combining technique is also discussed in the middle of this Chapter. For the doubly dispersive channel, the conventional OFDM and FrFT-OFDM systems are the best methods to achieve high signal quality. Therefore, the analyses of these techniques are also presented in this Chapter.

Based on the literature survey, the gaps are identified, and corresponding research objectives are defined. Further, based on research objectives, the research methodology is presented in the end of this Chapter.

2.1 Indoor Wireless Channel Measurements and Modeling

Modeling of the channel has a vital role to characterize the signal that propagates between transmitter and receiver. Indoor wireless communication includes technology such as WLAN, WPAN, and WBAN. In the indoor system, communication is possible between building-to-building, multi-floor buildings, office areas, conference room, hall, laboratory, etc. The indoor channel model is categorized in two ways:

- Statistical model
- Deterministic model

The statistical model requires a large number of measurements to obtained channel parameters like channel impulse response, power delay profile (PDP), and coherence bandwidth. The statistical-based channel model includes Saleh-Valenzuela (S-V) model [21], Extended S-V [22],

and 3GPP spatial channel model [23]. On the other hand, the deterministic model requires site-specific information such as dielectric constant, thickness, and the absorption coefficient of material (walls). The deterministic model characterizes the real effect of the environment but has high computational complexity. The main advantage of the deterministic model is that it does not require any complex measurement set up and unnecessary burden. Generally, the ray-tracing method is used in the deterministic model [24]. Some research papers based on statistical measurements over indoor communication channels are discussed below.

A. A. M. Saleh *et al*. [21] proposed a statistical model for indoor radio channels based on measured results. The clusters and rays within-cluster are modeled as a Poisson arrival process with different rates. **Spencer** *et al*. [22] included the Angle-of-Arrival (AOA) in Saleh-Valenzuela's model given in [21]. According to this technique, both clusters and rays are characterized by time and angle. The measurements and modeling of channels in the indoor office areas at 60 GHz were presented by **X. Wu** *et al*. [25]. An angular extended S-V model has been used to characterize the indoor channel measurement results [25].

The omnidirectional and maximum power path loss models for the indoor environment at 83.5 GHz have been presented by **J. Senic** *et al*. [26]. The measurements were conducted over 3000 transmitter-receiver antenna positions in different scenarios such as hallway, lobby, and conference room [26]. **K. Turbic** *et al*. [27] presented a shadowing model for the human body. The proposed model is based on body shadowing loss which is presented in the term of cosine function [27]. Off-body indoor channel measurements at 60 GHz were performed by **L. Petrillo** *et al*. [28]. The S-V model has been used to propose the impulse response model. The results have been obtained in the term of path loss and delay spread [28].

2.2 Shadowed Fading Models

Multiplicative shadowed fading is mostly used for better characterization of the wireless channel in comparison with LOS shadowed fading model. The reason behind this is that in the multiplicative shadowed fading model both specular component and diffuse power component of the multipath fading model follow the shadowing distribution. Table 2.1 listed the various shadowed fading model over the wireless communication channels. The shadowed fading model includes a wide range of applications not only in wireless communication but also in other fields such as image processing, and biomedical imaging [17, 29, 30]. Some significant applications

include body-centric communication, molecular communication, D2D communication, optical wireless communication, radar communication, unmanned aerial vehicle (UAV), LMS, and cellular communication.

Rayleigh/lognormal was the first shadowed fading model proposed by **H. Suzuki** in 1977 [16]. This model is a combination of Rayleigh and lognormal distribution, and it is suitable for the urban environment. **C. Loo** [10] proposed a Rice/lognormal shadowed fading model. In this model, the LOS component of Rice distribution follows the lognormal distribution. The model is suitable for LMS communication channels. After that, the Rice/lognormal model was modified by **G. E. Corazza** *et al*. [15] with the assumption that the total signal component of the Rice fading follows the lognormal distribution. The proposed model is adequate for LMS, rural, urban, and suburban environments. A Generalized Rice/lognormal model was proposed by **F. Vatalaro** *et al*. [31] with the assumption that the additive diffuse-multipath components have constant average power. The proposed model reduces to Rayleigh, Rice, lognormal, and Loo model. **S. H. Hwang** *et al*. [32] extended the Rice/lognormal model proposed by G.E. Corraza with the assumption of independent shadowing. The closed-form expression of PDF for Rayleigh/gamma (*K* distribution) model was obtained by **A. Abdi** *et al*. [17]. **T. T. Tjhung** *et al*. [33] proposed the Nakagami-*m*/lognormal model. The authors also derived the expressions of Level Crossing Rate (LCR) and Average Fade Duration (AFD) [33]. **A. Abdi** *et al*. [11] proposed Rice/Nakagami-*m* model for the LMS communication system. In this model, the LOS component of the Rice model follows the Nakagami-*m* model. In [11], the expressions of PDF, moments, MGF, LCR, and AFD have been derived. **P. M. Shankar** [18] proposed the Generalized *K* model. In this, the average power of Nakagami-*m* distribution follows the gamma distribution. **T. Eltoft** [34] introduced the Rician/inverse Gaussian model which is suitable for Synthetic Aperture Radar (SAR) and medical ultrasound images. **Karmeshu** *et al*. [35] proposed Rayleigh/inverse Gaussian distribution, which is adequate for biomedical imaging and optical wireless communication. **A. Laourine** *et al*. [36] proposed Nakagami-*m*/inverse Gaussian shadowed fading model (or G-distribution). **P. S. Bithas** [37] proposed Weibull/Gamma distribution. In [37], the closed-form expressions of PDF, Characteristic Function, Moments, Outage Probability, and ABER were derived. The extended Generalized *K* model was proposed by **F. Yilmaz** *et al*. [38]. In [38], the expressions for PDF, CDF, LCR, AFD, fractional moments, AF, ABER, Outage Probability, Average Capacity, and Outage Capacity have been provided.

Table 2.1: List of Shadowed Fading Model

Authors	Types	Shadowed Fading Model	Years	Applications
Suzuki	Multiplicative	Rayleigh/lognormal	1977	Urban Environment
C. Loo	LOS	Rice/lognormal	1985	Land Mobile Satellite
G. E. Corazza	Multiplicative	Rice /lognormal	1994	Rural, Urban, Suburban Environment
F. Vatalaro	Multiplicative	Generalized Rice/lognormal	1995	Wireless Communication
A. Abdi	Multiplicative	Rayleigh/gamma (K distribution)	1998	Radar Communication, Scattered Radiation, Medical Ultrasound Image
T. T. Tjhung	Multiplicative	Nakagami-*m*/lognormal	1999	Land Mobile Satellite
A. Abdi	LOS	Rice/Nakagami-m	2003	Land Mobile Satellite
P.M. Shankar	Multiplicative	Nakagami-*m*/gamma (Generalized K)	2004	Indoor, Outdoor
T. Eltoft	LOS	Rice/inverse Gaussian	2005	SAR, Medical Ultrasound Image
Karmeshu	Multiplicative	Rayleigh/inverse Gaussian	2007	Biomedical Imaging, Optical Wireless
A. Laourine	Multiplicative	Nakagami-*m*/inverse Gaussian	2009	Wireless Communication
P.S Bithas	Multiplicative	Weibull/gamma	2009	Wireless Communication
F. Yilmaz	Multiplicative	Extended Generalized K	2010	mmWave, Free Space Optical Channel
P. C. Sofotasios	Multiplicative	η-μ/gamma	2010	Wireless Communication
P. C. Sofotasios	Multiplicative	κ-μ/ inverse Gaussian	2013	RF, FSO
P. C. Sofotasios	Multiplicative	η-μ/inverse Gaussian	2013	RF, FSO, Ultrasound Imaging
J. F. Paris	LOS	κ-μ/Nakagami-*m*	2014	Underwater Acoustic Communication
I. Dey	Multiplicative	Rician/TWDP (JFTS)	2014	Indoor WLAN
S. L. Cotton	LOS	κ-μ/lognormal	2014	Body Centric Communications
S. L. Cotton	LOS	κ-μ/Nakagami-*m*	2015	Cellular D2D Communications
S.K. Yoo et al	Multiplicative	κ-μ/inverse gamma	2015	Wearable, Cellular D2D and Vehicular Communication
S.K. Yoo et al	Multiplicative	η-μ/inverse gamma	2015	Wearable, Cellular D2D and Vehicular Communication
S.K. Yoo et al	Multiplicative	κ-μ/gamma	2016	Off-body Communication
S.K. Yoo et al	Multiplicative	Fisher-Snedecor ($\mathcal{F}$)	2017	Wearable, Indoor D2D Communication

P. C. Sofotasios *et al*. [39] proposed η-μ/gamma fading distribution. Further, **P. C. Sofotasios** *et al*. [40] also introduced κ-μ/inverse Gaussian model in the year 2013. This model is suitable for Radio Frequency (RF) and Free-Space Optical (FSO) wireless communication. In [40], the analytical expressions of PDF, Moments, and AF were derived. In the same year, **P. C. Sofotaios** *et al*. [41] proposed η-μ/inverse Gaussian fading distribution which is suitable for RF, FSO, and ultrasound imaging.

The κ-μ shadowed fading model was proposed by **J. F. Paris** [12]. In this model, the LOS component of κ-μ distribution follows the Nakagami-*m* distribution. The proposed model is adequate for LMS and Underwater Acoustic Communication (UAC) systems. In [12], statistical parameters like PDF, CDF, and MGF were obtained. **S. L. Cotton** [13] proposed the κ-μ/lognormal LOS model in which the resultant dominant component of κ-μ distribution follows the lognormal model. In [13], the channel measurements were performed in the body-centric communication system.

I. Dey *et al*. [4] proposed a JFTS model which is the combination of TWDP and Rician distribution. In [4], the indoor channel measurements were conducted over frequencies 900, 2450, and 5000 MHz with different transmitter and receiver antenna positions. The measured PDF showed good agreement with the theoretical PDF of the JFTS model [4]. **S. L. Cotton** [14] proposed shadowed κ-μ distribution by considering the resultant dominant signal component of κ-μ distribution follows Nakagami-*m* model. The D2D field experiments at 868 MHz frequency have been performed in an outdoor environment. The experimental results better matched with the proposed shadowed κ-μ fading model [14].

S. K. Yoo *et al*. [19] proposed κ-μ/gamma model that was initially introduced by **P. C. Sofotasios** *et al*. [42]. **H. Shankar** *et al*. [43] proposed the Rayleigh/TWDP model which is adequate for indoor NLOS environment. In [43], the author derived the expression of PDF of the envelope signal. In the same year, POCA/TWDP model was provided by **H. Shankar** *et al*. [44]. In POCA/TWDP model, POCA is a small-scale fading distribution, and TWDP is the shadowing distribution.

The inverse gamma based shadowed fading distributions were proposed by **S. K. Yoo** *et al*. [45] that were initially proposed by **S. K. Yoo** *et al*. [46, 47]. In [45], the expressions of statistical parameters like PDF, MGF, CDF, Moments, and AF of both shadowed fading models were derived. In [45], further, the channel measurements were performed in three different wireless

applications like wearable, vehicular and cellular communication. The obtained measured results provide excellent fit, in both LOS and NLOS conditions, with both models [45]. **S. K. Yoo** *et al*. [48] proposed a shadowed fading model, coined as Fisher-Snedecor ($\mathcal{F}$), in which the RMS of Nakagami-*m* signal follow inverse Nakagami-*m* fading distribution. Particularly, the D2D experiments were performed in the indoor and outdoor scenario at 5.8 GHz. The author, in [48], further analyzed the ABER and Outage Probability performance. For the D2D communication system, channel measurement results best fitted to $\mathcal{F}$ shadowed fading model in comparison with the Generalized *K* fading model [48]. **O. S. Badaneh** *et al*. [49] proposed the product of $\mathcal{F}$ shadowed fading model. The product of two κ-μ random variables was presented by **N. Bhargav** *et al*. [50].

2.3 Performance Analysis over Single Channel

The capacity performance under various rate and power adaptive methods with and without diversity over Rayleigh channels was analyzed by **M. S. Alouini** *et al*. [51]. The MRC and Selection Combining (SC) diversity techniques were considered to derive Channel Capacity expressions [51]. The Symbol Error Rate (SER) performance for M-ary signaling over Rician channels was analyzed by **J. Sun** *et al*. [52]. **A. Abdi** *et al*. [53] proposed the closed-form expression of ABER over *K* channels. Further, the obtained results were compared with the Rayleigh/lognormal model that shows good agreement [53].

The closed-form MGF based expressions of Average SER (ASER) for binary and M-ary signal over Nakagami-*m* channels were derived by **H. Shin** *et al*. [54]. **P. S. Bithas** *et al*. [55] derived PDF, CDF, and MGF expressions in the term of SNR over the Generalized *K* fading channels. Further, the performance metrics like Average Channel Capacity (ACC), Outage Probability, and ABER were obtained. The ABER expressions were obtained for a large variety of modulation schemes like BPSK, square MQAM, non-coherent BFSK, BDPSK, gray coded MPSK, and MDPSK [55].

D. B. da Costa *et al*. [56] proposed ACC for several fading distributions. The ACC of Nakagami-*m* lower bounds the η-μ model however it upper bounds the κ-μ model. Moreover, it lower bounds the ACC of α-μ for $\alpha > 0$ and $\mu > m$ and upper bounds the ACC of α-μ for $\alpha > 2$ and $\mu < m$ [56]. In [57], the expressions of MGF and ABER using different modulation schemes for κ-μ and η-μ models were provided by **D. B. da Casta** *et al*. The obtained new results include

the result of Rician, Hoyt, and Nakagami-*m* fading channels [57]. The closed-form expressions of ACC under three adaptive transmission policies: ORA, OPRA, and CIFR for Generalized *K* model were provided by **A. Laourine** *et al*. [58].

K. P. Peppas [59] obtained the ACC expressions of η-μ fading distribution. These expressions were obtained for both single branch and MRC receiver operating over not necessarily identically distributed branches. The proposed expression includes several special cases like Hoyt and Nakagami-*m* distribution [59]. The performance over Generalized *K* fading channels was analyzed by **G. P. Efthymoglou** *et al*. [60]. **A. M. Magableh** *et al*. [61] proposed the MGF, Error Probabilities, and Outage Probabilities expressions of α-μ fading distribution.

M. D. Renzo *et al*. [62] proposed a new formula of Channel Capacity by using MGF and/or truncated MGF based approach. In [62], the author introduced E-transform to obtain the Channel Capacity under ORA and OPRA policy using MGF and/or truncated MGF expression. Also, the Mellin and Hankel transform of MGF was introduced to obtain the Channel Capacity under CIFR and Truncated CIFR policy, respectively [62]. **F. Yilmaz** *et al*. [63] derived a novel MGF based unified ABER and Channel Capacity expressions for single and multiple receiver with MRC. The MGF and ASER expressions for different modulation schemes over the Generalized *K* channels were derived by **G. P. Efthymoglou** [64]. Further, the closed-form expression of CDF of SNR (for integer *m*) was derived, which helps to achieve the expressions of Outage Probability, ACC, and ABER [64].

I. Dey *et al*. [65] derived the expressions of joint moments, mean, variance, and AF for JFTS distribution. The MGF and error rate expressions for JFTS model were derived in the work of **I. Dey** *et al*. [66]. **I. Dey** *et al*. [67] derived the expression for CDF over JFTS fading channels that further helps to obtain the expression of Outage Probability. The expression of pairwise error probability of turbo codes for PDF of square random variables for JFTS fading distribution was derived in the work of **I. Dey** *et al*. [68].

I. Dey *et al*. [69] analyzed the capacity performance over JFTS channels. The numerical results illustrated the effect of JFTS parameters on channel capacity [69]. The expressions of achievable bandwidth efficiency, cutoff rate, and channel capacity by considering the M-ary signaling and JFTS distribution were derived by **I. Dey** *et al*. [70]. Further, the author obtained the upper and lower bounds errors by truncating the infinite series expression of bandwidth efficiency [70]. The ABER expressions for various modulation techniques using CDF based approach over the JFTS

channels were derived by **I. Dey** *et al*. [71]. Further, the expression of achievable channel cutoff rates was derived in [71]. The expression of Outage Probability in the presence of self-interference over the JFTS channels was obtained by **I. Dey** *et al*. [72]. To this end, the author derived the expression for PDF of the difference between two correlated but not necessarily identically distributed squared JFTS variates [72].

Y. Xi *et al*. proposed a novel analytical method to calculate the Average Packet Error Rate (APER) of general packet transmission system for quasi-static fading channel [73]. **M. Rao** *et al*. analyzed the performance of Generalized Two Ray (GTR) distribution [74]. **A. Hamed** *et al*. [75] obtained the expressions of MGF and truncated MGF for *K* distribution. Based on derived MGF/truncated MGF, the expressions of ACC and ABER (MQAM) were obtained. Further, the performances of the adaptive MQAM system by considering the Outage Probability, system capacity, and ABER have been evaluated [75]. **D. Das** *et al*. [76] proposed a method of Automatic Modulation Classification (AMC) based on fourth-order cumulants to classify 8-PSK, 16-PSK, QPSK and OQPSK signaling schemes.

The capacity analysis of α-η-κ-μ distribution was performed by **X. Li** *et al*. [77]. In [77], the Channel Capacity performance improved by increasing the fading parameters like dominant power component (κ), multipath cluster (μ), and mean value (α). **T. Aldalgamouni** *et al.* analyzed the performance of α-η-μ fading distribution [78]. In [78], the proposed expressions reduced to Channel Capacity of α-μ, Nakagami-*m*, Weibull, and η-μ distributions. The closed-form expressions of Channel Capacity and ABER with interference for extended Generalized *K* distribution were derived by **S. P. Singh** *et al*. [79]. These expressions have been obtained by using the proposed unified conditional expression of ABER and channel capacity [79].

The exact and approximate expressions of MGF and SER for several fading models were derived by **E. Salahat** *et al*. [80]. **F. J. L. Martinez** *et al*. [81] presented a method for obtaining the incomplete MGF (IMGF). The derived IMGF expression of κ-μ shadowed has been used to obtain the channel capacity, outage probability, physical layer security, and ABER with adaptive modulation [81]. The generalized MGF based analysis of κ-μ extreme distribution has been performed in **J. Gong** *et al*. [82]. The expression of generalized MGF for the TWDP distribution was derived by **J. P. P. Martin** *et al*. [83]. Further, the performance in the term of energy detection, SER (NCMFSK), Outage Probability with interference and physical layer security were evaluated [83].

T. Aldalgamouni *et al*. [84] analyzed the error probabilities and capacity performance for $\mathcal{F}$ model. **J. Gong** *et al*. [85] proposed the generalized MGF and investigated the secrecy capacity performance for $\mathcal{F}$ model. The effective rates analysis for $\mathcal{F}$ model with multiple antenna systems was performed by **S. Chen** *et al*. [86]. The work on physical layer security for $\mathcal{F}$ model was provided by **L. Kong** *et al*. [87]. **H. Al-Hmood** *et al*. [88] investigated the energy detection performance for κ-μ shadowed and $\mathcal{F}$ models.

F. S. Almehmadi *et al*. obtained the effective capacity expression for $\mathcal{F}$ model [89]. The secrecy capacity analysis for $\mathcal{F}$ model was provided by **O. S. Badarneh** *et al*. [90]. The capacities performances using $\mathcal{F}$ model were analyzed by **S. K. Yoo** *et al*. [91], **H. Zhao** *et al*. [92], and **N. Kapacu** *et al*. [93]. **S. K. Yoo** *et al*. [94] evaluated the performance of entropy, and energy detection for $\mathcal{F}$ model. In [94], the analytical expressions of the average probability of detection, noise power uncertainty, square law diversity reception, and collaborative spectrum sensing were derived. Further, the author obtained the expressions of area under the curve (AUC) of instantaneous SNR, average AUC. Finally, to study the performance of entropy, the author obtained the expressions of Shannon entropy and cross-entropy [94].

2.4 Performance Analysis for Multiple Channels

The performance of the Generalized *K* fading model operating over multiple channel receivers was investigated by **P. M. Shankar** [95]. In [95], several statistics for SC and MRC receiver were derived. Further, the author studied the performance of error rate and AF for different fading and shadowing parameters. **P. S. Bithas** *et al*. [96] analyzed the performance of several diversity schemes over Generalized *K* fading channels. Further, with the assumption of i.n.i.d. channel, the performance measures such as average output SNR, AF, ABER, and Outage Probability were obtained [96].

P. Theofilakos *et al*. [97] presented the performance of Generalized SC (GSC) for i.i.d. *K* distribution using MGF based approach. In [97], the analytical expressions of marginal MGF were obtained, which is used to evaluate the ABER for GSC receiver. The performance of diversity receiver over on-body communication channels at 2.45GHz was studied by **I. Khan** *et al*. [98]. In [98], the experiments were taken in both anechoic and indoor environments with

random body movements. Mainly, three combining techniques (MRC, SC, and Equal Gain Combining (EGC)) were chosen for performance evaluation [98].

P. S. Bithas *et al*. [99] analyzed the capacity performance of selection diversity receiver for Generalized Gamma fading channels. Further, the channel capacities for Nakagami-*m* and Weibull fading models have been formulated using newly derived expressions [99]. **V. K. Dwivedi** *et al***.** [100] analyzed the capacity performance using MGF based approach for Generalized *K* fading model with MRC diversity. A novel unified MGF based method to obtain the ergodic capacity for diversity receivers (MRC and EGC) over the generalized fading channels was introduced by **F. Yilmaz** *et al*. [101]. **P. M. Shankar** [102] derived the expression of PDF with interference for the Generalized *K* distribution. Using derived PDF expression, the expression of ABER for BPSK has been obtained [102]. The expressions of MGF, ABER, Channel Capacity (CIFR), and Outage Probability for the Generalized *K* fading model were derived by **V. K. Dwivedi** *et al*. [103].

M. R. Bhatnagar *et al*. [104] evaluated the performance for shadowed Rician distribution using MRC receiver. The proposed ABER expression was used to obtain the diversity order and coding gain [104]. **E. Salahat** *et al*. [105] derived the analytical expression of PDF for κ-μ shadowed fading model operating over MRC receiver. Further, the author obtained the expressions of ACC and Error Probability for the Additive White Generalized Gaussian Noise (AWGGN) model [105]. The performance of several diversity techniques for η-μ/gamma fading distribution has been analyzed by **H. Al-Hmood** *et al*. [106].

The investigation on signal improvement and reliability over the off-body channel environment for switch diversity methods was reported by **S. K. Yoo** *et al*. [107]. The diversity equations of Nakagami-*m* fading model have been used to compare with experimental results of all three switch diversity techniques. In [107], the goodness of fit and Kullback-Leibler divergence test shows that both empirical and theoretical PDF good matched to each other. The generalized MGF based performance for Beckmann fading model was analyzed in the work of **J. P. P. Martin** *et al*. [108]. The derived generalized MGF was used to evaluate the expressions of the average probability of detection without and with diversity, AUC, and outage probability for the interference-limited case [108].

O. S. Badarneh *et al*. [109] analyzed the performance of MRC diversity for i.n.i.d. $\mathcal{F}$ model. **Y. A. Rahama** *et al*. [110] evaluated the performance of Fox's H function distribution for i.n.i.d.

case. **H. Al-Hmood** *et al*. [111] analyzed the performance of SC diversity for i.n.i.d. $\mathcal{F}$ model. The analysis of shadowed Hoyt/lognormal fading distribution using a mixture of gamma distribution was performed by **S. Kumar** *et al*. [112]. Particularly, the analytical expressions of PDF, CDF, Moments, Outage Probability, Channel Capacity for different adaptive transmission policies, and Error Probabilities for several signaling techniques were provided [112].

2.5 Performance Analysis for OFDM System

The Error Probability performance of uncoded and SFBC coded OFDM systems for Rayleigh fading model was analyzed by **M. Torabi** *et al* [113]. The ABER expressions of downlink SFBC with CDMA for Rayleigh model were derived by **T. Aldalgamouni** *et al*. [114]. **P. Dharmawansa** *et al*. [115] analyzed the BER/SER performance of OFDM system with Carrier Frequency Offset (CFO) over frequency selective, frequency flat Rayleigh, and Additive White Gaussian Noise (AWGN) channels. **F. J. L. Martinez** *et al*. [116] evaluated the BER performance of MIMO-OFDM systems for Rayleigh distribution with MRC receiver and beamforming by considering imperfect channel prediction and interpolation.

The Error Probability performance using BPSK signaling of flat/frequency-selective Rayleigh distribution for OFDM technique with CFO was analyzed by **R. U. Mahesh** *et al* [117]. **S. P. Majumder** *et al*. [118] evaluated the performance of error rate of SFBC coded OFDM for MSK signaling. **V. Bhaskar** *et al*. [119] analyzed adaptive modulation for the MIMO-OFDM with single and multiple antenna systems over Nakagami-*m* fading distribution. In [119], the expressions of spectral efficiency, error probability, and ACC were derived. The numerical results were obtained for different diversity order and Nakagami-*m* parameters [119]. **U. Raj** *et al*. [120] presented the performance of η-μ fading distribution using SFBC-OFDM.

The BER performance of uncoded OFDM and SFBC-OFDM systems for TWDP distribution was analyzed by **D. Singh** *et al*. [121]. **D. Singh** *et al*. [122, 123] analyzed the error probability performance of different fading distributions for SFBC coded OFDM. **D. Singh** *et al*. [124] analyzed the performance using Beaulieu-Xie fading model for single and multiple antennas OFDM system. The SER expressions of Space-Time Block Coding OFDM (STBC-OFDM) systems with CFO for generalized frequency-selective fading model were derived by **D. Singh** *et al*. [125]. Further, the ASER expression for imperfect Channel State Information (CSI) has been obtained [125].

S. Kumari *et al*. analyzed the error rate performance using BPSK modulation technique of FrFT-OFDM with CFO for Rayleigh distribution [126]. The BER performances for 1024-PSK and 1024-QAM modulation schemes of FrFT appended OFDM system over various channels like Nakagami-*m*, Rician, Rayleigh, and AWGN were presented in the work of **A. Kansal** *et al*. [127]. **M. R. Mousavi** *et al*. [128] obtained the BER expression of OFDM technique with FrFT for Rician distribution. The BER expressions using BPSK and 16-QAM of the FrFT-OFDM with CFO for frequency-selective Rician fading model were derived by **R. M. Ashri** *et al*. [129]. **Z. Mokhtari** *et al*. [130] derived the expression (tight bound) for Inter-Carrier Interference (ICI) power of OFDM system using FrFT.

The SER expression using QPSK modulation technique of Rayleigh distribution for OFDM system with discrete cosine FrFT was derived in the work of **A. Kumar** *et al*. [131]. **V. K. Trivedi** *et al*. [132] analyzed the performance of OFDM technique using FrFT for Nakagami-*m* distribution. The error probability expressions of uncoded and SFBC coded OFDM using FrFT for Rayleigh and TWDP fading models were derived by **T. Chawla** *et al*. [133]. **A. Kumar** *et al*. [134] analyzed the SER performance of OFDM technique with discrete FrFT for Rayleigh distribution with Symbol Timing Offset (STO) and CFO.

2.6 Motivation

The wireless system performance is based on the medium through which the information-carrying signal passes. In indoor scenarios, the transmitted signal may go through the highly-dense environment, which causes both shadowing and multipath fading effects. Thus, the shadowed fading model can be well characterized the received signal in this type of environment. Various shadowed fading models over indoor communication channels have been proposed, in which the multiplicative shadowed fading models are most adequate since it includes both LOS and NLOS obstructed signal components.

Also, the diversity combining technique mitigates the effect of fading using multiple receiving antennas. Thus, performances for shadowed fading models over indoor communication channels with and without diversity are necessary to evaluate. The performance can be analyzed in the term of ABER, Outage Probability, Channel Capacity, and AF. In multipath propagation, the signal spreads in the time domain which causes ISI. OFDM is a good technique to reduce ISI [1]. Practically, the channel is not stationary, therefore ICI introduces in the received signal.

Traditional OFDM systems cannot deal with this type of impairment. Recently, FrFT-OFDM is a good technique to deal with ICI. In a real environment, both ISI and ICI introduce in the receiving signal because of spreading in time and frequency. The OFDM and FrFT-OFDM systems can efficiently deal with this type of scenario.

2.7 Research Gaps

On the basis of reported literature, it is the point to notice that multiplicative shadowed fading distribution show excellent agreement with the channel measurement results in comparison with LOS shadowed fading distribution. The performance over shadowed fading distributions can be evaluated in the term of Outage Probability, ABER, Channel Capacity, and AF. Further, the enhancement in the performance can be achieved using the diversity mechanism and OFDM system. Based on the literature review, the following gaps are identified:

1. The performance of shadowed fading models is still needed to be elaborate in the term of ABER, AF, Channel Capacity, and Outage Probability. Both PDF and MGF based method can be used to obtain the performance measures. The ABER expressions can be obtained for various modulation techniques. The Channel Capacity expressions can be obtained for various power and rate adaptive methods [19, 48].
2. Further, the diversity techniques combat the fading effect at the receiver section with the use of multiple receiving antennas. The mostly used diversity combining techniques are SC, MRC, and EGC. By using these combining techniques, we can obtain various performance parameters such as Outage Probability, ABER for different modulation schemes, and different adaptive Channel Capacities [4, 12, 45, 48].
3. The OFDM technique reduces ISI and significantly provides higher data rates. Therefore, the performance measures like ABER and Channel Capacity can be evaluated for the OFDM system model. [4, 12, 13, 19]
4. It is found that the traditional OFDM technique fails in fast fading or doubly dispersive channels. The FrFT based OFDM technique is the right way to deal with this type of fading channels. Hence performance matrices like BER using the FrFT-OFDM technique can be obtained over fast fading or doubly dispersive channel which is not possible with the traditional OFDM system [4, 48].

2.8 Research Questions

The proposed research work is an attempt to answer the following questions:

1. How to select shadowed fading models which is suitable for indoor wireless communication?
2. Whether the multipath fading and shadowing parameter affects the system performance?
3. Whether the diversity combining technique combats the effect of fading? What is the role of number of diversity branch on system performance?
4. Whether the FrFT based OFDM scheme provides minimum error rate in comparison with FFT based OFDM?

2.9 Research Objectives

Based on previous studies and after going through the literature survey, the following research objectives are proposed

1. To study and analyze various composite fading model for Indoor Communication.
2. Performance analysis of composite fading model over single channel for Indoor scenarios.
3. To analyze the performance of composite fading model using diversity combining technique for Indoor Scenario
4. To analyze the performance of composite fading model using OFDM and FrFT-OFDM schemes.

2.10 Research Methodology

In this research work, the performance measures of shadowed fading models over indoor wireless communication channels are evaluated. First of all, the mathematical models of various fading distributions, diversity techniques, OFDM, and FrFT have been studied. The mathematical formulas of some essential performance parameters like ABER, Channel Capacity, Outage Probability, etc. have been presented. After that, the performance measures for the shadowed fading models over SISO channels have been computed. The diversity combining techniques mitigates the fading effects by enhancing the multiple antennas at the receiver with

intelligent combiner. The MRC is an optimum and straightforward technique for obtaining the best output SNR. Hence, analysis using MRC diversity technique over the shadowed fading channels has been performed. Further, the BER analyses of uncoded OFDM and SFBC-OFDM systems with FFT and FrFT over shadowed fading channels have been presented.

Chapter 3

Background and Overview

In the wireless communication system, both multipath fading and shadowing effects occur simultaneously. In other words, multipath fading is superimposed on shadowing; in such scenarios shadowed fading model can be well characterized to the received signal [8]. In this Chapter, the analytical models of some significant multipath fading, shadowing, and shadowed fading are presented that are used in this thesis for analyzing the performance of digital communication systems. The diversity mechanism is one of the well-known methods to mitigate the fading effects. Accordingly, this Chapter also introduces the basics of different diversity combining techniques.

The OFDM and FrFT-OFDM systems can efficiently deal with the doubly dispersive channel. Therefore, the basic principle of OFDM and FrFT are discussed in this Chapter which is helpful in this thesis to analyze the performance of OFDM and FrFT-OFDM systems. Further, the definition and mathematical formulas of some important performance matrices like ABER, Outage Probability, Channel Capacity, and Moments are presented in the end of this Chapter. Two methods of analysis i.e. PDF and MGF based approach, are discussed in this Chapter to evaluate the performance matrices.

3.1 Multipath Fading Model

The short-term fluctuation in the received signal amplitude is called multipath fading or small-scale fading. This type of fading is the cause of the multipath effect. The multipath fading occurs when the receiver moves over a small area. The multipath fading is characterized by Rayleigh, Nakagami-m, TWDP, Rician, Weibull, κ-μ, etc. These types of fading models are adequate for urban, suburban, and indoor scenarios. Some important multipath fading models are presented below

3.1.1 Rayleigh Model

The Rayleigh model consists of only multipath non-LOS components. Its density function in envelope form is [8]:

$$f_R(r) = \begin{cases} \frac{r}{\sigma^2} \exp\left[\frac{-r^2}{2\sigma^2}\right], & 0 \le r < \infty \\ 0, & r < 0 \end{cases} \tag{3.1}$$

where $2\sigma^2$ is the average fading power, and r is the envelope of the received signal.

3.1.2 Rician Model

Rician distribution consists of the strongest direct LOS component and weaker multipath component. The PDF of Rician model is given by [8]:

$$f_R(r) = \begin{cases} \frac{r}{\sigma^2} \exp\left[-\frac{r^2 + V_1^2}{2\sigma^2}\right] I_0\left(\frac{V_1 r}{\sigma^2}\right), & V_1 \ge 0, r \ge 0 \\ 0, & r < 0 \end{cases} \tag{3.2}$$

where I_0 (·) denotes the modified Bessel function of the first kind and zero-order [135, Eq. (8.447.1)] and the peak amplitude of the dominant signal is denoted by V_1. The Rician factor K (dB) is defined as:

$$K = \frac{V_1^2}{2\sigma^2} \tag{3.3}$$

When the dominant signal component (or LOS component) $V_1 = 0$ in (3.2), the Rician distribution reduces to Rayleigh distribution.

3.1.3 Nakagami-*m* Model

Nakagami-*m* distribution is adequate for indoor-mobile multipath propagation, and ionospheric propagation. The PDF of this tractable fading model is [8]:

$$f_R(r) = \frac{r^{2m-1} 2m^m}{\Gamma(m)\Omega^m} \exp\left(-\frac{mr^2}{\Omega}\right) \tag{3.4}$$

where $\Gamma(\cdot)$ represents the gamma function [135, Eq. (8.310)]. m and Ω are denoted as severity parameter and mean power, respectively. With m=1, this simple model converges to Rayleigh distribution. For m<1, it becomes Nakagami-q (Hoyt) model, where m is given by:

$$m = \frac{(1+q^2)^2}{2(1+2q^4)}, m \le 1 \tag{3.5}$$

3.1.4 TWDP Model

This model consists of the two strongest dominant signal components with multiple weaker additive components. Its PDF is given by [136]:

$$f_R(r) = \frac{r}{\sigma^2}\exp\left(-\frac{r^2}{2\sigma^2} - K\right)\sum_{j=1}^{M} a_j D\left(\frac{r}{\sigma}; K, \Delta\cos\frac{\pi(j-1)}{2M-1}\right) \tag{3.6}$$

where Rician factor K is defined as:

$$K = \frac{V_1^2 + V_2^2}{2\sigma^2}, \tag{3.7}$$

Δ defines the shape of TWDP pdf and its range is between 0 and 1 [136]:

$$\Delta = \frac{Peak \quad Specular \quad Power}{Average \quad Specular \quad Power} - 1 = \frac{2V_1V_2}{V_1 + V_2} \tag{3.8}$$

$$D(x; K, \nu) = \frac{1}{2} I_0\left(x\sqrt{(1-\nu)2K}\right)\exp(\nu K) + \frac{1}{2} I_0\left(x\sqrt{(1+\nu)2K}\right)\exp(-\nu K) \tag{3.9}$$

M is the order of approximate TWDP PDF. With the increase of M, the approximate PDF becomes more accurate of true TWDP PDF [136].

The order M is given by:

$$order(M) \ge \frac{1}{2} K\Delta \tag{3.10}$$

3.1.5 κ-μ Model

This generalized model represents the random fluctuations of the fading signal with LOS channel conditions. The density function in envelope form is represented as [137]:

$$f_R(r) = \frac{2\mu(1+\kappa)^{\frac{\mu+1}{2}}}{\kappa^{\frac{\mu-1}{2}}\exp(\mu\kappa)\Omega^{\frac{\mu+1}{2}}} r^{\mu}\exp\left(-\mu(1+\kappa)\frac{r^2}{\Omega}\right) I_{\mu-1}\left(2\mu\sqrt{\kappa(1+\kappa)}\frac{r}{\sqrt{\Omega}}\right) \tag{3.11}$$

where $I_v(\cdot)$ is the modified Bessel function of the first kind with order v [135, Eq. (8.406.1)].
The parameter κ is defined as:

$$\kappa = \frac{\delta^2}{2\mu\sigma^2}$$

δ^2, μ, and $2\mu\sigma^2$ are the total signal power of dominant component, number of multipath clustering, and total signal power of scattered waves, respectively. $\Omega = E[R^2] = \delta^2 + 2\mu\sigma^2$ is the average power. This generalized fading model can be reduced to classical small-scale fading models like Rician, Nakagami-*m,* Rayleigh, and one-sided Gaussian distribution.

3.2 Shadowing Model

The obstacles between the Tx and Rx causes shadowing effects. In other words, shadowing occurs when the user (Tx and/or Rx) moves in the shadow region of objects. This phenomenon causes random behavior in the transmitted signal. Generally, the lognormal distribution is used to characterize the shadowing and its PDF is discussed in the following section.

3.2.1 Log-Normal Model

The density function is [9]:

$$f_R(r) = \frac{1}{r\sqrt{2\pi\sigma^2}}\exp\left\{-\frac{[\ln(r)-m']^2}{2\sigma^2}\right\} \tag{3.12}$$

where the median value is denoted by m'

It is noted that the lognormal distribution characterizes the shadowing. However, this distribution forms a complex analytical solution for evaluating its performance over wireless communication channels. Because of the complexity of lognormal model, Gamma [138], inverse Gamma [139], inverse Gaussian [140], and inverse Nakagami-*m* distribution [141] are the best replacement for

the lognormal distribution. These models are simple and more manageable as compared to the lognormal model. In recent literature, TWDP distribution has also been used for evaluating the shadowing effects by replacing K factor to S_h factor [4].

The PDF of Gamma distribution can be given by [9, 138]:

$$f_R(r) = \frac{\left(\frac{r}{\beta}\right)^{c-1} \exp\left(-\frac{r}{\beta}\right)}{\beta \cdot \Gamma(c)} \tag{3.13}$$

where c is a positive number, and β is the parameter of Gamma distribution. This distribution is commonly used for characterizing the shadowing effect.

The PDF of the inverse Nakagami-m model is defined as follows [141]:

$$f_R(r) = \frac{2r^{-2\lambda-1}}{\Gamma(\lambda)} \exp\left(-\frac{\lambda}{r^2\omega}\right)\left(\frac{\lambda}{\omega}\right)^{\lambda} \tag{3.14}$$

where λ and ω is the shape and scale parameter, respectively.

3.3 Shadowed Fading Model

Shadowed fading models are suitable for indoor communication and their mathematical frameworks are presented as below:

3.3.1 $\mathcal{F}$ Model

This simple and tractable model is based on inverse Nakagami-m shadowing which is used to model the RMS value of Nakagami-m signal. The envelope PDF is [48]:

$$f_R(r) = \frac{2m^m \cdot (m_s\Omega)^{m_s} r^{2m-1}}{B(m, m_s)(mr^2 + m_s\Omega)^{m+m_s}} \tag{3.15}$$

where $B(\cdot,\cdot)$ is the beta function [135, Eq. (8.380.1)]. m_s and m represent the shadowing and severity parameters, respectively. $\Omega = E[r^2]$ is the mean square value. With $m_s \to \infty$, no shadowing of RMS signal power occurs and with $m_s \to 0$, the RMS signal power is deeply shadowed. Therefore, for m=1 and $m_s \to \infty$, it converges to Rayleigh distribution, and for m>0 and $m_s \to \infty$, it becomes Nakagami-m fading.

The density function of instantaneous SNR is expressed as [48]:

$$f_{\gamma}(\gamma) = \frac{\gamma^{m-1} m^{m} \cdot (m_s \bar{\gamma})^{m_s}}{B(m, m_s)(m\gamma + m_s \bar{\gamma})^{m+m_s}} \tag{3.16}$$

The MGF is given by [109]:

$$M_{\gamma}(s) = \frac{1}{\Gamma(m)\Gamma(m_s)} G_{2,1}^{1,2}\left(\frac{m}{m_s \bar{\gamma} s} \middle| \begin{matrix} 1-m_s, & 1 \\ m & \end{matrix} \right) \tag{3.17}$$

where $G_{p,q}^{m,n}[\cdot \mid \cdot]$ denotes the Meijer G function. $0 \le m \le q$, and $0 \le n \le p$, here m, n, p and q are the integer numbers [135, Eq. (9.301)].

3.3.2 *κ-μ*/gamma Model

This generalized model is based on gamma shadowing. In this, the average power of *κ-μ* distribution follows the gamma shadowing. The density function is [19]:

$$f_R(r) = \sum_{j=0}^{\infty} \frac{4\mu^{\frac{\alpha+\mu+3j}{2}} (1+\kappa)^{\frac{\alpha+\mu+j}{2}} \kappa^{j} r^{\alpha+\mu+j-1}}{\beta^{\frac{\alpha+\mu+j}{2}} j! \exp(\mu\kappa)\Gamma(\mu+j)\Gamma(\alpha)} K_{\alpha-\mu-j}\left(2r\sqrt{\frac{\mu(1+\kappa)}{\beta}} \right) \tag{3.18}$$

where $K_v(\cdot)$ is the modified Bessel function of the second kind with order v [135, Eq. (8.446)]. α and β represent the shape and scale parameters, respectively. By setting the several parameters values, the above model, as given in (3.18), converges to other fading distributions such as Nakagami-*m*, Rice/lognormal, *κ-μ*, Rayleigh/gamma, Generalized-*K*, Rice, and Rayleigh [19].

3.3.3 Rayleigh/TWDP Model

It is the mixture of Rayleigh and TWDP fading. The density function in envelope form is [43]

$$f_R(r) = \frac{r}{P_1 P_2} \exp(-S_h) \sum_{i=1}^{M} C_i D\left(\sqrt{\frac{r}{\sqrt{P_1 P_2}}}; S_h, \Delta M_i \right) K_m\left(\frac{r}{\sqrt{P_1 P_2}} \right) \tag{3.19}$$

where C_1, C_2, C_3, and C_4 are constant, and $M_i = \Delta\cos(\pi(i-1)/(2M-1))$. S_{h} and Δ represent the shadowing and shape parameters, respectively. P_2 and P_1 are the mean power. Rayleigh/TWDP

model is adequate for those scenarios where the transmitter and receivers are separated by surrounding objects like multi-floor buildings and wall partitions.

3.4 Diversity Techniques

The fading effects deteriorate the performance of digital communication systems. The diversity mechanism is a good technique to overcome the fading effects and improve the signal reliability at the receiver. Based on the nature of fading that deliberate to mitigate, the diversity technique is divided into two classes: micro, and macro diversity. The micro diversity technique reduces the short-term fading using multiple antennas at the base station whereas the macro-diversity scheme combats the effect of shadowing using numerous base stations [9].

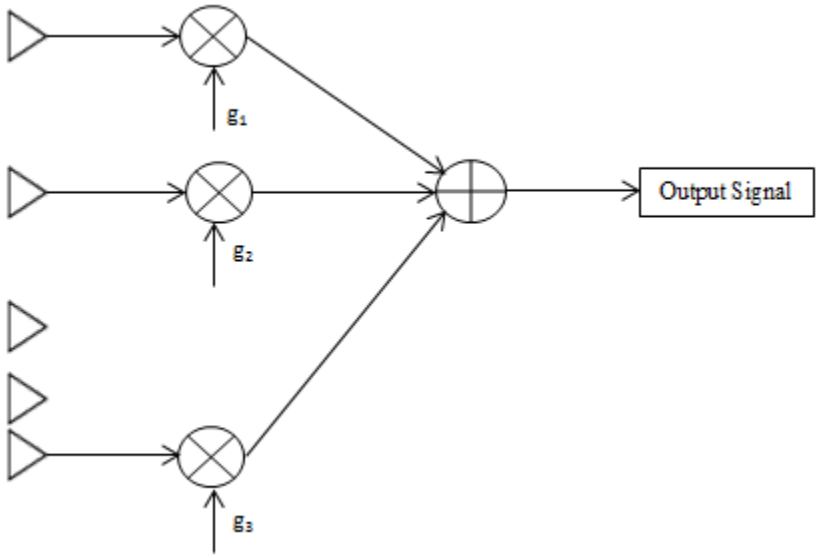

Figure 3.1: Concept of diversity combining technique [9].

In diversity combining technique, various replicas of the signal are received at the receiver section that must be intelligently combined to improve the quality of the signal. Figure 3.1 represents the outline of diversity combining algorithm. Through each branch, the signal is received and multiplied by a predefined weight factor and then combined intelligently to provide the output signal. Based on combining methods, the diversity technique is broadly classified into two groups:

(1) Switching based
(2) Weighting coefficients

In the switching method, one of the diversity branches is chosen; however, in the second technique, the result is obtained by summing the weighted portion of the signal from all diversity branches [1]. Figure 3.2 shows different types of diversity combining techniques:

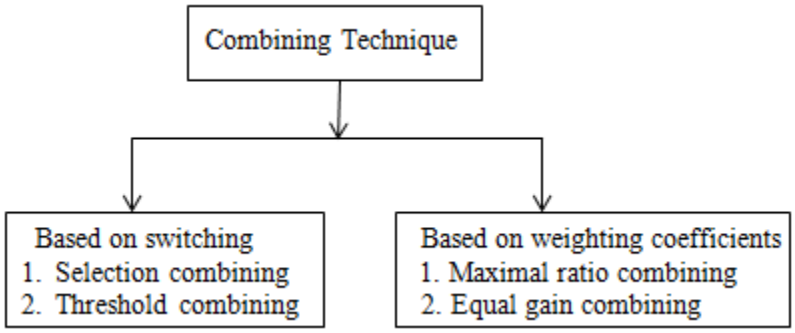

Figure 3.2: Types of diversity combining technique [1]

3.4.1 Maximum Ratio Combining (MRC)

By using this combining method, the best SNR with the highest probability can be obtained as compared to the other methods. MRC gives the best performance as compared to other combining techniques; however, it needs complex implementation [1].

In MRC diversity, the instantaneous output SNR is expressed as [9]:

$$\gamma_{MRC} = \sum_{i=1}^{L} \gamma_i = \frac{E_s}{N_0} \sum_{i=1}^{L} h_i^2 \tag{3.20}$$

where γ_i denotes the instantaneous SNR of i^{th} branch. h_i is randomness or fluctuations at i^{th} branch. The MRC algorithm provides the highest SNR improvement by combining the received SNR in all branches.

3.4.2 Equal Gain Combining (EGC)

EGC is a special case of the MRC algorithm. In EGC, gain factors are same. The SNR output at the EGC receiver is given by [9]:

$$\gamma_{EGC} = \frac{1}{L}\left[\sum_{i=1}^{L} \sqrt{\gamma_i}\right]^2 \tag{3.21}$$

The EGC scheme is less complicated than the MRC scheme. EGC diversity has better output SNR in comparison to SC and SSC diversity.

3.4.3 Selection Combining (SC)

In the SC technique, the single path that has a signal with the highest instantaneous SNR, as compared to all other individual paths, is selected for demodulation. This technique improves the receiver performance without any additional transmit power or sophisticated receiving circuitry. The SC algorithm with the selection of g_i can be given as [9]:

$$g_k = \begin{cases} 1 & \gamma = \max\{\gamma_i\}_{i=1,2,..L} \\ 0 & otherwise \end{cases} \tag{3.22}$$

The branch with highest SNR value can be express as:

$$\gamma_{SC} = \max\{\gamma_i\}_{i=1,2,...L} \tag{3.23}$$

For i.i.d. case, the distribution function becomes:

$$F_{SC}(\gamma) = [prob\{\gamma_i \le \gamma\}]^L \tag{3.24}$$

Thus, the density function of SC diversity is expressed as:

$$f_{SC}(\gamma) = \frac{d}{d\gamma} F_{SC}(\gamma) = L[F(\gamma_i)]^{L-1} f(\gamma_i) \tag{3.25}$$

It is noted that the SC algorithm is least complicated than all other combining techniques since it requires only a single branch that has maximum instantaneous SNR. The SC scheme requires the scanning of all diversity branches and selection of one branch for obtaining the maximum SNR at a time is practically difficult. To avoid this difficulty threshold combining algorithm is used.

3.4.4 Threshold Combining (TC)

In TC technique, the threshold SNR is fixed. In this algorithm, the branch that has the highest SNR is selected to receiver for processing. It chooses another branch (having high SNR) when the SNR of current branch falls below the predefined threshold [1]. The improvement in received SNR depends on the level of the threshold value. For performance improvement, the threshold

level should be adaptive according to variable wireless environmental conditions. TC scheme has the least complex receiver circuit and does not require unnecessary switching from one diversity branch to another diversity branches.

3.5 Orthogonal Frequency Division Multiplexing

In multipath propagation, the signal spreads in the time domain which causes ISI. Accordingly, the signal may undergo frequency-selective fading which distorts the shape of the signal and also challenging to detect the signal. Multicarrier modulation is an excellent technique to deal with these impairments. OFDM is the particular case of multicarrier modulation. In the OFDM technique, the system bandwidth is divided into sets of sub-band and these sub-bands are orthogonal and independent to each other [1].

In Frequency Division Multiplexing (FDM) technique, the net bandwidth is partitioned into smaller sub-bands with some space to avoid mutual interference. This space is provided by introducing a guard band between two sub-bands. Therefore FDM technique uses an inefficient frequency spectrum. However, the OFDM technique provides the sub-bands to be spaced much closer to each other by using overlapping. OFDM technique saves up to 50% of the total spectrum [1]. Figure 3.3 depicts the block diagram of transmitting and receiving OFDM model.

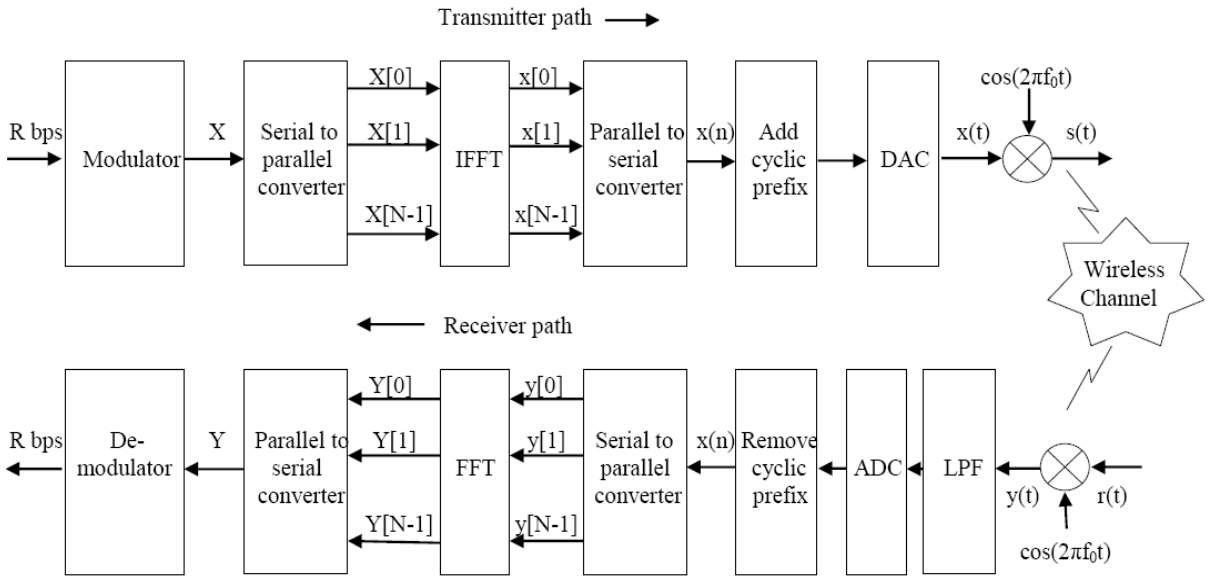

Figure 3.3: OFDM System Model [1].

Considering, the incoming signal data rate is *R* bits per second (bps). It passes through the modulator that modulates the incoming signal. In other words, the modulator maps the incoming signal onto the carrier signal. After getting the modulated signal *X*, it changes into the parallel data stream. Now, the *N* parallel discrete-frequency components are passes through the Inverse FFT (IFFT) to obtain the *N* parallel discrete-time components. After IFFT, the discrete-time component passes through the parallel to serial converter to get a signal in the time domain. Cyclic Prefix (CP) is added to remove ISI. After that, the data is up-converted before transmission through the wireless channel.

After passes through the wireless channel, the carrier signal component gets remove and obtain a baseband signal component. Followed by the filtering circuit, and CP, the discrete-time signal component is obtained. A serial to parallel converter collects *N* sample data in the time domain. These time-domain samples are passes through the FFT to output the frequency domain samples. These frequency domain samples are then serially converted and pass through the demodulator to map the received signal *Y* and produce the data *R* bps.

3.5.1 Applications

OFDM technologies are being widely used in several WLAN and Wireless Metropolitan Area Networks (WMAN). This technology is also used in Digital Video Broadcasting (DVB), Digital Audio Broadcasting (DAB) system, and Long-Term Evolution (LTE) [1]. Further OFDM has a highly desirable feature for wireless transmission; therefore, it has more considerable interest in the research community as well as industrial purposes.

3.5.2 Advantages

- It provides spectrally efficient transmission (sub-bands are densely packed). Hence realize high data rate over a given bandwidth.
- For fast and efficient signal processing, OFDM can be digitally implemented using IFFT and FFT.
- OFDM can efficiently deal with ISI. OFDM makes symbol duration *N* times larger than the original symbol duration. This resultant symbol duration is significantly large as compared to delay spread causes in the channel.

- OFDM converts frequency-selective fading into flat-fading conditions that simplify the processing at the receiver for recovering the data.

3.5.3 Drawback

OFDM technique suffers from the specific drawback that degrades the performance of OFDM based system

- It is sensitive to CFO
- It is also sensitive to the timing offset

3.6 Fractional Fourier Transform

It is the generalized form of the FT [142]. With the increase of order between 0 and 1, the FrFT can represent the signal characteristic between the time and frequency axis. Suppose *s*(t) is any signal quantity in time domain and therefore, its FrFT is given as [143,144]:

$$S_p(v) = F_p[s](v) = \int_{-\infty}^{\infty} K_p(t,v)s(t)dt \tag{3.26}$$

where $F_p[\cdot]$ is the FrFT operator with transform order *P*. The FrFT kernel $K_p(t,v)$ is represented as:

$$K_p(t,v) = \begin{cases} \exp\left(-jut\csc\phi + j\dfrac{t^2+v^2}{2}\cot\phi\right)\sqrt{(1-j\cot\phi)/2\pi} & , \quad \phi \neq n\pi \\ \delta(t-v) & , \quad \phi = 2n\pi \\ \delta(t+v) & , \quad \phi = (2n+1)\pi \end{cases} \tag{3.27}$$

where $\phi = p\pi/2$ is the angle of rotation. The IFrFT can be defined as:

$$s(t) = F_{-p}[S_p](t) = \int_{-\infty}^{\infty} K_{-p}(t,v)S_p(u)dv \tag{3.28}$$

3.6.1 Applications of FrFT

FrFT is the best technique to deal with non-stationary signals. It has many applications as given below [142]

- Optical information processing
- Phase retrieval and signal reconstruction
- Signal detection and parameter estimation
- Filtering in the FrFT domain
- Neural networks
- Sound analysis
- Image processing
- Applications in radar, sonar, and communication

In frequency-selective channels, the ISI can be easily resolved by using the OFDM technique. However, when the channel is frequency dispersive (that causes ICI), the orthogonality between subcarriers is destroyed using a traditional OFDM system. Thus, to reduce ICI, FrFT based OFDM is used that improves the system performance as compared to FT based ODFM system [143].

3.7 Performance Measures

For implementing any wireless system, the analysis of performance measures is necessary. Performance analysis parameters include ABER, Channel Capacity, Outage Probability, Moments, AF, AFD, and LCR [8]. Some important performance parameters are discussed as below.

3.7.1 Moments

The Moments has a vital role in performance analysis over the radio communication channels. With the help of the Moments, the Average Output SNR, second Moment, and AF can be evaluated. The n^{th} moment is given by [8]:

$$E[\gamma^n] = \int_0^\infty \gamma^n f_\gamma(\gamma) d\gamma \tag{3.29}$$

where n is the order of moment and E[·] is the expectation. By putting n = 1, the first moment or mean value can be calculated. Likewise, by putting n = 2 and 3, the second and third moment can be calculated.

An alternate way (using MGF based approach) to obtain the Moment is given by [8]:

$$E[\gamma^n] = \left. \frac{dM_\gamma(s)}{ds} \right|_{s=0} \tag{3.30}$$

where $M_\gamma(\gamma)$ is the MGF and it is given as:

$$M_\gamma(s) = \int_0^\infty \exp(-s\gamma) f_\gamma(\gamma) d\gamma \tag{3.31}$$

3.7.2 Amount of Fading (AF)

The AF can be computed using second and fourth Moment of any fading model. AF is related to the severity parameter and is defined as [8]:

$$AF = \frac{E[\gamma^4] - \left(E[\gamma^2]\right)^2}{\left(E[\gamma^2]\right)^2} \tag{3.32}$$

3.7.3 Average Bit Error Rate (ABER)

The Error Probability depends on the types of modulation technique, modulation index, average SNR, fading factors, etc. The formula to calculate the ABER is given as below [8]:

$$P_e(E) = \int_0^\infty P(E \mid \gamma) \cdot f_\gamma(\gamma) d\gamma \tag{3.33}$$

where $P(E \mid \gamma)$ represents the Conditional Error Probability (CEP) in AWGN channels. Table 3.1 shows the conditional BER for several modulation techniques.

The formula of ABER for several signaling techniques using MGF method is shown in Table 3.2. The calculation of ABER using MGF based approach is easy because this method avoids the computations of mathematically complex integration. For example, the ABER for BDPSK can be directly obtained using given MGF expression (as shown in Table 3.2). Using this method, generally, the solutions are obtained in the closed-form if the PDF is available in closed-form. The ABER using MGF based approach is given by [8]:

$$P_e(\gamma) = \frac{1}{2\pi j} \int_{\sigma - j\infty}^{\sigma + j\infty} \frac{M_\gamma(-s)}{s} ds \tag{3.34}$$

Table 3.1: Conditional error rate for several modulation techniques

Modulation Scheme	ξ_1	ξ_2	Conditional Error Probability $P(E/\gamma)$
BPSK	0.5	1	$\xi_1 erfc\left(\sqrt{\xi_2 \gamma}\right)$
BFSK	0.5	0.5	
QPSK and MSK	1	0.5	
BDPSK	0.5	1	$\xi_1 \exp(-\xi_2 \gamma)$
NCFSK	0.5	0.5	
NCMFSK	$\frac{1}{M}\sum_{i=2}^{M}(-1)^i\binom{M}{i}$	$\left(1-\frac{1}{i}\right)$	
MPSK	$1/\pi$	$\frac{\sin^2(\pi/M)}{\sin^2(\theta)}$	$\xi_1 \int_0^{\pi-\pi/M} \exp(-\xi_2(\theta))d\theta$
MDPSK	$1/\pi$	$\frac{\sin^2(\pi/M)}{1+\cos(\pi/M)\cos(\theta)}$	
π/4 DQPSK	$1/2\pi$	$\frac{2}{2-\sqrt{2}\cos(\theta)}$	$\xi_1 \int_0^{\pi} \exp(-\xi_2(\theta))d\theta$

Table 3.2: ABER for several modulation techniques using MGF based approach

Modulation Scheme	ABER
BDPSK	$0.5\, M_\gamma(a)$, a=1
NCFSK	$0.5\, M_\gamma(a)$, a=0.5
BPSK	$\frac{1}{\pi}\int_0^{\pi/2} M_\gamma\left(\frac{a}{\sin^2(\theta)}\right)d\theta$, a=1
BFSK	$\frac{1}{\pi}\int_0^{\pi/2} M_\gamma\left(\frac{a}{\sin^2(\theta)}\right)d\theta$, a=0.5
BFSK with min. corre.	$\frac{1}{\pi}\int_0^{\pi/2} M_\gamma\left(\frac{a}{\sin^2(\theta)}\right)d\theta$, a=0.715
MAM	$\frac{2(M-1)}{M\pi\log_2(M)}\int_0^{\pi/2} M_\gamma\left(\frac{g_{AM}}{\sin^2(\theta)}\right)d\theta,\ g_{AM}=\frac{3\log_2(M)}{M^2-1}$
Square MQAM	$\frac{4}{M\pi\log_2(M)}\left\{\left(1-\frac{1}{\sqrt{M}}\right)\int_0^{\pi/2} M_\gamma\left(\frac{g_{QAM}}{\sin^2(\theta)}\right)d\theta-\left(1-\frac{1}{\sqrt{M}}\right)^2\int_0^{\pi/4} M_\gamma\left(\frac{g_{QAM}}{\sin^2(\theta)}\right)d\theta\right\}, g_{QAM}=\frac{3\log_2(M)}{2(M-1)}$
MPSK	$\frac{1}{\pi\log_2(M)}\int_0^{\Theta} M_\gamma\left(\frac{g_{PSK}}{\sin^2(\theta)}\right)d\theta,\ g_{PSK}=\log_2(M)\sin^2\left(\frac{\pi}{M}\right),\ \Theta=\pi-\pi/M$
MDPSK	$\frac{1}{\pi\log_2(M)}\int_0^{\Theta} M_\gamma\left(\frac{g_{PSK}}{1+\cos(\theta)\cos(\pi/M)}\right)d\theta$

3.7.4 Outage Probability

It is the probability that SNR (γ) falls below the certain threshold SNR level (γ_0) and mathematically can be represented as [8]:

$$P_{out} = P_r\{\gamma \le \gamma_0\} = \int_0^{\gamma_0} f_\gamma(\gamma)d\gamma = F_\gamma(\gamma_0) \tag{3.35}$$

The P_{out} using MGF based approach is given by [8]:

$$P_{out} = \frac{1}{2\pi j}\int_{\sigma-j\infty}^{\sigma+j\infty} \frac{M_\gamma(-s)}{s}\exp(s\gamma_0)ds \tag{3.36}$$

3.7.5 Channel Capacity

The amount of data transmitted through the wireless medium is said to be Channel Capacity. In the case of ideal condition (or no fading), the maximum capacities are obtained. The capacity improvement depends on some parameters such as code rate, constellation size, and transmitted power. The capacity with different variable data rate and power methods are given below

3.7.5.1 ORA

This method has variable data rates and fixed transmitted power. Only Rx knows the CSI. The C_{ORA} is defined as [62]:

$$C_{ORA} = \int_0^{\infty} \log_2(1+\gamma) f_\gamma(\gamma)d\gamma \tag{3.37}$$

The Channel Capacity for ORA policy using MGF based approach is [62]:

$$C_{ORA} = \frac{1}{\ln(2)}\int_0^{\infty} E_i(-s)\frac{d}{ds}M_\gamma(s)ds \tag{3.38}$$

where $E_{\text{i}}(\cdot)$ denotes an exponential integral function [135, Eq. (8.211.1)].

The capacity in the low SNR region (C_{ORA}) is given by [62]:

$$C_{ORA}^{LSNR} \cong \frac{1}{\ln(2)} \int_0^{\infty} \gamma \cdot f_{\gamma}(\gamma) d\gamma \tag{3.39}$$

The capacity at high SNR under ORA method is [77]:

$$C_{ORA}^{HSNR} = \int_0^{\infty} \log_2(\gamma) f_{\gamma}(\gamma) d\gamma \tag{3.40}$$

3.7.5.2 OPRA

In this method, both Rx and Tx know the CSI. Because of CSI availability, this method can easily vary the data rate and transmitting power. Channel Capacity under OPRA schemes is given by [62]

$$C_{OPRA} = \int_{\gamma_0}^{\infty} \log_2\left(\frac{\gamma}{\gamma_0}\right) \cdot f_{\gamma}(\gamma) d\gamma \tag{3.41}$$

where γ_0 is the cut off SNR below which no transmission of data occurs.

Given an average transmit power constraint; the optimal power cutoff SNR level γ_0 for adaptive transmission technique must satisfy the following relationship [62]

$$\int_{\gamma_0}^{\infty} \left(\frac{1}{\gamma_0} - \frac{1}{\gamma}\right) f_{\gamma}(\gamma) d\gamma = 1 \tag{3.42}$$

The Channel Capacity for OPRA policy using MGF based approach is given by [62]

$$C_{OPRA} = \frac{\gamma_0}{\ln(2)} \int_0^{\infty} E_i(-s) \Psi_{\gamma}(s; \gamma_0) ds \tag{3.43}$$

where

$$\Psi_{\gamma}(s; \gamma_0) = \frac{\exp(s)}{\gamma_0} \left[M_{\gamma}\left(\frac{s}{\gamma_0}\right) - \hat{M}_{\gamma}\left(\frac{s}{\gamma_0}; \gamma_0\right) \right] + \frac{\exp(s)}{\gamma_0^2} \left[M'_{\gamma}(t)\Big|_{t=\frac{s}{\gamma_0}} - \gamma_0 \hat{M}'_{\gamma}(t; \gamma_0)\Big|_{t=\frac{s}{\gamma_0}} \right] \tag{3.44}$$

Here $\hat{M}_{\gamma}(\cdot;\cdot)$ is the truncated MGF.

3.7.5.3 CIFR

This method has fixed data rate. Both Tx and Rx know the CSI. The C_{CIFR} is defined by the following formula [62]

$$C_{CIFR} = \log_2\left(1 + \frac{1}{\int_0^{\infty} \frac{f_\gamma(\gamma)}{\gamma} d\gamma}\right) \tag{3.45}$$

The Channel Capacity for CIFR scheme using MGF approach is given by [62]

$$C_{CIFR} = \log_2\left(1 + \frac{1}{\int_0^{\infty} M_\gamma(s) ds}\right) \tag{3.46}$$

3.7.5.4 TIFR

In the CIFR method, the Tx sends the transmitting power to Rx in huge amount. Due to which the penalty introduces on capacity under CIFR transmission protocol. Therefore, the TIFR method is preferred so that the capacity losses could be overcome. In this, the Tx sends the power to Rx above the predetermined cutoff SNR γ_0. The C_{TIFR} is [62]

$$C_{TIFR} = \log_2\left(1 + \frac{1}{\int_{\gamma_0}^{\infty} \frac{f_\gamma(\gamma)}{\gamma} d\gamma}\right)(1 - P_{out}(\gamma_0)) \tag{3.47}$$

The Channel Capacity for TIFR scheme using MGF based approach is given by [62]

$$C_{TIFR} = \log_2\left(1 + \frac{1}{\overline{P}_{out}\left(\frac{1}{\gamma_0}\right)}\right)(1 - P_{out}(\gamma_0)) \tag{3.48}$$

where $\overline{P}_{out}(\cdot)$ is the Outage Probability of $\bar{\gamma}$ whose PDF and MGF are given in [62].

In this Chapter, the mathematical models of different fading channels, different diversity techniques, OFDM system, and FrFT model have been presented. Also, some mathematical formulas to calculate the performance measures such as ABER, Channel Capacity, AF, Moments, and Outage Probability have been presented. The MRC diversity provides better SNR improvements in comparison with SC, EGC, and TC diversity. Moreover, the employment of OFDM model at Tx and Rx gives better performance in time-varying wireless channels.

Chapter 4

Shadowed Fading Model over Single Channel

In indoor wireless system, the transmitter (Tx) and/or receiver (Rx) may be located in the corridor, office room, laboratory, seminar hall, and also on the human body. Multipath fading occurs due to scattering and reflections from the surrounding objects. However, the obstruction in the signal components from the surrounding objects and the human body is the main cause of shadowing. Therefore, the characterization of signal components can be well modeled by a combination of both multipath fading and shadowing (or shadowed fading).

In the indoor scenarios, the performance can be evaluated in the respect of ABER, Outage Probabilities, AF, and Channel Capacities. Different methods of analysis such as PDF, MGF, CDF, and Characteristic Function based approach can be used for obtaining the performance parameters of single channel. In this Chapter, two shadowed fading models i.e. κ-μ/gamma and Rayleigh/TWDP, are presented for performance evaluation of channel. Correspondingly, the statistical parameters are derived for both models. With the help of these statistics, the performance matrices are computed. Finally, in this Chapter, the numerical results are obtained from the derived expressions and compared with the existing fading models.

4.1 Introduction

The multipath fading signal under LOS channel conditions is characterized by κ-μ fading. Based on several μ and κ values, this generalized multipath model converges to other distributions like Nakagami-*m*, Rician, Rayleigh, and one-sided Gaussian. The κ-μ distribution based new shadowed models were developed in [12-14, 19, 40]. One of these is κ-μ/gamma, which is the composition of κ-μ and gamma model, is derived in [19]. This paper presents the expressions of the Density Function, CDF, MGF, Moments, and AF as the function of received envelope signal for κ-μ/gamma fading [19].

TWDP model characterizes the multipath fading which consists of two specular components and multiple diffuse power components [136]. Further, it can be reduced to Rician and Rayleigh

distribution. In reported literature, the TWDP distribution has been used as a shadowing model by replacing the K factor to S_h factor [4, 43, 44]. TWDP based new shadowed fading models are Rician/TWDP (also known as JFTS model), Rayleigh/TWDP, and POCA/TWDP [4, 43, 44]. These models are adequate for the indoor WLAN communication system. Rician/TWDP model had been proposed by I. dey *et al.* [4] which is the mixture of Rician and TWDP distribution. The Rician/TWDP shadowed fading model is analytically complex.

In this Chapter, the performances of two new shadowed models: Rayleigh/TWDP and κ-μ/gamma have been evaluated over the indoor wireless communication. Following parameters have been evaluated and compared in this Chapter:

- Density Function, MGF, Moments, and Distribution Function for κ-μ/gamma fading are computed.
- The expressions of Error Probability using several modulation techniques, Outage Probability, and Capacity for ORA, OPRA, CIFR, and TIFR methods for κ-μ/gamma fading are derived.
- The key statistics such as PDF and MGF for Rayleigh/TWDP model are derived.
- The expression of CDF as the function of the envelope signal for Rayleigh/TWDP model is derived.
- Performance matrices such as ABER using BDPSK, NCFSK, BPSK, and BFSK modulation schemes and Outage Probability for Rayleigh/TWDP fading distribution are computed.
- The new results of derived expression for κ-μ/gamma and Rayleigh/TWDP model are presented and compared with existing fading model.

Research hypothesis test: Both multipath fading and shadowing parameter of shadowed fading model influence the system performance.

4.2 System Model

Assuming, signal $x(t)$ is transmitted over the shadowed fading channels. The received signal $y(t)$ can be expressed as

$$y(t) = h \cdot x(t) + c(t) \tag{4.1}$$

where, h is the multipath fading and shadowing envelope. $c(t)$ denotes the additive white Gaussian noise. Two shadowed fading models are considered in this Chapter for evaluating the performance matrices. The formulation of these two shadowed fading models is given below.

(A) Formulation of κ-μ/gamma model

Integrating the κ-μ conditional envelope PDF with respect to random variation of mean signal power Ω, the κ-μ/gamma PDF can be represented as,

$$f_R(r) = \int_0^\infty f_{R|\Omega}(r \mid \omega) f_\Omega(\omega) d\omega \tag{4.2}$$

With the assumption of constant Ω, the κ-μ/gamma PDF in (4.2) becomes [137]

$$f_{R|\Omega}(r \mid \omega) = \frac{2\mu(\kappa+1)^{\frac{\mu+1}{2}} r^{\mu}}{\kappa^{\frac{\mu-1}{2}} \exp(\mu\kappa)\omega^{\frac{\mu+1}{2}}} \exp\left(-\frac{\mu(1+\kappa)r^2}{\omega}\right) I_{\mu-1}\left(2\mu\sqrt{\kappa(1+\kappa)}\frac{r}{\sqrt{\omega}}\right) \tag{4.3}$$

It is noted that (4.3) represents the PDF of κ-μ distribution. κ denotes the ratio of the total power of dominant components (δ^2) to the total power of the scattered waves ($2\mu\sigma^2$). The parameter μ is the multipath clustering, and σ^2 denoted the power of the scattered wave in each cluster. Hence, the corresponding mean signal power is given as $E[R^2] = \Omega = \delta^2 + 2\mu\sigma^2$.

Now by assuming Ω follows the gamma PDF [9, 138]

$$f_\Omega(\omega) = \frac{\omega^{\alpha-1}}{\Gamma(\alpha)\beta^{\alpha}} \exp\left(-\frac{\omega}{\beta}\right) \tag{4.4}$$

By plugging (4.3) and (4.4) into (4.2), (4.2) becomes

$$f_R(r) = \frac{2\mu(\kappa+1)^{\frac{\mu+1}{2}} r^{\mu}}{\kappa^{\frac{\mu-1}{2}} \exp(\mu\kappa)\Gamma(\alpha)\beta^{\alpha}} \int_0^\infty \omega^{\frac{2\alpha-\mu-3}{2}} \exp\left(-\frac{\mu(1+\kappa)r^2}{\omega}\right) \exp\left(-\frac{\omega}{\beta}\right) I_{\mu-1}\left(2\mu\sqrt{\kappa(1+\kappa)}\frac{r}{\sqrt{\omega}}\right) d\omega \tag{4.5}$$

So, the PDF of envelope signal over κ-μ/gamma channels in infinite series form can be given as [19]

$$f_R(r)=\sum_{j=0}^{\infty}\frac{4\mu^{\frac{\alpha+\mu+3j}{2}}\kappa^j(1+\kappa)^{\frac{\alpha+\mu+j}{2}}r^{\alpha+\mu+j-1}}{j!\exp(\mu\kappa)\Gamma(\alpha)\Gamma(\mu+j)\beta^{\frac{\alpha+\mu+j}{2}}}K_{\alpha-\mu-j}\left(2r\sqrt{\frac{\mu(1+\kappa)}{\beta}}\right) \tag{4.6}$$

(B) Formulation of Rayleigh/TWDP model

The density function of Rayleigh model is [8]

$$f_X(x)=f_X(x;P_1)=\frac{x}{P_1}\exp\left(-\frac{x^2}{2P_1}\right) \tag{4.7}$$

The PDF of TWDP distribution, which is characterized as shadowing, is given as [43]

$$f_Y(y)=\frac{y}{P_2}\exp\left(-\frac{y^2}{2P_2}-S_h\right)\sum_{i=1}^{M}a_iD\left(\frac{y}{\sqrt{P_2}};S_h,\Delta b_i\right) \tag{4.8}$$

where

$$D(\xi;u,v)=\frac{1}{2}\exp(vu)I_0\left(\xi\sqrt{2u(1-v)}\right)+\frac{1}{2}\exp(-vu)I_0\left(\xi\sqrt{2u(1+v)}\right) \tag{4.9}$$

and, y is the received signal envelope of TWDP distribution, S_h denotes the shadowing parameter, Δ is the shape parameter and P_2 is the mean signal of TWDP distribution. M is the approximation index and $b_i=\cos(i-1)\pi/7$.

The joint PDF $f_{XY}(x,y)$ can be given as [43]

$$f_{XY}(x,y)=\frac{xy}{P_1P_2}\exp\left(-\frac{x^2}{2P_1}-\frac{y^2}{2P_2}-S_h\right)\left[a_4T_4+a_3T_3+a_2T_2+a_1T_1\right] \tag{4.10}$$

where,

$$T_i=\exp(-\Delta S_hb_i)I_0(y\sqrt{2S_h(1+\Delta b_i)/P_2})+\exp(\Delta S_hb_i)I_0(y\sqrt{2S_h(1-\Delta b_i)/P_2}) \tag{4.11}$$

and, a_1, a_2, a_3 and a_4 has constant value.

Therefore, the density function of envelope signal for Rayleigh/TWDP shadowed fading model is evaluated as [43]

$$f_R(r) = \frac{r}{P_1 P_2} \exp(-S_h) \sum_{i=1}^{M} C_i D\left(\sqrt{\frac{r}{\sqrt{P_1 P_2}}}; S_h, \Delta M_i \right) K_m\left(\frac{r}{\sqrt{P_1 P_2}} \right) \tag{4.12}$$

4.3 κ-μ/gamma Model

4.3.1 PDF

The mathematical formula to obtain the PDF of γ is given as [8]

$$f_\gamma(\gamma) = f_R\left(\sqrt{\frac{\Omega\gamma}{\bar{\gamma}}} \right) \Bigg/ \left(2\sqrt{\frac{\bar{\gamma}\gamma}{\Omega}} \right) \tag{4.13}$$

By plugging (4.6) into (4.13), the density function of κ-μ/gamma becomes

$$f_\gamma(\gamma) = \sum_{j=0}^{\infty} \frac{2\mu^j \kappa^j}{j!\Gamma(\alpha)\Gamma(\mu+j)\exp(\mu\kappa)} \cdot \gamma^{\frac{\alpha+\mu+j-2}{2}} \left(\frac{\mu(1+\kappa)\Omega}{\beta\bar{\gamma}} \right)^{\frac{\alpha+\mu+j}{2}} K_{\alpha-\mu-j}\left(2\sqrt{\frac{\mu(1+\kappa)\Omega\gamma}{\beta\bar{\gamma}}} \right) \tag{4.14}$$

By using [135, Eq. (9.34.3)], an alternate expression of PDF (SNR) is computed as

$$f_\gamma(\gamma) = \sum_{j=0}^{\infty} \frac{\mu^j \kappa^j}{j!\exp(\mu\kappa)\Gamma(\alpha)\Gamma(\mu+j)} \left(\frac{\mu(1+\kappa)\Omega}{\beta\bar{\gamma}} \right) G_{0,2}^{2,0}\left(\frac{\mu(1+\kappa)\Omega\gamma}{\beta\bar{\gamma}} \middle| \alpha-1, \quad \mu+j-1 \right) \tag{4.15}$$

4.3.2 MGF

The definition of MGF is given in (3.31). By substituting (4.14) into (3.31), the MGF of γ is given as

$$M_\gamma(s) = \sum_{j=0}^{\infty} \frac{2\mu^j \kappa^j}{j!\Gamma(\alpha)\Gamma(\mu+j)\exp(\mu\kappa)} \left(\frac{\mu(1+\kappa)\Omega}{\beta\bar{\gamma}} \right)^{\frac{\alpha+\mu+j}{2}} \int_0^{\infty} \exp(-s\gamma)\gamma^{\frac{\alpha+\mu+j-2}{2}} K_{\alpha-\mu-j}\left(2\sqrt{\frac{\mu(1+\kappa)\Omega\gamma}{\beta\bar{\gamma}}} \right) d\gamma \tag{4.16}$$

The $G_{p,q}^{m,n}[\cdot|\cdot]$ and $K_{\mathrm{v}}(\cdot)$ function is related through the following mathematical formula [135, Eq. (9.34.3)]

$$x^\mu K_v(x) = 2^{\mu-1} G_{0,2}^{2,0}\left(\frac{x^2}{4} \middle| \frac{\mu}{2}+\frac{v}{2}, \frac{\mu}{2}-\frac{v}{2} \right) \tag{4.17}$$

On plugging (4.17) into (4.16), (4.16) becomes

$$M_{\gamma}(s)=\sum_{j=0}^{\infty}\frac{(1+\kappa)\kappa^{j}\mu^{j+1}}{j!\Gamma(\mu+j)\Gamma(\alpha)\exp(\mu\kappa)\beta}\left(\frac{\Omega}{\bar{\gamma}}\right)\int_{0}^{\infty}\exp(-s\gamma)G_{0,2}^{2,0}\left(\frac{\mu(1+\kappa)\Omega}{\beta\bar{\gamma}}\gamma\middle|\begin{matrix}\\ \alpha-1,\mu+j-1\end{matrix}\right)d\gamma \quad (4.18)$$

By using [135, Eq. (7.813.1)], the MGF becomes

$$M_{\gamma}(s)=\sum_{j=0}^{\infty}\frac{\mu^{j}\kappa^{j}}{j!\exp(\mu\kappa)\Gamma(\alpha)\Gamma(\mu+j)}\left(\frac{\mu(1+\kappa)\Omega}{s\beta\bar{\gamma}}\right)G_{1,2}^{2,1}\left(\frac{\mu(1+\kappa)\Omega}{s\beta\bar{\gamma}}\middle|\begin{matrix}0\\ \alpha-1,\mu+j-1\end{matrix}\right) \quad (4.19)$$

4.3.3 CDF

The CDF of γ is given by [9]

$$F_{\gamma}(\gamma)=\int_{0}^{\gamma}f_{\gamma}(\gamma)d\gamma \quad (4.20)$$

On substituting (4.15) into (4.20), (4.20) is expressed as

$$F_{\gamma}(\gamma)=\sum_{j=0}^{\infty}\frac{\mu^{j}\kappa^{j}}{j!\exp(\mu\kappa)\Gamma(\mu+j)\Gamma(\alpha)}\left(\frac{\mu(1+\kappa)\Omega}{\beta\bar{\gamma}}\right)\int_{0}^{\gamma}G_{0,2}^{2,0}\left(\frac{\mu(1+\kappa)\Omega\gamma}{\beta\bar{\gamma}}\middle|\begin{matrix}\\ \alpha-1,\quad \mu+j-1\end{matrix}\right)d\gamma \quad (4.21)$$

Using [135, Eq. (7.811.2)], after algebraic calculation, (4.21) becomes

$$F_{\gamma}(\gamma)=\sum_{j=0}^{\infty}\frac{\mu^{j}\kappa^{j}}{j!\exp(\mu\kappa)\Gamma(\alpha)\Gamma(\mu+j)}\left(\frac{\mu(1+\kappa)\Omega\gamma}{\beta\bar{\gamma}}\right)G_{1,3}^{2,1}\left(\frac{\mu(1+\kappa)\Omega\gamma}{\beta\bar{\gamma}}\middle|\begin{matrix}0\\ \alpha-1 \quad \mu+j-1 \quad -1\end{matrix}\right) \quad (4.22)$$

4.3.4 Moments

The Moments associated with instantaneous SNR has been defined in the previous Chapter in (3.29). By substituting (4.15) into (3.29), the Moment becomes

$$E[\gamma^{n}]=\sum_{j=0}^{\infty}\frac{\mu^{j}\kappa^{j}}{j!\exp(\mu\kappa)\Gamma(\alpha)\Gamma(\mu+j)}\left(\frac{\mu(1+\kappa)\Omega}{\beta\bar{\gamma}}\right)\int_{0}^{\infty}\gamma^{n}G_{0,2}^{2,0}\left(\frac{\mu(1+\kappa)\Omega\gamma}{\beta\bar{\gamma}}\middle|\begin{matrix}\\ \alpha-1,\quad \mu+j-1\end{matrix}\right)d\gamma \quad (4.23)$$

With the help of [135, Eq. (7.811.4)], the above equation can be expressed as

$$E[\gamma^{n}]=\sum_{j=0}^{\infty}\frac{\mu^{j}\kappa^{j}\Gamma(\alpha+n)\Gamma(\mu+j+n)}{j!\exp(\mu\kappa)\Gamma(\alpha)\Gamma(\mu+j)}\left(\frac{\mu(1+\kappa)\Omega}{\beta\bar{\gamma}}\right)^{-(n+1)} \quad (4.24)$$

4.3.5 Average Bit Error Rate

The expressions of conditional BER for different modulation schemes over the AWGN channels are mentioned in Table 3.1. Moreover, Table 3.2 presents the formulas for obtaining the ABER using MGF based approach. The ABER expressions for different modulation schemes for κ-μ/gamma model are derived as follows

(A) BDPSK and NCFSK

With the help of Table 3.2, the error probability for BDPSK and NCFSK is expressed as

$$P_e(E) = 0.5 \cdot M_\gamma(a) \tag{4.25}$$

Now, by substituting (4.19) into (4.25), the ABER can be obtained as

$$P_e(E) = 0.5\sum_{j=0}^{\infty} \frac{\mu^j \kappa^j}{j!\exp(\mu\kappa)\Gamma(\alpha)\Gamma(\mu+j)} \left(\frac{\mu(1+\kappa)\Omega}{a\beta\bar{\gamma}}\right) G_{1,2}^{2,1}\left(\frac{\mu(1+\kappa)\Omega}{a\beta\bar{\gamma}}\middle| \begin{matrix} 0 \\ \alpha-1, \mu+j-1 \end{matrix}\right) \tag{4.26}$$

(B) BPSK and BFSK

By using Table 3.2, the expression of error probability for BPSK and BFSK modulation can be given as

$$P_e(E) = \frac{1}{\pi}\int_0^{\pi/2} M_\gamma\left(\frac{a}{\sin^2(\theta)}\right) d\theta \tag{4.27}$$

By putting (4.19) into (4.27), (4.27) becomes

$$P_e(E) = \frac{1}{\pi}\sum_{j=0}^{\infty} \frac{\mu^j \kappa^j}{j!\exp(\mu\kappa)\Gamma(\alpha)\Gamma(\mu+j)} \int_0^{\pi/2} \left(\frac{\mu(1+\kappa)\Omega\sin^2(\theta)}{a\beta\bar{\gamma}}\right) G_{1,2}^{2,1}\left(\frac{\mu(1+\kappa)\Omega\sin^2(\theta)}{a\beta\bar{\gamma}}\middle| \begin{matrix} 0 \\ \alpha-1, \mu+j-1 \end{matrix}\right) d\theta \tag{4.28}$$

Putting $sin^2(\theta)=x$ in (4.28) and after performing integration by substitution, (4.28) can be written as

$$P_e(E) = \frac{1}{2\pi}\sum_{j=0}^{\infty} \frac{\mu^j \kappa^j}{j!\exp(\mu\kappa)\Gamma(\alpha)\Gamma(\mu+j)} \left(\frac{\mu(1+\kappa)\Omega}{a\beta\bar{\gamma}}\right) \int_0^1 x^{1/2}\cdot(1-x)^{-1/2} G_{1,2}^{2,1}\left(\frac{\mu(1+\kappa)\Omega}{a\beta\bar{\gamma}} x\middle| \begin{matrix} 0 \\ \alpha-1, \mu+j-1 \end{matrix}\right) dx \tag{4.29}$$

With the help of [135, Eq. (7.811.2)], the ABER (BPSK/BFSK) can be obtained as

$$P_e(E)=\frac{1}{2\pi}\sum_{j=0}^{\infty}\frac{\mu^j\kappa^j\Gamma(0.5)}{j!\exp(\mu\kappa)\Gamma(\alpha)\Gamma(\mu+j)}\left(\frac{\mu(1+\kappa)\Omega}{a\beta\bar{\gamma}}\right)G_{2,3}^{2,2}\left(\frac{\mu(1+\kappa)\Omega}{a\beta\bar{\gamma}}\middle|\begin{matrix}-0.5 & 0\\ \alpha-1 & \mu+j-1 & -1\end{matrix}\right) \tag{4.30}$$

(C) MAM

With the help of Table 3.2, the ABER for MAM scheme is given as

$$P_e(E)=\frac{2(M-1)}{M\pi\log_2(M)}\int_0^{\pi/2}M_\gamma\left(\frac{g_{AM}}{\sin^2(\theta)}\right)d\theta \tag{4.31}$$

By substituting (4.19) into (4.31), (4.31) can be written as

$$P_e(E)=\frac{2(M-1)}{M\pi\log_2(M)}\sum_{j=0}^{\infty}\frac{\mu^j\kappa^j}{j!\exp(\mu\kappa)\Gamma(\alpha)\Gamma(\mu+j)}\int_0^{\pi/2}\left(\frac{\mu(1+\kappa)\Omega\sin^2(\theta)}{g_{AM}\beta\bar{\gamma}}\right)G_{1,2}^{2,1}\left(\frac{\mu(1+\kappa)\Omega\sin^2(\theta)}{g_{AM}\beta\bar{\gamma}}\middle|\begin{matrix}0\\ \alpha-1,\mu+j-1\end{matrix}\right)d\theta \tag{4.32}$$

By putting $sin^2(\theta)=x$, after performing integration by substitution, (4.32) can be obtained as

$$P_e(E)=\frac{2(M-1)}{M\pi\log_2(M)}\sum_{j=0}^{\infty}\frac{\mu^j\kappa^j}{j!\exp(\mu\kappa)\Gamma(\alpha)\Gamma(\mu+j)}\left(\frac{\mu(1+\kappa)\Omega}{2g_{AM}\beta\bar{\gamma}}\right)\int_0^1 x^{1/2}\cdot(1-x)^{-1/2}G_{1,2}^{2,1}\left(\frac{\mu(1+\kappa)\Omega}{g_{AM}\beta\bar{\gamma}}x\middle|\begin{matrix}0\\ \alpha-1,\mu+j-1\end{matrix}\right)d\theta \tag{4.33}$$

By using [135, Eq. (7.811.2)], (4.33) can be written as

$$P_e(E)=\frac{(M-1)}{M\pi\log_2(M)}\sum_{j=0}^{\infty}\frac{\mu^j\kappa^j\Gamma(0.5)}{j!\exp(\mu\kappa)\Gamma(\alpha)\Gamma(\mu+j)}\left(\frac{\mu(1+\kappa)\Omega}{g_{AM}\beta\bar{\gamma}}\right)G_{2,3}^{2,2}\left(\frac{\mu(1+\kappa)\Omega}{g_{AM}\beta\bar{\gamma}}x\middle|\begin{matrix}-0.5, & 0\\ \alpha-1, & \mu+j-1, & -1\end{matrix}\right) \tag{4.34}$$

(D) MQAM

The tight bound CEP is expressed by [75]

$$P_e(E\mid\gamma)\le\int_0^{\infty}0.2\cdot\exp\left(-\frac{1.5}{M-1}\gamma\right),\quad \gamma\ge 0,\quad M\ge 4 \tag{4.35}$$

By plugging (4.35) into (3.33), the expression of ABER can be obtained as

$$P_e(E)=\int_0^{\infty}0.2\cdot\exp\left(-\frac{1.5}{M-1}\gamma\right)f_\gamma(\gamma)d\gamma \tag{4.36}$$

Using (3.31), (4.36) can be written as

$$P_e(E) = 0.2 \cdot M_\gamma(s)\Big|_{s=\frac{1.5}{M-1}} \tag{4.37}$$

On putting (4.19) into (4.37), the corresponding error probability is expressed as

$$P_e(E) = 0.2\sum_{j=0}^{\infty} \frac{\mu^j \kappa^j}{j!\exp(\mu\kappa)\Gamma(\alpha)\Gamma(\mu+j)} \left(\frac{(M-1)\mu(1+\kappa)\Omega}{1.5\beta\bar{\gamma}}\right) G_{1,2}^{2,1}\left(\frac{(M-1)\mu(1+\kappa)\Omega}{1.5\beta\bar{\gamma}}\middle| \begin{matrix} 0 \\ \alpha-1 \quad \mu+j-1 \end{matrix}\right) \tag{4.38}$$

(E) MPSK

The ASER for MPSK in the term of MGF, using Table 3.2, is given as

$$P_e(E) = \frac{1}{\pi}\int_0^{\Theta} M_\gamma\left(\frac{g_{MPSK}}{\sin^2(\theta)}\right) d\theta \tag{4.39}$$

By the definition of MGF, as given in (3.31), the above equation can be written as

$$P_e(E) = \frac{1}{\pi}\int_0^{\infty}\int_0^{\Theta} \exp\left(-\frac{g_{MPSK}}{\sin^2(\theta)}\gamma\right) f_\gamma(\gamma) d\gamma d\theta \tag{4.40}$$

By using integration property, the above expression becomes

$$P_e(E) = \int_0^{\infty}\left[\frac{1}{\pi}\int_0^{\pi/2} \exp\left(-\frac{g_{MPSK}}{\sin^2(\theta)}\gamma\right) d\theta + \frac{1}{\pi}\int_{\pi/2}^{\Theta} \exp\left(-\frac{g_{MPSK}}{\sin^2(\theta)}\gamma\right) d\theta\right] f_\gamma(\gamma) d\gamma \tag{4.41}$$

By using [145, Eq. (7)] and [145, Eq. (8)], the above integration can be approximated as

$$\left.\begin{aligned} &\frac{1}{\pi}\int_0^{\pi/2} \exp\left(-\frac{g_{MPSK}}{\sin^2(\theta)}\gamma\right) d\theta \approx \frac{1}{12}\exp\left(-g_{MPSK}\gamma\right) + \frac{1}{4}\exp\left(\frac{-4g_{MPSK}}{3}\gamma\right) \\ &\frac{1}{\pi}\int_{\pi/2}^{\pi-\pi/M} \exp\left(-\frac{g_{MPSK}}{\sin^2(\theta)}\gamma\right) d\theta \approx \frac{1}{2\pi}\left(\exp(-g_{MPSK}\gamma) + \exp\left(\frac{-g_{MPSK}\gamma}{\sin^2(\Theta)}\right)\right)\left(\Theta - \frac{\pi}{2}\right) \end{aligned}\right\} \tag{4.42}$$

By substituting (4.42) into (4.41), (4.41) can be simplified as

$$\begin{aligned} P_e(E) = &\left(\frac{\Theta}{2\pi} - \frac{1}{6}\right)\int_0^{\infty} \exp\left(-g_{MPSK}\gamma\right) f_\gamma(\gamma) d\gamma + \frac{1}{4}\int_0^{\infty} \exp\left(-\frac{4}{3}g_{MPSK}\gamma\right) f_\gamma(\gamma) d\gamma \\ &+ \left(\frac{\Theta}{2\pi} - \frac{1}{4}\right)\int_0^{\infty} \exp\left(-\frac{g_{MPSK}}{\sin^2(\theta)}\gamma\right) f_\gamma(\gamma) d\gamma \end{aligned} \tag{4.43}$$

Now, by the definition of MGF, as given in (3.31), (4.43) becomes

$$P_e(E)=\left(\frac{\Theta}{2\pi}-\frac{1}{6}\right)M_\gamma(g_{MPSK})+\frac{1}{4}M_\gamma\left(\frac{4}{3}g_{MPSK}\right)+\left(\frac{\Theta}{2\pi}-\frac{1}{4}\right)M_\gamma\left(\frac{g_{MPSK}}{\sin^2\Theta}\right) \tag{4.44}$$

By plugging (4.19) into (4.44), the ABER for MPSK can be obtained as

$$P_e(E)=\sum_{j=0}^{\infty}\frac{\mu^j\kappa^j}{j!\exp(\mu\kappa)\Gamma(\alpha)\Gamma(\mu+j)}\left(\frac{\mu(1+\kappa)\Omega}{\beta\bar{\gamma}}\right)\left[\left(\frac{\Theta}{2\pi}-\frac{1}{6}\right)\frac{1}{g_{MPSK}}G_{1,2}^{2,1}\left(\frac{\mu(1+\kappa)\Omega}{g_{MPSK}\beta\bar{\gamma}}\middle|\begin{matrix}0\\ \alpha-1,\mu+j-1\end{matrix}\right)\right.$$

$$\left.+\frac{3}{16g_{MPSK}}G_{1,2}^{2,1}\left(\frac{3\mu(1+\kappa)\Omega}{4g_{MPSK}\beta\bar{\gamma}}\middle|\begin{matrix}0\\ \alpha-1,\mu+j-1\end{matrix}\right)+\left(\frac{\Theta}{2\pi}-\frac{1}{4}\right)\frac{\sin^2\Theta}{g_{MPSK}}G_{1,2}^{2,1}\left(\frac{\mu(1+\kappa)\Omega\sin^2\Theta}{g_{MPSK}\beta\bar{\gamma}}\middle|\begin{matrix}0\\ \alpha-1,\mu+j-1\end{matrix}\right)\right] \tag{4.45}$$

(F) NCMFSK

With the help of Table 3.1, the expression of conditional SER for NCMFSK modulation scheme over the AWGN channels is given as

$$P_e(E/\gamma)=\frac{1}{M}\sum_{i=2}^{M}(-1)^i\binom{M}{i}\exp\left(-\left(1-\frac{1}{i}\right)\gamma\right) \tag{4.46}$$

By plugging (4.46) in (3.33), the expression of ASER for NCMFSK can be obtained as

$$P_e(E)=\frac{1}{M}\sum_{i=2}^{M}(-1)^i\binom{M}{i}\int_0^{\infty}\exp\left(-\left(1-\frac{1}{i}\right)\gamma\right)f_\gamma(\gamma)d\gamma \tag{4.47}$$

With the help of (3.31), (4.47) becomes

$$P_e(E)=\frac{1}{M}\sum_{i=2}^{M}(-1)^i\binom{M}{i}M_\gamma\left(\left(1-\frac{1}{i}\right)\right) \tag{4.48}$$

By substituting (4.19) into (4.48), the corresponding ASER is given as

$$P_e(E)=\frac{1}{M}\sum_{i=2}^{M}(-1)^i\binom{M}{i}\sum_{j=0}^{\infty}\frac{\mu^j\kappa^j}{j!\exp(\mu\kappa)\Gamma(\alpha)\Gamma(\mu+j)}\left(\frac{\mu(1+\kappa)\Omega}{\left(1-\frac{1}{i}\right)\beta\bar{\gamma}}\right)G_{1,2}^{2,1}\left(\frac{\mu(1+\kappa)\Omega}{\left(1-\frac{1}{i}\right)\beta\bar{\gamma}}\middle|\begin{matrix}0\\ \alpha-1,\mu+j-1\end{matrix}\right) \tag{4.49}$$

4.3.6 Channel Capacity

The Channel Capacity is an essential performance parameter since it represents how much data is transmitted through the channel under fading conditions. The Channel Capacity for different power and rate adaptive methods has been discussed in the previous Chapter. The capacities under various adaptive transmission protocols for κ-μ/gamma model are derived as follows

(A) ORA

By putting (4.14) into (3.37), the Channel Capacity for ORA policy in bit/s/Hz is expressed as

$$C_{ORA} = \sum_{j=0}^{\infty} \frac{2\mu^j \kappa^j}{j!\Gamma(\mu+j)\Gamma(\alpha)\exp(\mu\kappa)} \left(\frac{\mu(1+\kappa)\Omega}{\beta\bar{\gamma}}\right)^{\frac{\alpha+\mu+j}{2}} \int_0^{\infty} \log_2(1+\gamma)\gamma^{\frac{\alpha+\mu+j-2}{2}} K_{\alpha-\mu-j}\left(2\sqrt{\frac{\mu(1+\kappa)\Omega\gamma}{\beta\bar{\gamma}}}\right) d\gamma \quad (4.50)$$

The relation between logarithmic and Meijer G function is given as [146, Eq. (8.4.6.5)]

$$\ln(1+\gamma) = G_{2,2}^{1,2}\left(\gamma \middle| \begin{matrix} 1,1 \\ 1,0 \end{matrix}\right) \quad (4.51)$$

By substituting (4.51) into (4.50) and using logarithmic property, (4.50) can be written as

$$C_{ORA} = \frac{1}{\ln(2)} \sum_{j=0}^{\infty} \frac{2\mu^j \kappa^j}{j!\Gamma(\alpha)\Gamma(\mu+j)\exp(\mu\kappa)} \left(\frac{\mu(1+\kappa)\Omega}{\beta\bar{\gamma}}\right)^{\frac{\alpha+\mu+j}{2}} \int_0^{\infty} \gamma^{\frac{\alpha+\mu+j-2}{2}} G_{2,2}^{1,2}\left(\gamma \middle| \begin{matrix} 1,1 \\ 1,0 \end{matrix}\right) K_{\alpha-\mu-j}\left(2\sqrt{\frac{\mu(1+\kappa)\Omega\gamma}{\beta\bar{\gamma}}}\right) d\gamma \quad (4.52)$$

With the help of [135, Eq. (7.821.3)] and after performing some mathematical steps, the Channel Capacity for ORA scheme can be obtained as

$$C_{ORA} = \sum_{j=0}^{\infty} \frac{\mu^j \kappa^j}{j!\Gamma(\mu+j)\exp(\mu\kappa)\Gamma(\alpha)\ln(2)} G_{4,2}^{1,4}\left(\frac{\beta\bar{\gamma}}{\mu(1+\kappa)\Omega} \middle| \begin{matrix} -\alpha+1 & -\mu-j+1 & 1 & 1 \\ 1 & 0 & & \end{matrix}\right) \quad (4.53)$$

An alternative method to obtain the Channel Capacity for ORA policy is MGF based approach, as defined in the previous Chapter in (3.38). Therefore, to get the Channel Capacity for ORA policy using the MGF method, first of all, the first-order derivative of MGF $M_\gamma(s)$ has to derive which is given as

$$M'_\gamma(s) = \frac{d}{ds} M_\gamma(s) = \sum_{j=0}^{\infty} \frac{\mu^j \kappa^j}{j!\exp(\mu\kappa)\Gamma(\alpha)\Gamma(\mu+j)} \left(\frac{\mu(1+\kappa)\Omega}{\beta\bar{\gamma}}\right) \frac{d}{ds} s^{-1} G_{1,2}^{2,1}\left(\frac{\mu(1+\kappa)\Omega}{s\beta\bar{\gamma}} \middle| \begin{matrix} 0 \\ \alpha-1, \mu+j-1 \end{matrix}\right) \quad (4.54)$$

With the help of [146, Eq. (8.2.2.30)], the above equation becomes

$$M'_{\gamma}(s)=\sum_{j=0}^{\infty}\frac{-\mu^{j}\kappa^{j}}{j!\exp(\mu\kappa)\Gamma(\alpha)\Gamma(\mu+j)}\left(\frac{\mu(1+\kappa)\Omega}{s^{2}\beta\bar{\gamma}}\right)G_{1,2}^{2,1}\left(\frac{\mu(1+\kappa)\Omega}{s\beta\bar{\gamma}}\middle|\begin{matrix}-1\\ \alpha-1,\mu+j-1\end{matrix}\right) \tag{4.55}$$

By plugging (4.55) into (3.38), the Channel Capacity for ORA is obtained as

$$C_{ORA}=\frac{1}{\ln(2)}\sum_{j=0}^{\infty}\frac{-\mu^{j}\kappa^{j}}{j!\exp(\mu\kappa)\Gamma(\alpha)\Gamma(\mu+j)}\left(\frac{\mu(1+\kappa)\Omega}{\beta\bar{\gamma}}\right)\int_{0}^{\infty}E_{i}(-s)\left(\frac{1}{s^{2}}\right)G_{1,2}^{2,1}\left(\frac{\mu(1+\kappa)\Omega}{s\beta\bar{\gamma}}\middle|\begin{matrix}-1\\ \alpha-1,\mu+j-1\end{matrix}\right)ds \tag{4.56}$$

The exponential integration and Meijer G function is related by the following formula [146, Eq. (8.4.11.1)]

$$E_{i}(-s)=-G_{1,2}^{2,0}\left(s\middle|\begin{matrix}1\\ 0,\quad 0\end{matrix}\right) \tag{4.57}$$

By substituting (4.57) into (4.56), (4.56) becomes

$$C_{ORA}=\frac{1}{\ln(2)}\sum_{j=0}^{\infty}\frac{\mu^{j}\kappa^{j}}{j!\exp(\mu\kappa)\Gamma(\alpha)\Gamma(\mu+j)}\left(\frac{\mu(1+\kappa)\Omega}{\beta\bar{\gamma}}\right)\int_{0}^{\infty}\left(\frac{1}{s^{2}}\right)G_{1,2}^{2,0}\left(s\middle|\begin{matrix}1\\ 0,\quad 0\end{matrix}\right)G_{1,2}^{2,1}\left(\frac{\mu(1+\kappa)\Omega}{s\beta\bar{\gamma}}\middle|\begin{matrix}-1\\ \alpha-1,\mu+j-1\end{matrix}\right)ds \tag{4.58}$$

Using $G_{p,q}^{m,n}[\cdot\,|\,\cdot]$ function property and [146, Eq. (2.24.1.1)], C_{ORA} can be obtained as

$$C_{ORA}=\frac{1}{\ln(2)}\sum_{j=0}^{\infty}\frac{\mu^{j}\kappa^{j}}{j!\Gamma(\alpha)\Gamma(\mu+j)\exp(\mu\kappa)}\left(\frac{\mu(1+\kappa)\Omega}{\beta\bar{\gamma}}\right)G_{4,2}^{1,4}\left(\frac{\beta\bar{\gamma}}{\mu(1+\kappa)\Omega}\middle|\begin{matrix}2-\alpha,\quad 2-\mu-j,\quad 2,\quad 2\\ 2,\qquad 1\end{matrix}\right) \tag{4.59}$$

(B) OPRA

In this policy, both transmitter and receiver know CSI. The optimal power cutoff SNR level γ_0 for adaptive transmission policy must satisfy the following condition [62]

$$\int_{\gamma_0}^{\infty}\left(\frac{1}{\gamma_0}-\frac{1}{\gamma}\right)f_{\gamma}(\gamma)d\gamma=1 \tag{4.60}$$

or,

$$\frac{\overline{F}_{\gamma}(\gamma_0)}{\gamma_0}-\int_{\gamma_0}^{\infty}\frac{f_{\gamma}(\gamma)}{\gamma}d\gamma=1 \tag{4.61}$$

where $\overline{F}_{\gamma}(\cdot)$ denotes the complementary CDF of SNR.

With the help of (4.15), the integral term in (4.61) is expressed as

$$\int_{\gamma_0}^{\infty}\frac{f_{\gamma}(\gamma)}{\gamma}d\gamma=\sum_{j=0}^{\infty}\frac{\mu^{j}\kappa^{j}}{j!\exp(\mu\kappa)\Gamma(\alpha)\Gamma(\mu+j)}\left(\frac{\mu(1+\kappa)\Omega}{\beta\overline{\gamma}}\right)\int_{\gamma_0}^{\infty}\gamma^{-1}G_{0,2}^{2,0}\left(\frac{\mu(1+\kappa)\Omega\gamma}{\beta\overline{\gamma}}\middle|\begin{matrix}\alpha-1, & \mu+j-1\end{matrix}\right)d\gamma \quad (4.62)$$

Let $\gamma/\gamma_0=t$, so $d\gamma=\gamma_0 dt$. After performing integration by substitution, (4.62) can be obtained as

$$\int_{\gamma_0}^{\infty}\frac{f_{\gamma}(\gamma)}{\gamma}d\gamma=\sum_{j=0}^{\infty}\frac{\mu^{j}\kappa^{j}}{j!\exp(\mu\kappa)\Gamma(\alpha)\Gamma(\mu+j)}\left(\frac{\mu(1+\kappa)\Omega}{\beta\overline{\gamma}}\right)\int_{1}^{\infty}t^{-1}G_{0,2}^{2,0}\left(\frac{\mu(1+\kappa)\Omega\gamma_0 t}{\beta\overline{\gamma}}\middle|\begin{matrix}\alpha-1, & \mu+j-1\end{matrix}\right)dt \quad (4.63)$$

With the help of [135, Eq. (7.811.3)], (4.63) can be simplified as

$$\int_{\gamma_0}^{\infty}\frac{f_{\gamma}(\gamma)}{\gamma}d\gamma=\sum_{j=0}^{\infty}\frac{\mu^{j}\kappa^{j}}{j!\exp(\mu\kappa)\Gamma(\alpha)\Gamma(\mu+j)}\left(\frac{\mu(1+\kappa)\Omega}{\beta\overline{\gamma}}\right)G_{1,3}^{3,0}\left(\frac{\mu(1+\kappa)\Omega\gamma_0}{\beta\overline{\gamma}}\middle|\begin{matrix}1\\0, & \alpha-1, & \mu+j-1\end{matrix}\right) \quad (4.64)$$

By substituting (4.64) into (4.61), the condition for optimal data transmission is obtained as

$$\frac{\overline{F}_{\gamma}(\gamma_0)}{\gamma_0}-\sum_{j=0}^{\infty}\frac{\mu^{j}\kappa^{j}}{j!\exp(\mu\kappa)\Gamma(\alpha)\Gamma(\mu+j)}\left(\frac{\mu(1+\kappa)\Omega}{\beta\overline{\gamma}}\right)G_{1,3}^{3,0}\left(\frac{\mu(1+\kappa)\Omega\gamma_0}{\beta\overline{\gamma}}\middle|\begin{matrix}1\\0, & \alpha-1, & \mu+j-1\end{matrix}\right)=1 \quad (4.65)$$

It is noted that no transmission of data takes place when the received SNR level γ falls below the optimal power cutoff SNR level γ_0.

Now, the expression of Channel Capacity under OPRA policy can be obtained by plugging (4.14) into (3.41)

$$C_{OPRA}=\sum_{j=0}^{\infty}\frac{\mu^{j}\kappa^{j}}{j!\exp(\mu\kappa)\Gamma(\alpha)\Gamma(\mu+j)}\left(\frac{\mu(1+\kappa)\Omega}{\beta\overline{\gamma}}\right)\int_{\gamma_0}^{\infty}\log_2\left(\frac{\gamma}{\gamma_0}\right)G_{0,2}^{2,0}\left(\frac{\mu(1+\kappa)\Omega\gamma}{\beta\overline{\gamma}}\middle|\begin{matrix}\alpha-1, & \mu+j-1\end{matrix}\right)d\gamma \quad (4.66)$$

Let $\gamma/\gamma_0=x$ or $d\gamma=\gamma_0 dx$ and after performing integration by substitution, (4.66) becomes

$$C_{OPRA}=\frac{1}{\ln(2)}\sum_{j=0}^{\infty}\frac{\mu^{j}\kappa^{j}}{j!\Gamma(\mu+j)\Gamma(\alpha)\exp(\mu\kappa)}\left(\frac{\mu(1+\kappa)\Omega\gamma_0}{\beta\overline{\gamma}}\right)\int_{1}^{\infty}\ln(x)\cdot G_{0,2}^{2,0}\left(\frac{\mu(1+\kappa)\Omega\gamma_0 x}{\beta\overline{\gamma}}\middle|\begin{matrix}\alpha-1, & \mu+j-1\end{matrix}\right)dx \quad (4.67)$$

The relation between logarithmic and hypergeometric function is given as [135, Eq. (9.121.6)]

$$\ln(1+x)=x_2F_1(1,1;2;-x) \quad (4.68)$$

By plugging (4.68) into (4.67), (4.67) becomes

$$C_{OPRA} = \frac{1}{\ln(2)} \sum_{j=0}^{\infty} \frac{\mu^j \kappa^j}{j! \exp(\mu\kappa)\Gamma(\mu+j)\Gamma(\alpha)} \left(\frac{\mu(1+\kappa)\Omega\gamma_0}{\beta\bar{\gamma}} \right)$$
$$\times \int_1^{\infty} (x-1)\cdot {}_2F_1(1,1;2;1-x) G_{0,2}^{2,0}\left(\frac{\mu(1+\kappa)\Omega\gamma_0 x}{\beta\bar{\gamma}} \middle| \begin{matrix} \alpha-1, & \mu+j-1 \end{matrix} \right) dx \tag{4.69}$$

With the help of [135, Eq. (7.831)], the Channel Capacity for OPRA scheme is obtained as

$$C_{OPRA} = \frac{1}{\ln(2)} \sum_{j=0}^{\infty} \frac{\mu^j \kappa^j}{j! \exp(\mu\kappa)\Gamma(\alpha)\Gamma(\mu+j)} \left(\frac{\mu(1+\kappa)\Omega\gamma_0}{\beta\bar{\gamma}} \right) G_{2,4}^{4,0}\left(\frac{\mu(1+\kappa)\Omega\gamma_0}{\beta\bar{\gamma}} \middle| \begin{matrix} 0, & 0 \\ -1, & -1, \quad \alpha-1, \quad \mu+j-1 \end{matrix} \right) \tag{4.70}$$

(C) CIFR

The Channel Capacity under CIFR scheme using MGF based approach can be obtained by solving the integration presented in (3.46), and it is given as

$$\int_0^{\infty} M_{\gamma}(s) ds = \sum_{j=0}^{\infty} \frac{\mu^j \kappa^j}{j! \exp(\mu\kappa)\Gamma(\alpha)\Gamma(\mu+j)} \int_0^{\infty} s^{-1} G_{1,2}^{2,1}\left(\frac{\mu(1+\kappa)\Omega}{s\beta\bar{\gamma}} \middle| \begin{matrix} 0 \\ \alpha-1, \mu+j-1 \end{matrix} \right) ds \tag{4.71}$$

By putting $1/s = t$ into (4.71) and follow some mathematical steps, (4.71) becomes

$$\int_0^{\infty} M_{\gamma}(s) ds = \sum_{j=0}^{\infty} \frac{\mu^j \kappa^j}{j! \exp(\mu\kappa)\Gamma(\alpha)\Gamma(\mu+j)} \int_0^{\infty} t^{-1} G_{1,2}^{2,1}\left(\frac{t\mu(1+\kappa)\Omega}{\beta\bar{\gamma}} \middle| \begin{matrix} 0 \\ \alpha-1, \mu+j-1 \end{matrix} \right) dt \tag{4.72}$$

With the help of [135, Eq. (7.811.4)], the above equation can be obtained as

$$\int_0^{\infty} M_{\gamma}(s) ds = \sum_{j=0}^{\infty} \frac{\mu^j \kappa^j}{j! \exp(\mu\kappa)\cdot(\alpha-1)\cdot(\mu+j-1)} \left(\frac{\mu(1+\kappa)\Omega}{\beta\bar{\gamma}} \right) \tag{4.73}$$

By substituting (4.73) into (3.46), C_{CIFR} can be written as

$$C_{CIFR} = \log_2 \left(1 + 1 \Big/ \sum_{j=0}^{\infty} \frac{\mu^j \kappa^j}{j!(\mu+j)\alpha \exp(\mu\kappa)} \left(\frac{\mu(1+\kappa)\Omega}{\beta\bar{\gamma}} \right) \right) \tag{4.74}$$

(D) TIFR

The Channel Capacity for TIFR policy has been defined in the previous Chapter in (3.47). By plugging (4.64) into (3.47), the C_{TIFR} is expressed as

$$C_{TIFR} = \log_2\left(1+\left(\sum_{j=0}^{\infty}\frac{\mu^j\kappa^j}{j!\exp(\mu\kappa)\Gamma(\alpha)\Gamma(\mu+j)}\left(\frac{\mu(1+\kappa)\Omega}{\beta\bar{\gamma}}\right)G_{1,3}^{3,0}\left(\frac{\Omega\gamma_0\mu(1+\kappa)}{\beta\bar{\gamma}}\middle|\begin{matrix}1\\0,\quad \alpha-1,\quad \mu+j-1\end{matrix}\right)\right)^{-1}\right)\left(1-F_\gamma(\gamma_0)\right) \quad (4.75)$$

where

$$F_\gamma(\gamma_0) = \sum_{j=0}^{\infty}\frac{\mu^j\kappa^j}{j!\exp(\mu\kappa)\Gamma(\mu+j)\Gamma(\alpha)}\left(\frac{\mu(1+\kappa)\Omega\gamma_0}{\beta\bar{\gamma}}\right)G_{1,3}^{2,1}\left(\frac{(1+\kappa)\Omega\gamma_0\mu}{\beta\bar{\gamma}}\middle|\begin{matrix}0\\\alpha-1,\quad \mu+j-1,\quad -1\end{matrix}\right) \quad (4.76)$$

4.3.7 Outage Probability

Using [19, Eq. (8)] and (3.35), the P_{out} is expressed as

$$P_{out} = \sum_{j=0}^{\infty}\frac{\pi\kappa^j\mu^{\alpha+j}(1+\kappa)^\alpha\left(\frac{\gamma_0\Omega}{\bar{\gamma}}\right)^\alpha {}_1F_2\left(\alpha;\alpha-\mu-j+1,1+\alpha;\frac{\mu(1+\kappa)\gamma_0\Omega}{\beta\bar{\gamma}}\right)}{j!\sin((\mu-\alpha+j)\pi)\exp(\mu\kappa)\beta^\alpha\Gamma(1+\alpha)\Gamma(\mu+j)\Gamma(1+\alpha-\mu-j)}$$

$$-\sum_{j=0}^{\infty}\frac{\pi\kappa^j\mu^{\mu+2j}(1+\kappa)^{\mu+j}\left(\frac{\gamma_0\Omega}{\bar{\gamma}}\right)^{\mu+j} {}_1F_2\left(\mu+j;1+\mu-\alpha+j,1+\mu+j;\frac{\mu(1+\kappa)\gamma_0\Omega}{\beta\bar{\gamma}}\right)}{j!\sin((\mu-\alpha+j)\pi)\exp(\mu\kappa)\beta^{\mu+j}\Gamma(\alpha)\Gamma(1+\mu+j)\Gamma(1-\alpha+\mu+j)} \quad (4.77)$$

An alternate and tractable expression of P_{out} can also be evaluated using (3.35) and (4.22)

$$P_{out} = \sum_{j=0}^{\infty}\frac{\mu^j\kappa^j}{j!\exp(\mu\kappa)\Gamma(\alpha)\Gamma(\mu+j)}\left(\frac{\mu(1+\kappa)\Omega\gamma_0}{\beta\bar{\gamma}}\right)G_{0,2}^{2,0}\left(\frac{\mu(1+\kappa)\Omega\gamma_0}{\beta\bar{\gamma}}\middle|\begin{matrix}0\\\alpha-1\quad \mu+j-1\quad -1\end{matrix}\right) \quad (4.78)$$

4.3.8 Results

The performance of κ-μ/gamma fading distribution is analyzed in this section by considering the matrices such as Error Probability, Capacity, and Outage Probability. The performances depend on the shadowing parameter, Mean SNR, Modulation Index, Fading Parameter, and type of signaling techniques. The newly obtained results converge to special cases of κ-μ/gamma fading model. Figure 4.1 depicts the ABER for BDPSK ((4.26) with a = 1) and NCFSK ((4.26) with a = 0.5) and its comparison with previous results of Nakagami-m/gamma [55] and Rayleigh [52, 147]. As presented in Figure 4.1, the curve overlapping with Nakagami-m/gamma fading has minimum error rates than the curve overlapping with Rayleigh fading. Moreover, BDPSK technique shows better error rate performance in comparison to NCFSK.

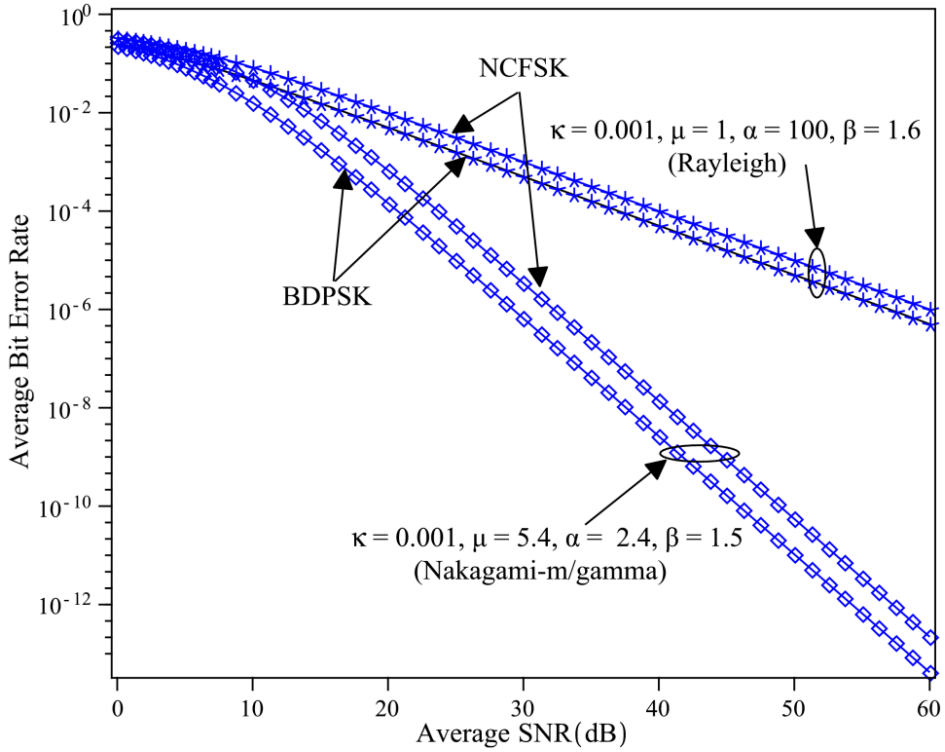

Figure 4.1: ABER comparisons using BDPSK and NCFSK with several fading distributions.

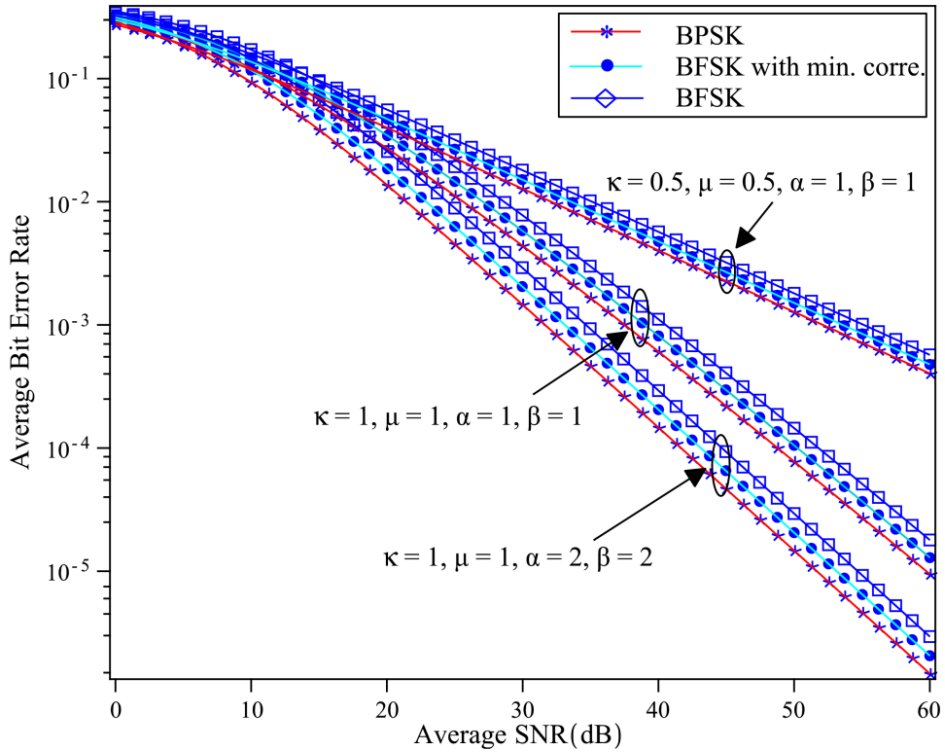

Figure 4.2: ABER using BPSK, BFSK, and BFSK with minimum correlation.

The error rates comparison curve between BPSK ((4.30) with a = 1), BFSK ((4.30) with a = 0.5), and BFSK with min. corr. ((4.30) with a = 0.707) is shown in Figure 4.2. The BPSK technique has lowest error probability than BFSK as can be easily seen in Figure 4.2. The reduction in BER is achieved as μ,κ increases with constant β,α. Moreover, slight reduction in BER is achieved as β,α increases with constant μ,κ. In Figure 4.2, the ABER for any signaling schemes (BPSK or BFSK) decreases by varying the average SNR.

Table 4.1: Required number of terms in (4.30) to achieve an error rate less than 10^{-6}

Parameters (κ,μ,α,β)	Number of Terms in (4.30)
κ=1,μ=1,α=2,β=2	9
κ=1,μ=1,α=0.5,β=0.5	11
κ=2,μ=2,α=2,β=2	17

Table 4.1 shows the number of terms in (4.30) for obtaining the error rate less than 10^{-6}. It is clear that only few terms are required to obtained better accuracy of results. Also, larger values of κ,μ,α,β requires large number of terms as clearly depicted in Table 4.1. In a similar way, the number of terms can also be provided for all proposed mathematical expressions of κ-μ/gamma model.

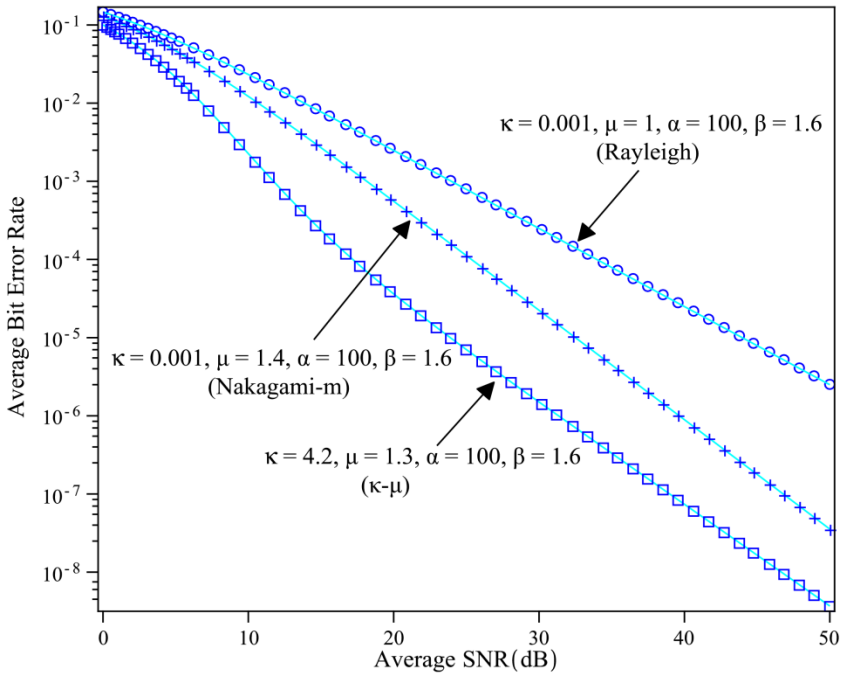

Figure 4.3: ABER comparison using BPSK with several fading distributions.

Figure 4.3 depicts the error rates of BPSK (((4.30) with a = 1). The error rates result is compared with the corresponding result of κ-μ [57, Eq. (12)], Nakagami-m [9, Eq. (4.138)] and Rayleigh [9, Eq. (4.134)] distribution. The proposed results have good match with exiting results. The error rate curve having higher value of multipath cluster (μ=1.4) goes downwards rapidly than lower one as the mean SNR level increases, which means that large number of multipath clusters gives better performance improvement.

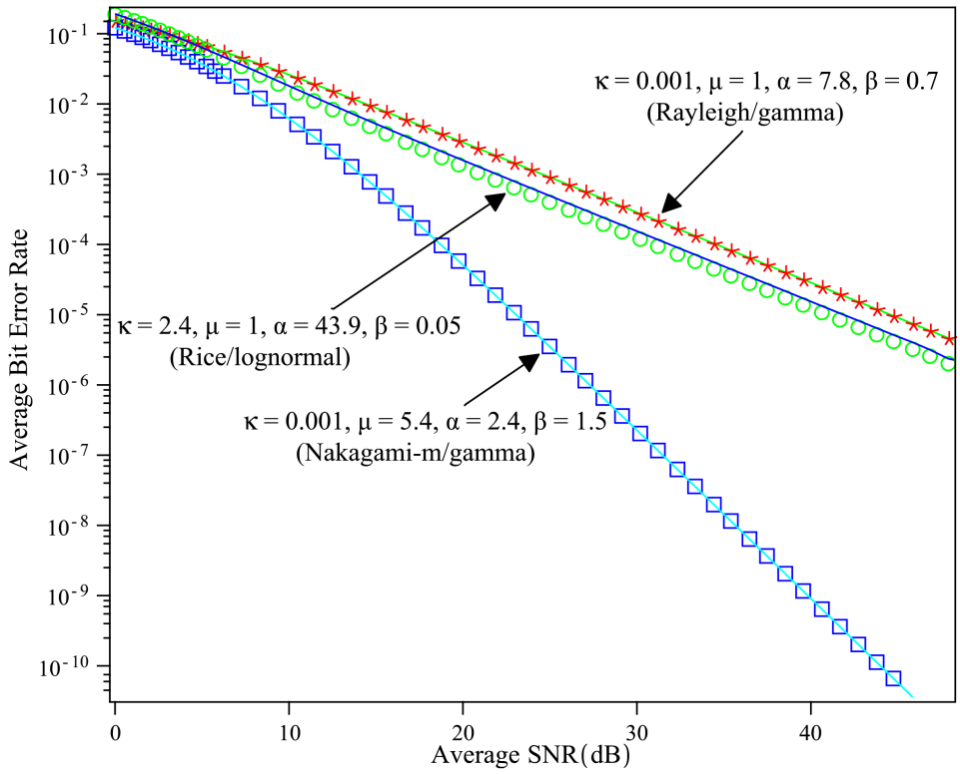

Figure 4.4: ABER comparisons using BPSK with several shadowed fading distributions.

Figure 4.4 represents the ABER using BPSK and its comparison with previous results of Rice/lognormal [148, Eq. (6)], Nakagami-m/gamma [9, Eq. (4.152)] and Rayleigh/gamma [9, Eq. (4.152)]. The curve coinciding with Nakagami-m/gamma model has minimum error probability than the curve overlapping with Rayleigh/gamma and Rice/lognormal distribution. In Figure 4.4, the ABER reduces as average SNR increases for constant κ,μ,α,β.

Figure 4.5 shows the ABER for MAM and its comparison with existing results of Rayleigh [8, Eq. (8.103)] and Nakagami-m [8, Eq. (8.106)] model. The result is obtained by using the derived expression given in (4.34). In Figure 4.5, the error rate reduces as μ increases with constant β, α, and κ. Also, 4-AM has lowest error probability than the other two with higher modulation index.

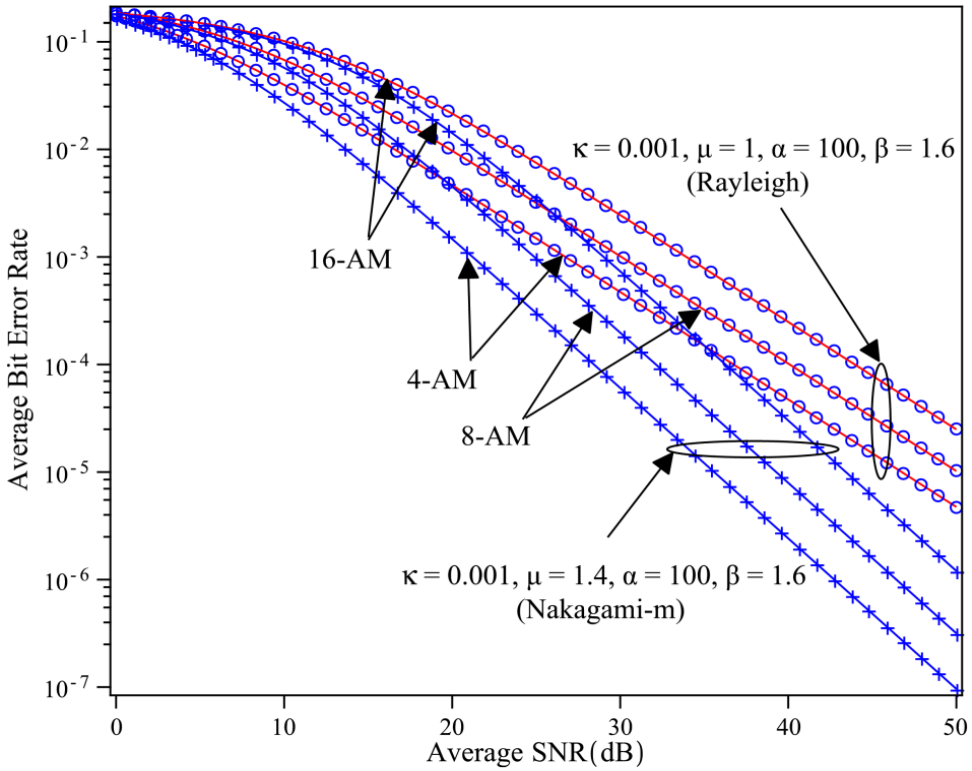

Figure 4.5: ABER comparison using MAM with several fading distributions.

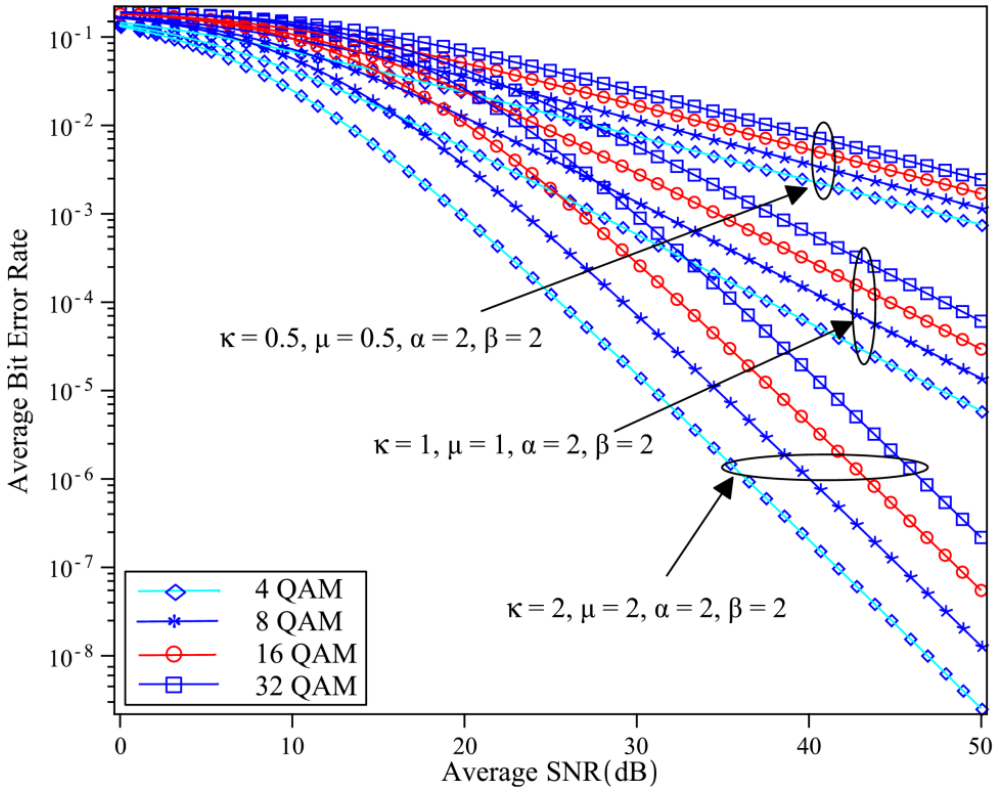

Figure 4.6: Error probability using MQAM signaling for several parameters.

Figure 4.6 depicts the ABER for MQAM (4.38) with μ,κ= 0.5,1,2 and β,α=2. In Figure 4.6, on increasing M (4to32), ABER performance degrades. The error rate using 4-QAM is minimum and it increases as M varies. Also, the error rate reduces as the fading parameters (μ,κ) increases between 0.5 and 1 with constant modulation index and shadowing parameter.

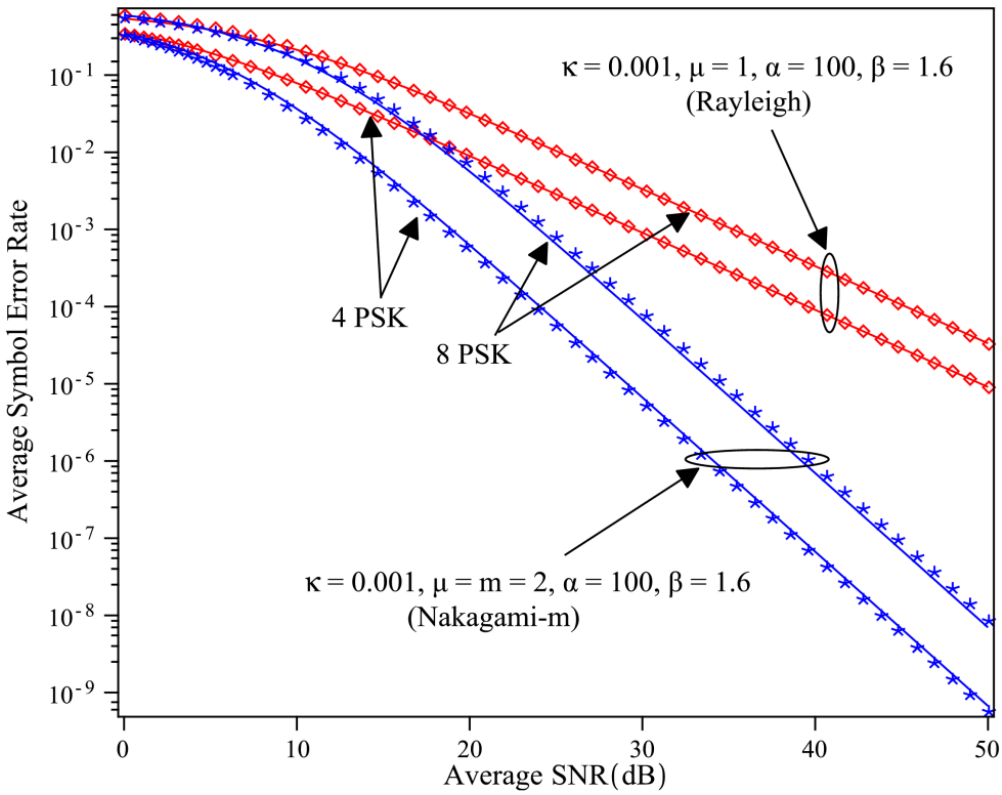

Figure 4.7: ASER comparison using MPSK (M=4,8) with several fading distributions.

The error rates comparison graph using MPSK (4.45) is shown in Figure 4.7. The results obtained are compared with the ASER of Rayleigh [8, Eq. (8.113)] and Nakagami-m [8, Eq. (8.115)] model; which have shown excellent agreement. The higher value of μ has minimum SER. The SER performance improves by varying μ between 1 and 2, as shown in Figure 4.7. Also, 4-PSK modulation scheme shows excellent SER performance in comparison with 8-PSK modulation scheme.

Figure 4.8 depicts the plot of ASER for NCMFSK (4.49) with M=2,4 and its comparison with the results of Rayleigh [52, Eq. (9)] and Rician model [52, Eq. (8)]. In Figure 4.8, with μ=1, α=100, β=1.6 and M=2 (or 4), the ASER reduces as κ varying between 0.001 and 3.2. Also, the ASER increases, as M increases from 2 to 4 with constant κ,μ,α,β.

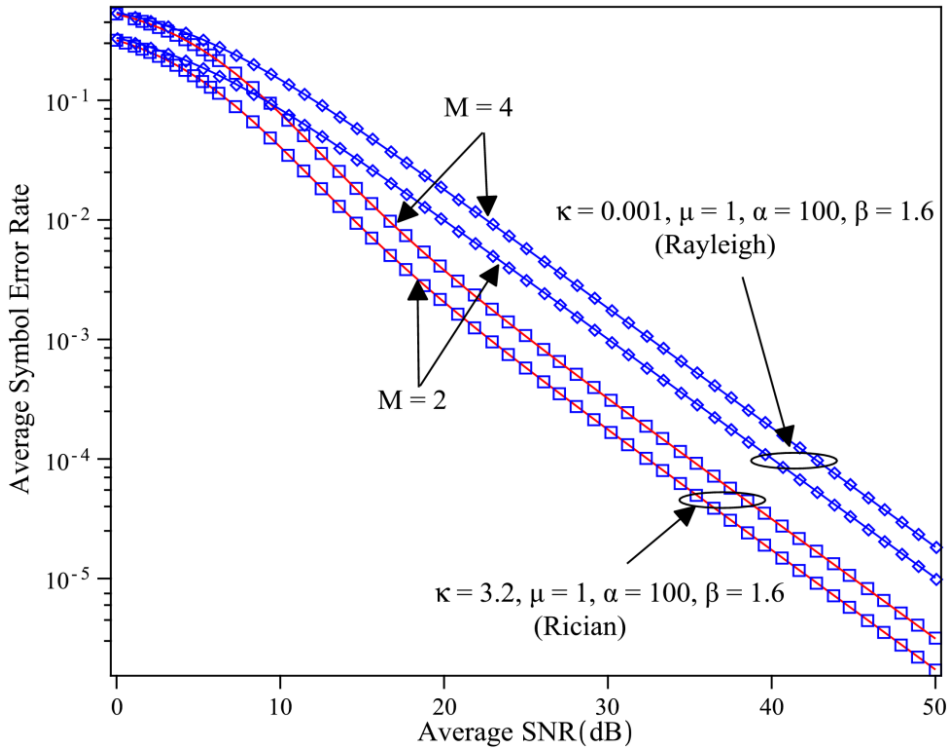

Figure 4.8: ASER comparison using NCMFSK (*M*=2,4) with several fading distributions.

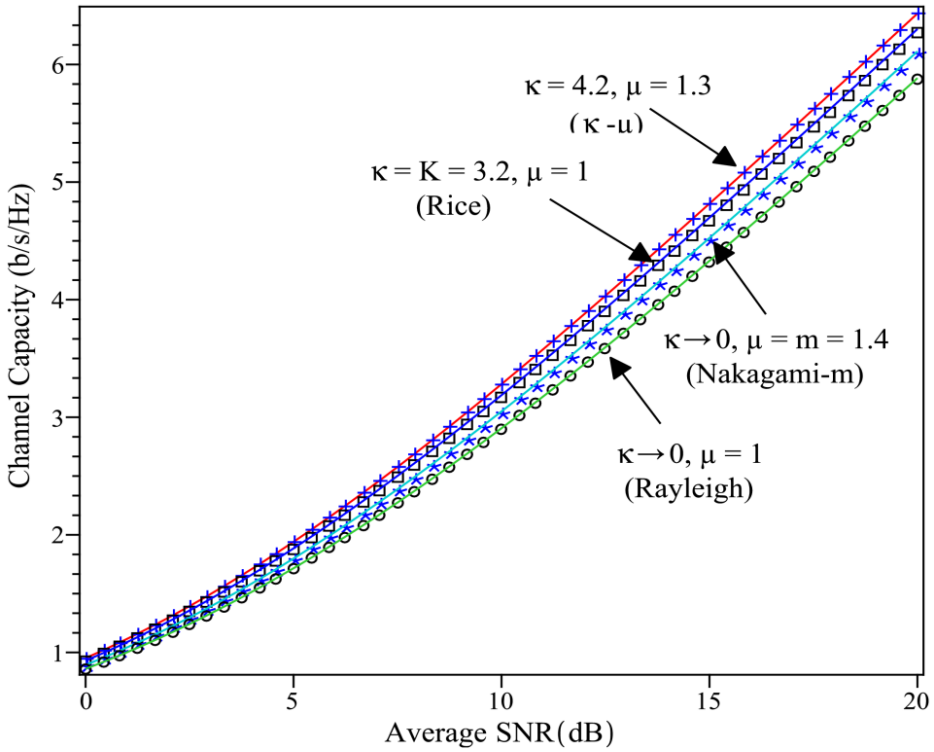

Figure 4.9: Channel capacity comparison using ORA method with several fading distributions.

Figure 4.9 depicts the Channel Capacity for ORA transmission protocol (4.53) of κ-μ/gamma model and is compared with Rayleigh [9, Eq. (4.208)], Nakagami-m [9, Eq. (4.207)], Rice [9, Eq. (4.210)], and κ-μ [56, Eq. (6)] distribution. The Channel Capacity becomes higher as μ increases.

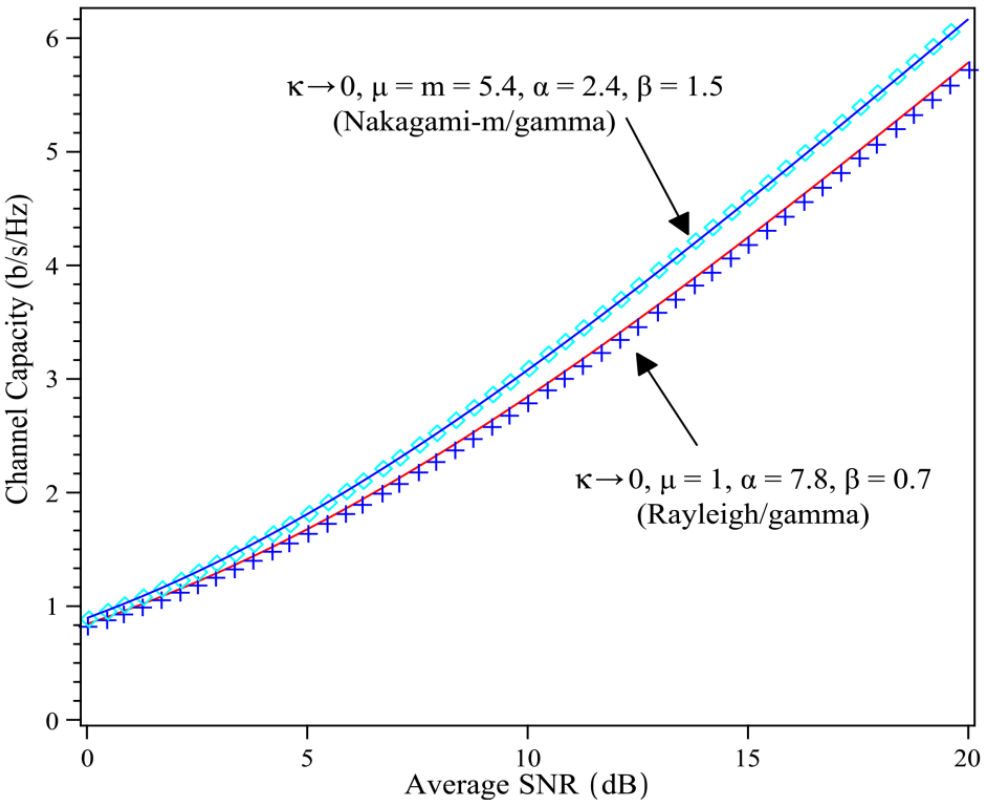

Figure 4.10: Channel capacity comparison using ORA method with several shadowed fading distributions.

Figure 4.10 illustrates the graph of C_{ORA} (4.53) and its comparison with the corresponding results of Rayleigh/gamma [9, Eq. (4.214)], and Nakagami-m/gamma [9, Eq. (4.214)] model. As expected, the higher capacity is achieved as the mean SNR increases.

Figure 4.11 depicts the Channel Capacity comparisons (ORA) using PDF and MGF based analysis with different κ,μ,α and β values. The capacity plot using both PDF (4.53) and MGF (4.59) based approach shows an excellent agreement. In Figure 4.11, on increasing κ,μ (1 to 2) with α=β=1, the Channel Capacity increases. The Channel Capacity also increases by varying α,β (0.5 to 1) with fixed κ,μ.

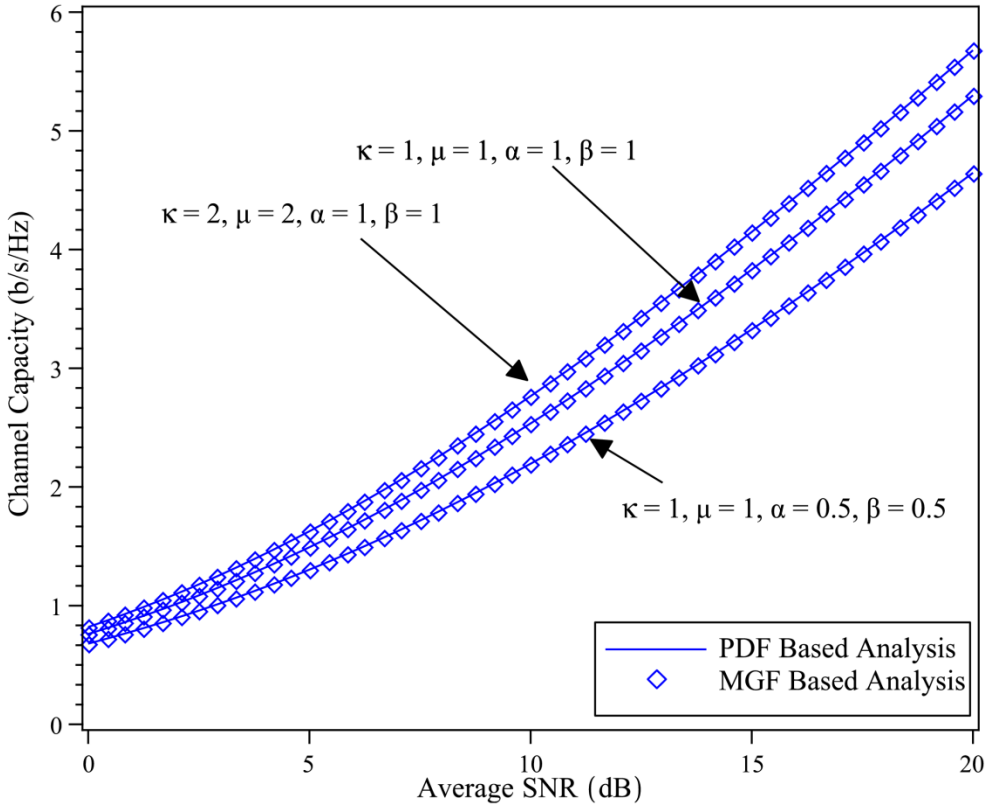

Figure 4.11: Channel capacity comparison for ORA method using PDF and MGF based analysis.

Figure 4.12 depicts the Channel Capacity comparisons of various adaptive transmission protocols. In Figure 4.12, the AWGN channel shows the highest Channel Capacity as compared to the capacity of various adaptive transmission protocols over the κ-μ/gamma channels. The capacity for ORA (4.53) scheme shows the best performance in comparison with OPRA (4.70), CIFR (4.74), and TIFR (4.75) schemes since it uses a fixed amount of transmitting power. Also, the Channel Capacity for all the presented adaptive transmission protocols improves as the average SNR increases. From Figure 4.12, it is also observed that the TIFR yields an increase in capacity over the CIFR but this increase in capacity diminishes as average SNR increases. The capacity for the CIFR scheme is minimum because of high capacity loss. This capacity penalty is recovered by the TIFR protocol since it transmits the power only above the fixed cutoff SNR.

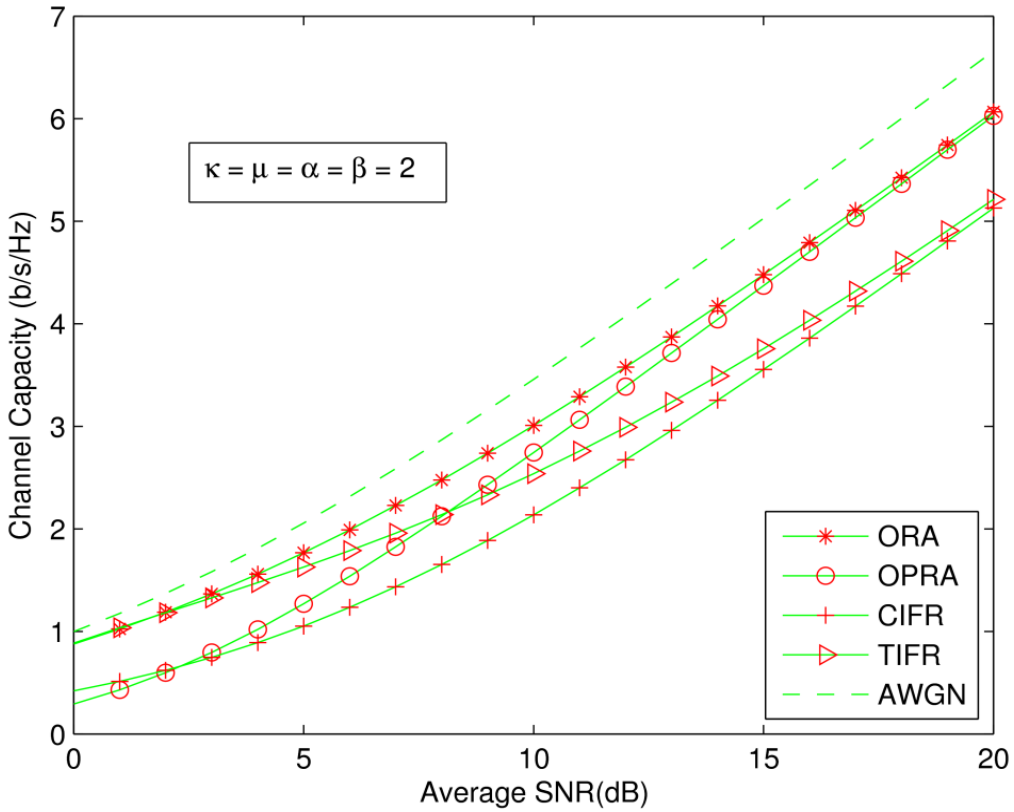

Figure 4.12: All channel capacities comparison with ideal AWGN channel.

Table 4.2: Channel capacities for various rate and power adaptive methods at 12 dB average SNR with $\kappa=\mu=\alpha=\beta=1$.

Methods	Channel Capacity (bits/s/Hz)
AWGN	4.074
ORA	3.577
OPRA	3.388
TIFR	2.990
CIFR	2.675

As shown in Table 4.2, at 12 dB average SNR, the values of C_{ORA}, C_{OPRA}, C_{TIFR}, and C_{TIFR} are 3.577, 3.388, 2.990, and 2.675, respectively. Thus, it is clear that ORA scheme has better capacity performance in comparison with the other policies. Also, the AWGN channel has a maximum capacity (4.074) as expected. The CIFR has minimum channel capacity because a large amount of power is transmitted using this scheme.

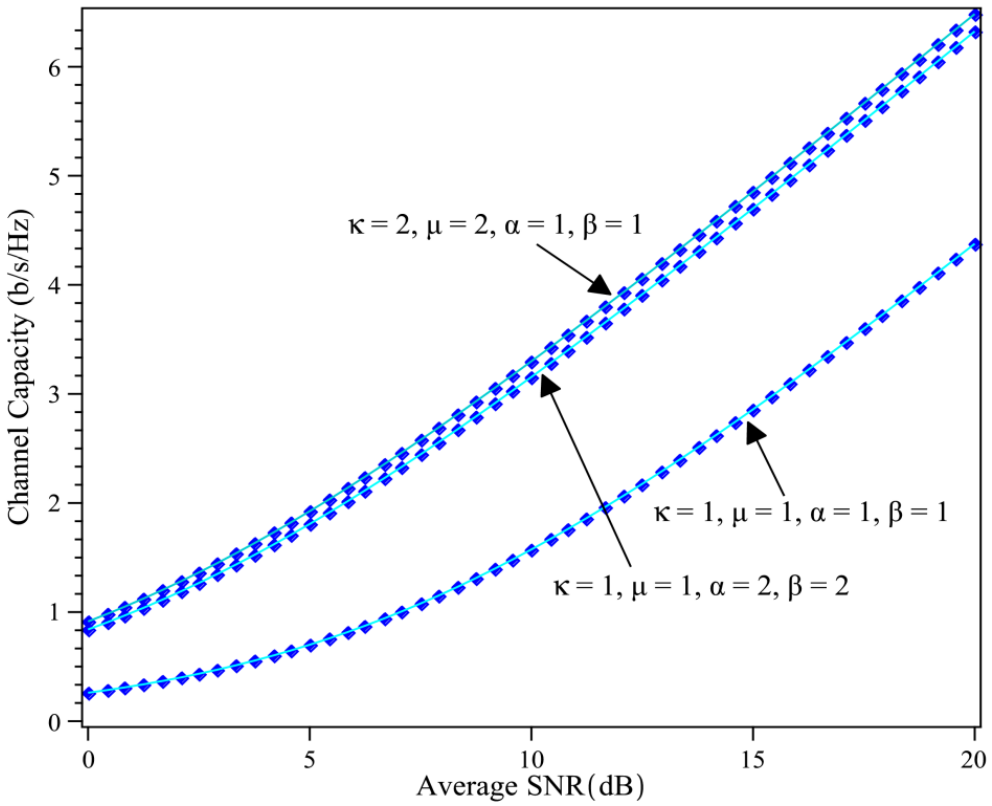

Figure 4.13: Capacity of CIFR method with several shadowing and fading parameters.

Figure 4.13 represents the Channel Capacity for CIFR policy (4.74) for several β,α,μ,κ. The capacity increases as the fading parameter (μ,κ) vary from 1 to 2. However, a slightly low capacity improvement is observed as the shadowing (β,α) parameter increases between 1 and 2. Figure 4.14 illustrates the Channel Capacity for TIFR policy (4.75) with $\{\mu,\kappa =1,2,3\}$, $\{\beta,\alpha=1\}$ and γ_0=0.5,4. With the higher level of average SNR (> 6 dB), at γ_0=4 dB, the higher value of capacity is achieved and lower capacity is observed at γ_0=0.5 dB. Moreover, a large value of fading parameter (μ,κ) provides higher Channel Capacity as depicted in Figure 4.14.

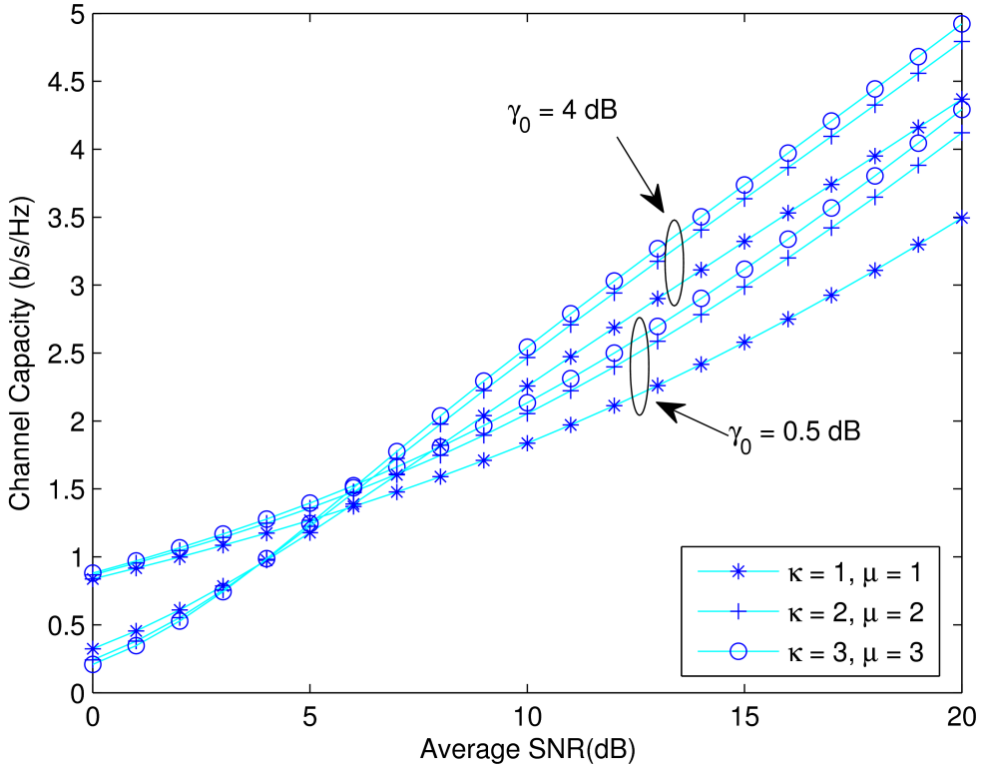

Figure 4.14: Capacity of TIFR method for κ,μ={1, 2, 3}, α=1, β=1 and γ_0=0.5,4 dB.

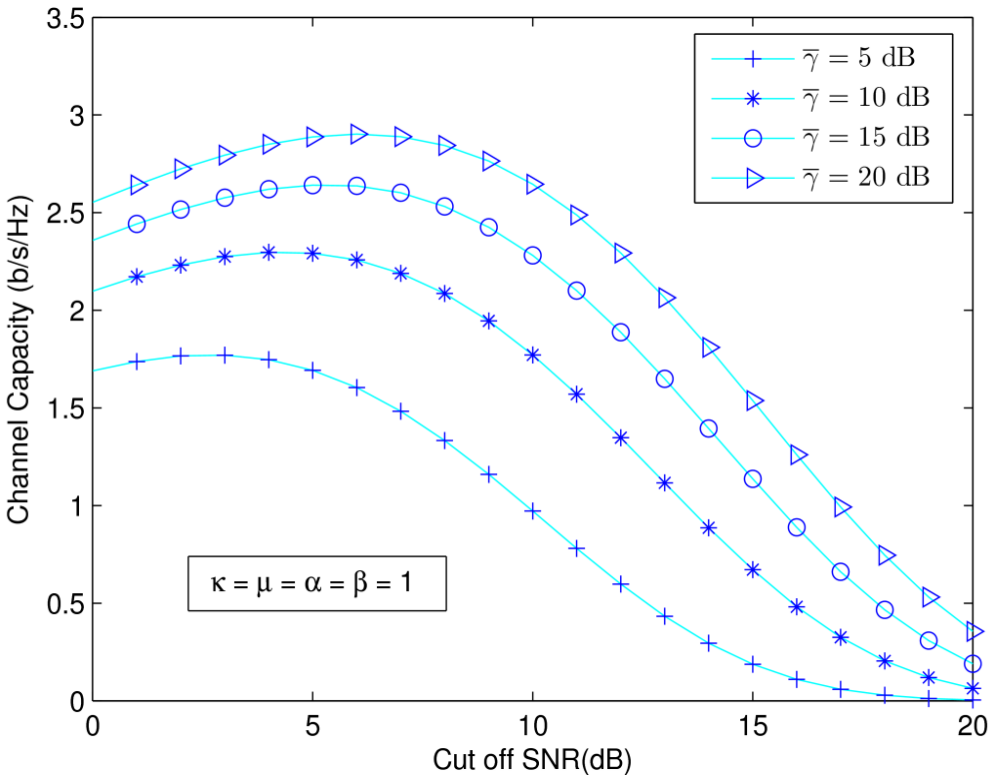

Figure 4.15: Channel capacity under TIFR policy with $\bar{\gamma}$ =5,10,15,20 dB and κ=μ=α=β=1.

Figure 4.15 illustrates the Channel Capacity under TIFR scheme versus cut-off SNR (dB) with different value of $\bar{\gamma}$ (5, 10, 15, 20 dB). Figure 4.15 depicts that higher value of average SNR (20dB) has high capacity and the capacity becomes lower as average SNR decreases from 20dB to 5dB. Moreover, on increasing the cut-off SNR (dB), the Channel Capacity for TIFR policy (at fixed average SNR) increases slightly and then gets decreases sharply. Thus it can be concluded that the higher value of cut-off SNR (dB) has high capacity loss for constant average SNR.

Figure 4.16 shows the Outage Probabilities comparison curve with 10 dB threshold SNR. In Figure 4.16, P_{out} of κ-μ/gamma model (4.77) coincides with corresponding results of Rayleigh [9, Table 4.4], Rician [8, Table 9.5], Nakagami-*m* [9, Eq. (4.157)], Rayleigh/gamma [9, Table 4.4] and Nakagami-*m*/gamma [9, Table 4.4] model. With β=1.6, α=100, $\kappa \to 0$, the P_{out} reduces as μ varies.

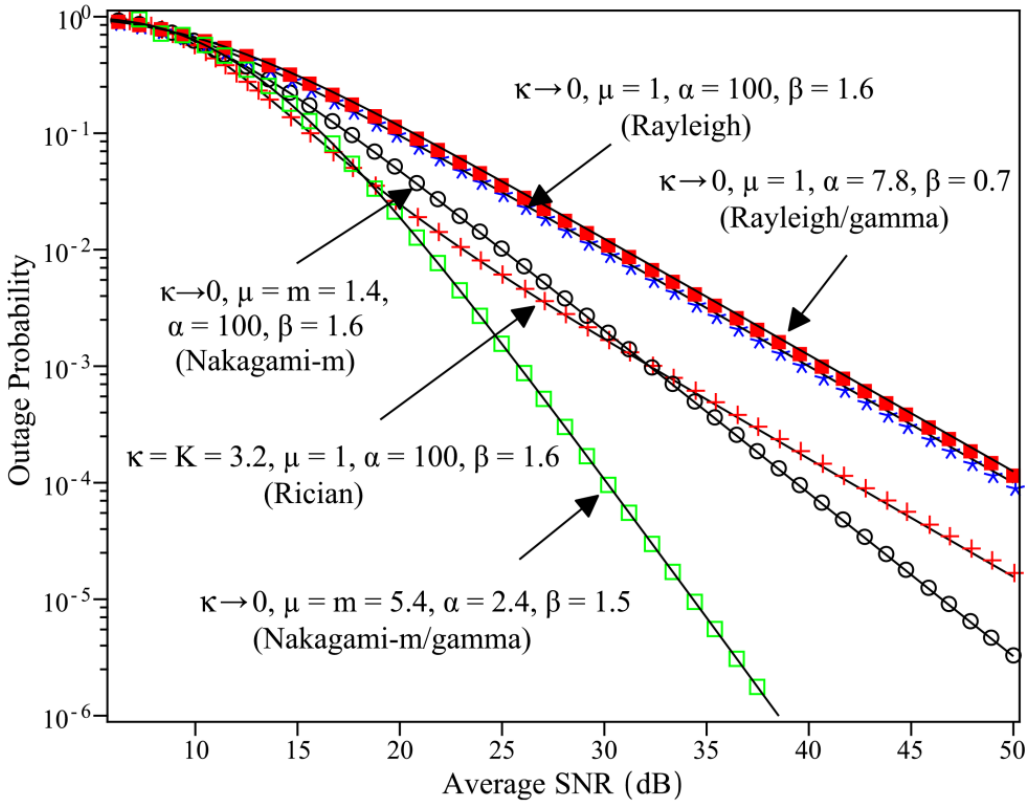

Figure 4.16: Outage probability comparisons with several fading distributions using 10 dB threshold SNR.

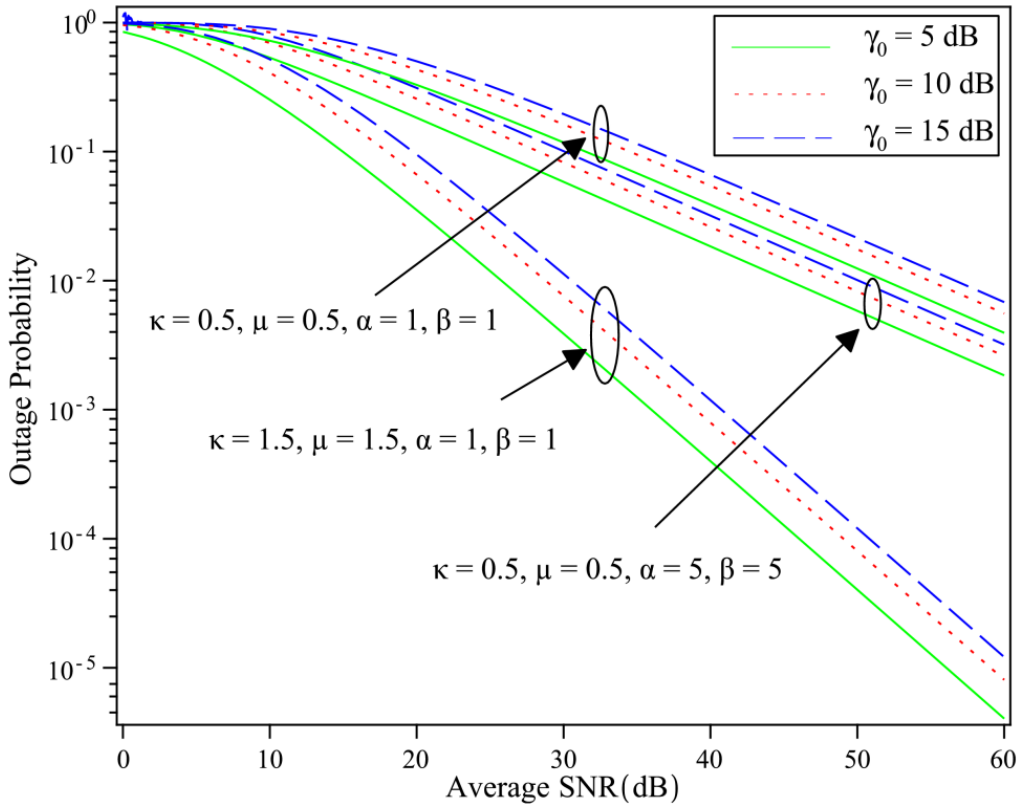

Figure 4.17: Outage probability with different threshold SNR (5, 10, and 15 dB).

Figure 4.17 depicts the plot of Outage Probability at 5, 10, and 15 dB threshold SNR. In Figure 4.17, 5 dB threshold SNR value achieve minimum Outage Probability in comparison with 10 dB and 15 dB threshold SNR. Also, with fixed α,β and γ_0, the Outage Probability decreases sharply as μ,κ varies. However, on varying the value of β,α (1 to 5) with fixed μ,κ,γ_0, the slight improvement in Outage Probability performance is observed.

Table 4.3: Outage probability of *κ*-*μ*/gamma model for different threshold SNR at 40 dB average SNR with *κ*=*μ*=1.5 and *β*=*α*=1.

Threshold SNR(dB)	Outage Probability
5	3.92×10^{-4}
10	7.04×10^{-4}
15	1.13×10^{-3}

Table 4.3 depicts the Outage Probability for several threshold SNR with $\kappa=\mu=1.5$ and $\beta=\alpha=1$. It is clear that the Outage Probability for 5dB threshold SNR at fixed average SNR (40 dB) is minimum as compared to 10 dB and 15 dB threshold SNR.

From the all presented results of κ-μ/gamma fading model, it is clear that the system performance improved as the fading parameter (μ,κ) increases with constant shadowing parameter (β,α) and vice versa. Moreover, the proposed results of κ-μ/gamma distribution have shown closely overlapped to the existing results.

4.4 Rayleigh/TWDP Model

The mathematical work and analysis of Rayleigh/TWDP model have been evaluated in this Section. The performance matrices like Error Rates and Outage Probabilities are computed using derived statistical parameters.

4.4.1 PDF

The density function of γ can be obtained by substituting (4.12) into (4.13) such that

$$f_{\gamma}(\gamma)=\frac{\Omega}{2P_1P_2\bar{\gamma}}\exp(-S_h)\sum_{i=1}^{4}C_iD\left(\sqrt{\sqrt{\frac{\Omega\gamma}{\bar{\gamma}\cdot P_1P_2}}};S_h,\Delta M_i\right)K_m\left(\sqrt{\frac{\Omega\gamma}{\bar{\gamma}\cdot P_1P_2}}\right)d\gamma \tag{4.79}$$

4.4.2 MGF

The MGF can be obtained by substituting (4.79) into (3.31)

$$M_{\gamma}(s)=\int_0^{\infty}\exp(-s\gamma)\frac{\Omega}{2P_1P_2\bar{\gamma}}\exp(-S_h)\sum_{i=1}^{4}C_iD\left(\sqrt{\sqrt{\frac{\Omega\gamma}{\bar{\gamma}\cdot P_1P_2}}};S_h,\Delta M_i\right)K_m\left(\sqrt{\frac{\Omega\gamma}{\bar{\gamma}\cdot P_1P_2}}\right)d\gamma \tag{4.80}$$

With the help of (4.9), (4.80) becomes

$$M_{\gamma}(s)=\sum_{i=1}^{4}C_i\frac{\Omega}{2P_1P_2\bar{\gamma}}\exp(-S_h)\left[\exp(\Delta M_iS_h)\int_0^{\infty}\exp(-s\gamma)I_0\left(\sqrt{\sqrt{\frac{\Omega\gamma}{\bar{\gamma}\cdot P_1P_2}}2S_h(1-\Delta M_i)}\right)K_m\left(\sqrt{\frac{\Omega\gamma}{\bar{\gamma}\cdot P_1P_2}}\right)d\gamma\right.$$

$$\left.+\exp(-\Delta M_iS_h)\int_0^{\infty}\exp(-s\gamma)I_0\left(\sqrt{\sqrt{\frac{\Omega\gamma}{\bar{\gamma}\cdot P_1P_2}}2S_h(1+\Delta M_i)}\right)K_m\left(\sqrt{\frac{\Omega\gamma}{\bar{\gamma}\cdot P_1P_2}}\right)d\gamma\right] \tag{4.81}$$

The Bessel function in the infinite series form can be represented as [135]

$$I_\alpha(x)=\sum_{m=0}^{\infty}\frac{1}{m!\Gamma(m+\alpha+1)}\left(\frac{x}{2}\right)^{2m+\alpha} \tag{4.82}$$

By putting (4.82) into (4.81), (4.81) can be written as

$$M_\gamma(s)=\sum_{i=1}^{4}C_i\frac{\Omega}{4P_1P_2\bar{\gamma}}L(S_h,\Delta M_i)\left[\int_0^{\infty}e^{-s\gamma}\gamma^{m/2}K_m\left(\sqrt{\frac{\Omega\gamma}{\bar{\gamma}\cdot P_1P_2}}\right)d\gamma\right] \tag{4.83}$$

where

$$L(S_h,\Delta M_i)=\exp(-(1-M_i\Delta)S_h)\sum_{m=0}^{\infty}\frac{\left(\sqrt{\frac{\Omega}{\bar{\gamma}P_1P_2}}\cdot\frac{2S_h(1-\Delta M_i)}{4}\right)^m}{(m!)^2}+\exp(-(1+M_i\Delta)S_h))\sum_{m=0}^{\infty}\frac{\left(\sqrt{\frac{\Omega}{\bar{\gamma}P_1P_2}}\cdot\frac{2S_h(1+\Delta M_i)}{4}\right)^m}{(m!)^2} \tag{4.84}$$

By using [135, Eq. (6.631.3)], the MGF expression can be obtained as

$$M_\gamma(s)=\frac{1}{4}\sum_{i=1}^{4}C_iL(S_h,\Delta M_i)s^{-(m+1)/2}\left(\sqrt{\frac{\Omega}{\bar{\gamma}P_1P_2}}\right)\Gamma(m+1)\exp\left(\frac{\Omega}{8sP_1P_2\bar{\gamma}}\right)W_{-(m+1)/2,m/2}\left(\frac{\Omega}{4sP_1P_2\bar{\gamma}}\right) \tag{4.85}$$

4.4.3 CDF

The distribution function in the term of envelope signal is presented as [9]

$$F_R(r)=P_R(R\le r)=\int_0^{r}f_R(r)dr \tag{4.86}$$

By plugging the PDF of envelope signal of the Rayleigh/TWDP model (as given in (4.12)) into (4.86), the expression of CDF can be written as

$$F_R(r)=\int_0^{r}\frac{r}{P_1P_2}\exp(-S_h)\sum_{i=1}^{M}C_iD\left(\sqrt{\frac{r}{\sqrt{P_1P_2}}};S_h,\Delta\cos\frac{\pi(j-1)}{2M-1}\right)K_m\left(\frac{r}{\sqrt{P_1P_2}}\right)dr \tag{4.87}$$

By using (4.9) and (4.82), the above expression can be written as

$$F_R(r)=\int_0^r \frac{r}{2P_1P_2}\exp(-S_h)\sum_{i=1}^{M}C_i\left[\exp(S_h\Delta M_i)\sum_{m=0}^{\infty}\frac{\left(\frac{2rS_h(1-\Delta M_i)}{4\sqrt{P_1P_2}}\right)^m}{(m!)^2}+\exp(-S_h\Delta M_i)\sum_{m=0}^{\infty}\frac{\left(\frac{2rS_h(1+\Delta M_i)}{4\sqrt{P_1P_2}}\right)^m}{(m!)^2}\right]K_m\left(\frac{r}{\sqrt{P_1P_2}}\right)dr \tag{4.88}$$

Now, (4.88) can be simplified as

$$F_R(r)=\frac{1}{2P_1P_2}Q(S_h,\Delta M_i)\sum_{i=1}^{M}C_i\int_0^r r^{m+1}K_m\left(\frac{r}{\sqrt{P_1P_2}}\right)dr \tag{4.89}$$

where,

$$Q(S_h,\Delta M_i)=\exp(-S_h(1-\Delta M_i))\sum_{m=0}^{\infty}\frac{\left(\frac{(1-\Delta M_i)S_h}{2\sqrt{P_1P_2}}\right)^m}{(m!)^2}+\exp(-S_h(1+\Delta M_i))\sum_{m=0}^{\infty}\frac{\left(\frac{(1+\Delta M_i)S_h}{2\sqrt{P_1P_2}}\right)^m}{(m!)^2} \tag{4.90}$$

With the help of [149, Eq. (7.14.1.3)], (4.89) can be written as

$$F_R(r)=2\left(\sqrt{P_1P_2}\right)^m\sum_{i=1}^{4}a_i\cdot Q(S_h,\Delta M_i)\left[\frac{2^m\cdot\pi}{\sin((m+1)\pi)\cdot\Gamma(-m)}-\left(r/\sqrt{P_1P_2}\right)^{m+1}K_{m+1}\left(r/\sqrt{P_1P_2}\right)\right] \tag{4.91}$$

4.4.4 Outage Probability

The expression of the Outage Probability can be obtained by plugging (4.91) into (3.35) such that

$$P_{out}=F_R\left(\sqrt{\frac{\gamma_0\Omega}{\bar{\gamma}}}\right)=2\sum_{i=1}^{4}a_iQ(S_h,\Delta M_i)\left[\frac{2^m\pi}{\sin((m+1)\pi)\Gamma(-m)}-\left(\sqrt{\frac{\gamma_0\Omega}{\bar{\gamma}\cdot P_1P_2}}\right)^{m+1}K_{m+1}\left(\sqrt{\frac{\gamma_0\Omega}{\bar{\gamma}\cdot P_1P_2}}\right)\right] \tag{4.92}$$

4.4.5 Average Bit Error Rate

The expressions of Error Probability using several signaling techniques for Rayleigh/TWDP model are derived in this Section.

(A) BFSK and BPSK

With the help of (4.85) and Table 3.2, the ABER for coherent modulation scheme can be obtained as

$$P_e(E)=\frac{1}{\pi}\int_0^{\pi/2}\frac{1}{4}\sum_{i=1}^{4}C_iL(S_h,\Delta M_i)\left(\frac{a}{\sin^2\theta}\right)^{-\frac{m+1}{2}}\left(\sqrt{\frac{\Omega}{\bar{\gamma}P_1P_2}}\right)\Gamma(m+1)\exp\left(\frac{\Omega\cdot\sin^2\theta}{8aP_1P_2\bar{\gamma}}\right)W_{-(m+1)/2,m/2}\left(\frac{\Omega\cdot\sin^2\theta}{4aP_1P_2\bar{\gamma}}\right)d\theta \quad (4.93)$$

By putting $\sin^2\theta=x$, after performing integration by substitution, and using [135], (4.93) is expressed as

$$P_e(E)=\frac{1}{4\pi}\sum_{i=1}^{4}C_iL(S_h,\Delta M_i)\left(\sqrt{\frac{\Omega}{\bar{\gamma}P_1P_2}}\right)\frac{\Gamma(m+1)}{2a^{(m+1)/2}}\int_0^1 x^{\frac{m}{2}}(1-x)^{-1/2}\left\{\Gamma(-m)\left(\frac{\Omega\cdot x}{4aP_1P_2\bar{\gamma}}\right)^{(m+1)/2}\right.$$

$$\left.\times\,{}_1F_1\left(m+1;m+1;\frac{\Omega\cdot x}{4aP_1P_2\bar{\gamma}}\right)+\left(\frac{\Omega\cdot x}{4aP_1P_2\bar{\gamma}}\right)^{-\frac{m-1}{2}}\frac{\Gamma(m)}{\Gamma(m+1)}{}_1F_1\left(1;m+1;\frac{\Omega\cdot x}{4aP_1P_2\bar{\gamma}}\right)\right\}dx \quad (4.94)$$

With the help of [135, Eq. (7.512.12)], the ABER for coherent binary modulation schemes can be obtained as

$$P_e(E)=\frac{\Omega}{16\pi\cdot a^{(m+2)/2}P_1P_2\bar{\gamma}}\sum_{i=1}^{4}C_iL(S_h,\Delta M_i)\left\{\left(\frac{\Omega}{4aP_1P_2\bar{\gamma}}\right)^{m/2}\frac{\Gamma(-m)\Gamma(m+1.5)\Gamma(0.5)}{(m+1)}\right.$$

$$\left.\times\,{}_2F_2\left(m+1.5,m+1;m+2,m+1;\frac{\Omega}{4aP_1P_2\bar{\gamma}}\right)+\left(\frac{\Omega}{4aP_1P_2\bar{\gamma}}\right)^{-\frac{m}{2}}\Gamma(m)\Gamma(0.5)\Gamma(1.5)\,{}_2F_2\left(1.5,1;2,m+1;\frac{\Omega}{4aP_1P_2\bar{\gamma}}\right)\right\} \quad (4.95)$$

(B) BDPSK and NCFSK

The ABER for binary non-coherent modulation scheme can be obtained by substituting (4.85) into Table 3.2. Hence it can be written as

$$P_e(E)=\frac{1}{8}\sum_{i=1}^{4}C_iL(S_h,\Delta M_i)(a)^{-(m+1)/2}\left(\sqrt{\frac{\Omega}{\bar{\gamma}P_1P_2}}\right)\Gamma(m+1)\exp\left(\frac{\Omega}{8aP_1P_2\bar{\gamma}}\right)W_{-(m+1)/2,m/2}\left(\frac{\Omega}{4aP_1P_2\bar{\gamma}}\right) \quad (4.96)$$

4.4.6 Results

The analytical analysis of Rayleigh/TWDP distribution is demonstrated in this Section. The performance is dependent on the Mean SNR, Average Fading Power, Shadowing (S_h), and Scale Parameter (Δ). The plots of the Distribution Function, Outage Probability, and Error Probabilities for several modulation techniques are illustrated in this section.

Figure 4.18 illustrates the CDF for different shape parameter (Δ = 0, 0.5, 0.8, 1). Usually, average fading power P_1=0.2 and P_2=0.2 are considered to plot the CDF curve.

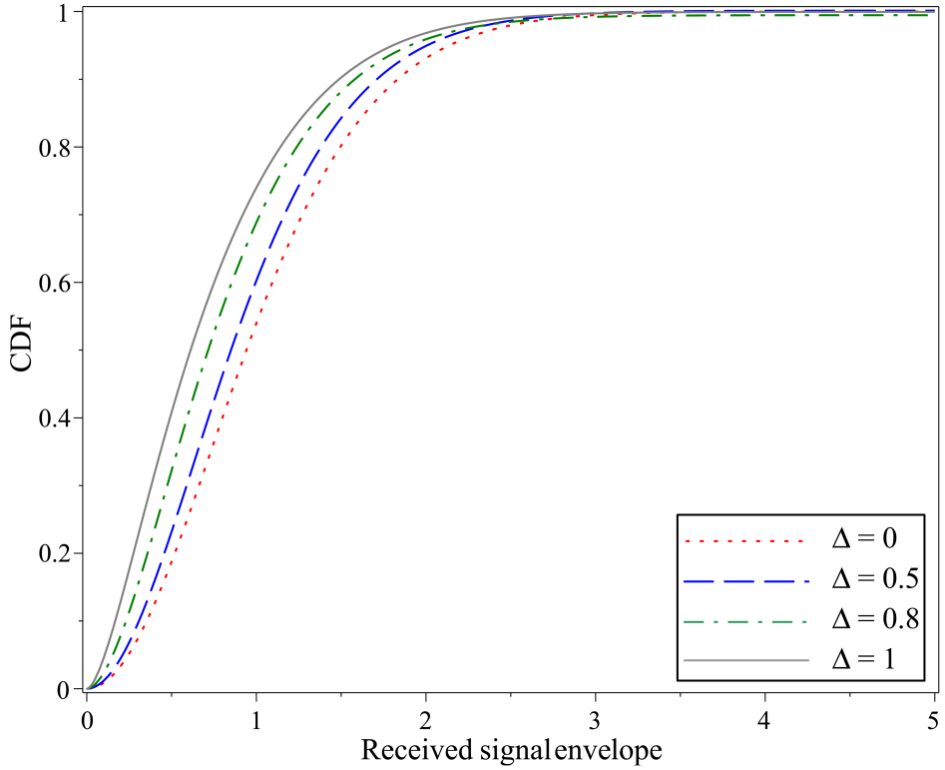

Figure 4.18: CDF for Δ = 0, 0.5, 0.8, 1 with S_h=2 dB and P_1=P_2 =0.2.

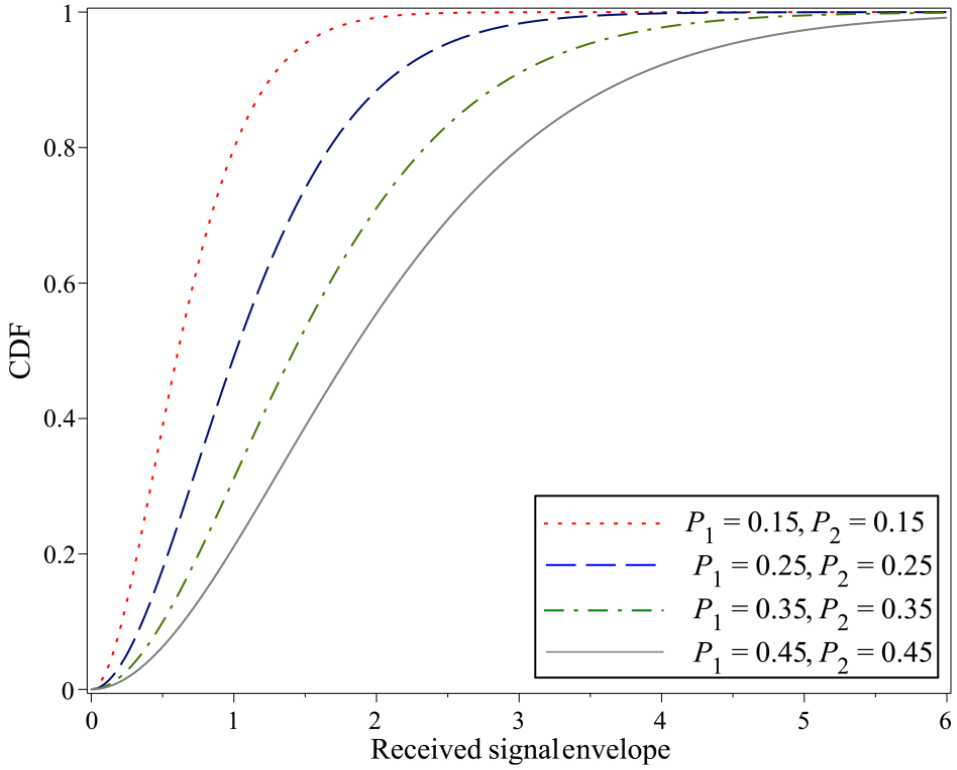

Figure 4.19: CDF for different P_2 and P_1 values with S_h=10 dB and Δ=0.6.

Figure 4.19 represents the CDF versus received signal envelope for different P_1, P_2 values with S_h=10dB and Δ=0.6. In Figure 4.19, for P_1=P_2=0.15, on increasing the received signal envelope, the CDF increases sharply.

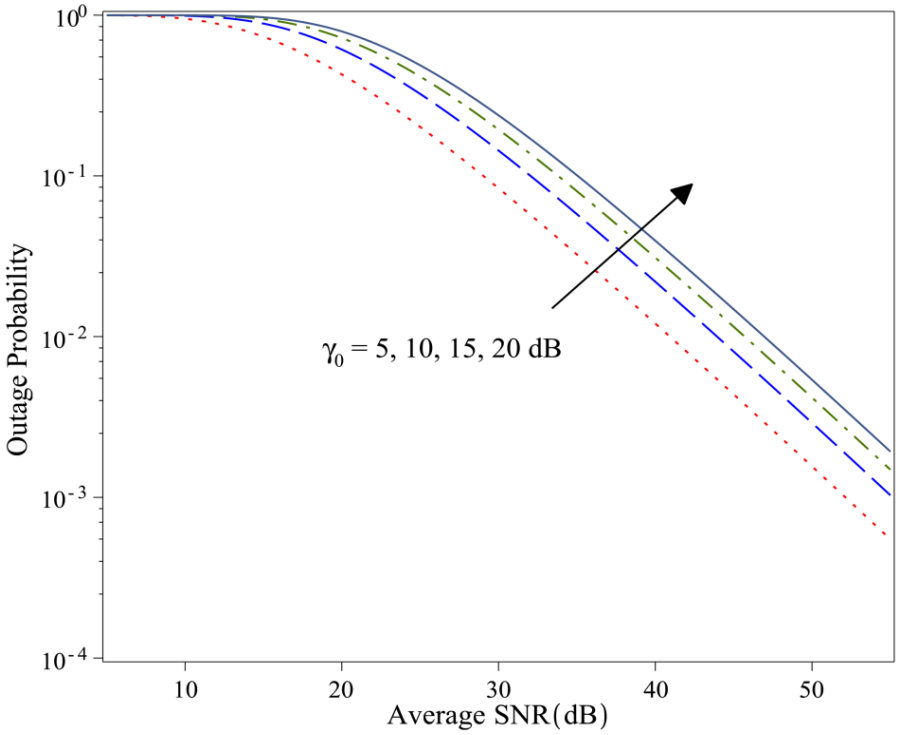

Figure 4.20: Outage probability for various threshold SNR with S_h=2 dB and Δ=0.1.

Figure 4.20 illustrates the plot of Outage Probability for Δ=0.1 and S_h=2 dB with different values of threshold SNR γ_0 = 5, 10, 20, and 30 dB. In Figure 4.20, on increasing the threshold SNR (5 to 20 dB), the Outage Probability increases. Moreover, the Outage Probability reduces as the mean SNR varies for fixed threshold SNR as expected.

Figure 4.21 illustrates the ABER for BPSK modulation scheme (4.95) with different shadowing parameter (S_h = 2, 5, 8, 10 dB) and constant shape parameter (Δ = 0.6). A lower S_h factor has very small range of discrete shadowing values that encountered rapidly and therefore causes the higher severity in shadowing. However, a large S_h factor shows large variations in main wave amplitude contributed by each scattering neighborhood that causes approximately equal number of low and high discrete shadowing values and therefore lower severity in shadowing occurs. In Figure 4.21, the error rates become lower as the average SNR varies with any fixed value of S_h. Also, on increasing the shadowing parameter (2 to 10 dB) with Δ = 0.6, the ABER decreases that improve the system performance. The larger S_h factor (10dB) shows lower BER because of

lower severity in shadowing. However, lower S_h factor represents higher BER because of high severity in shadowing.

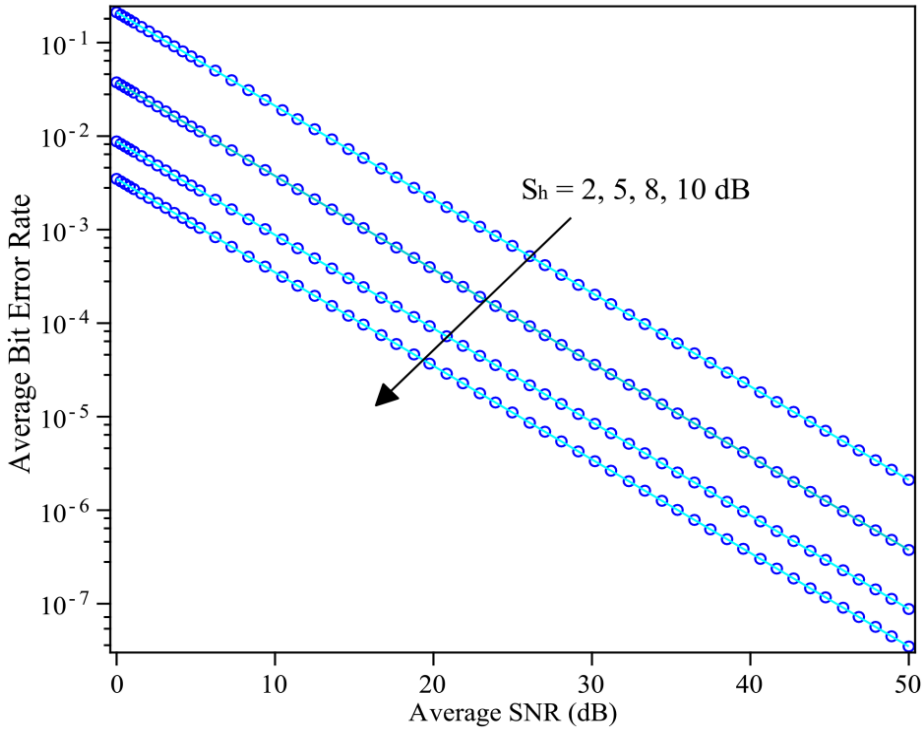

Figure 4.21: ABER for BPSK with Δ = 0.6 and S_h = 2, 5, 8, 10 dB.

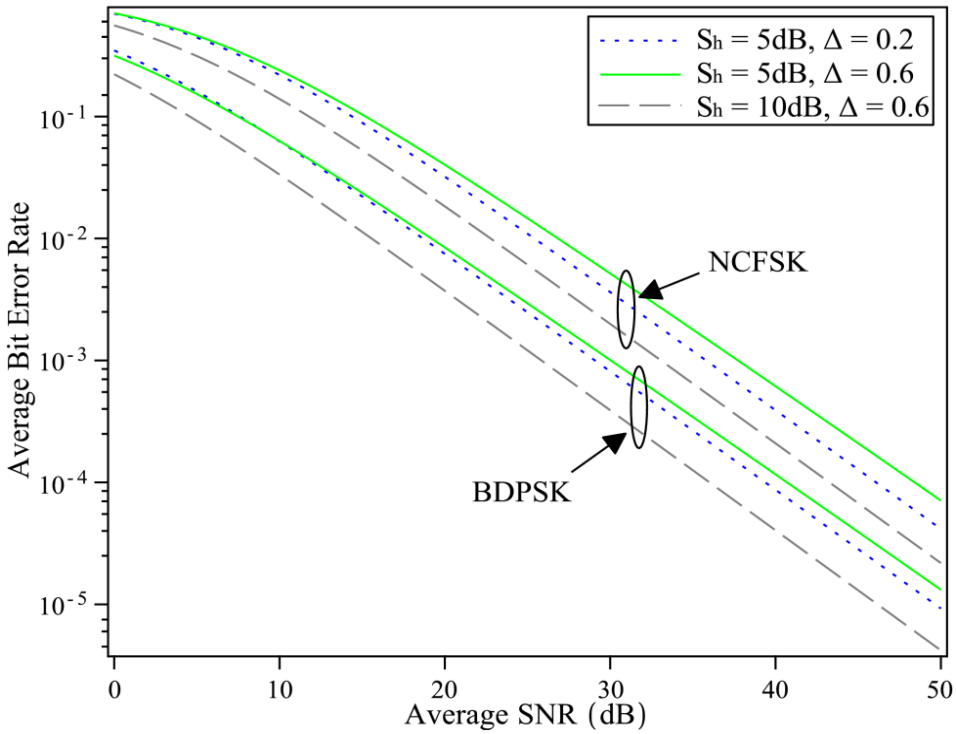

Figure 4.22: ABER for BDPSK and NCFSK with different Δ and S_h.

Figure 4.22 represents the error rate comparison curve between BDPSK and NCFSK with S_h = 5, 10, Δ = 0.2, 0.6 and P_1, P_2 = 0.1, 0.3. In Figure 4.22, for any modulation schemes, on increasing Δ parameter (0.2 to 0.6) with constant S_h = 5 dB, a slight degradation in BER performance is observed. However, for any modulation schemes, on increasing the shadowing parameter (S_h = 5 to 10 dB) with constant Δ = 0.6, the BER performance improves.

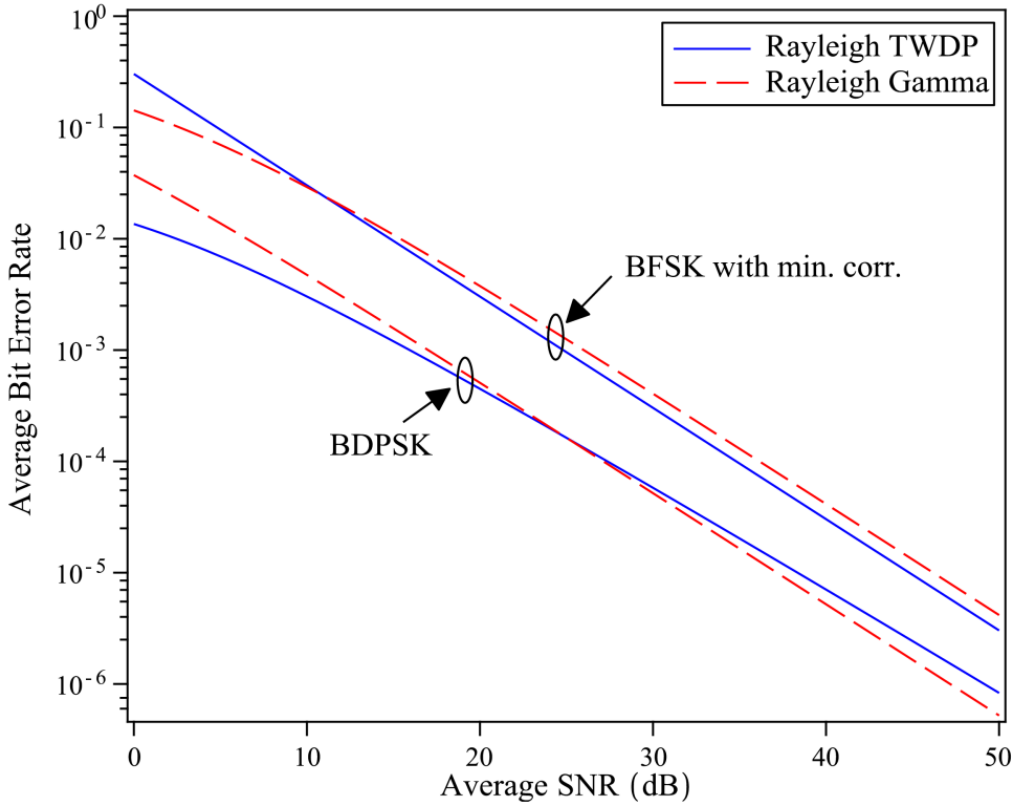

Figure 4.23: ABER for BDPSK and BFSK with minimum correlation with Δ = 0.6 and S_h = 2 dB. Rayleigh/TWDP (solid line), Rayleigh/gamma (dash line).

Figure 4.23 illustrates the ABER for BDPSK and BFSK with minimum correlation for Δ = 0.6 and S_h = 2dB and its comparison with Rayleigh/gamma shadowed fading model [53]. In Figure 4.23, BDPSK modulation scheme shows minimum error rate in comparison with BFSK with minimum correlation. Also, as depicted in Figure 4.23, the BER for BFSK signaling of the Rayleigh/TWDP model is minimum as compared to BER of Rayleigh/gamma model at high SNR region (>10dB).

4.5 Contribution

In this Chapter, the performances of κ-μ/gamma and Rayleigh/TWDP models have been evaluated. The contributions of this Chapter are as follows:

- The statistical parameters such as PDF, MGF, Moments, and Distribution Function of κ-μ/gamma model have been computed.
- Channel Capacity for different power and rate adaptive methods, Outage Probability, and Error Probabilities expressions have been derived mathematically.
- The performances have been examined by varying few terms such as Average SNR, Modulation Index, Scaling, and Shaping factors.
- The improvement in overall performance has been observed as μ,κ varies with the shadowing factor kept constant.
- The analytical expressions of some statistical parameters such as PDF, CDF, and MGF of Rayleigh/TWDP fading have been computed which helps to derive the Error Probability and Outage Probability expressions.
- The performance of the Rayleigh/TWDP model depends on the Shape (Δ) and the Shadowing parameter (S_h). The numerical results have been presented that demonstrated the derived expressions of the Rayleigh/TWDP model.

Based on the research outcomes reported in this Chapter, it is concluded that both multipath fading and shadowing parameter has considerable role in system performance. Thus, the research hypothesis testing is successfully achieved.

Published paper related to this Chapter:

(1) Hari Shankar, Ankush Kansal, "CDF and MGF based analysis over Rayleigh TWDP shadowed fading channel for indoor communication". International Journal of Electronics, Taylor & Francis, vol. 105 (12), pp. 2099-2113, 2018.

(2) Hari Shankar, Ankush Kansal, "Performance analysis of κ-μ/gamma shadowed fading model over indoor off body communication channel. International Journal of Electronics and Communication (AEU), Elsevier, vol. 93, pp. 283-288, 2018.

(3) Hari Shankar, Ankush Kansal, "MGF-based analysis of κ-μ/gamma composite fading model for indoor off body communication". Transactions on Emerging Telecommunications Technologies, Wiley, e3566, pp. 1-17, 2019.

Chapter 5

Shadowed Fading Model over Multiple Channels

In indoor wireless communication, when the signal passes through the channels, it becomes faded by surrounding objects like building, walls, doors, chairs, and the human body. Also, both scattered and dominant components of the signal may be obscured by surrounding objects and the human body which causes shadowing. These factors may degrade the indoor wireless system performances.

The diversity combining is a good method to overcome the effects of fading by setup the several antennas at the Rx. In the diversity mechanism, the signal quality can be improved without increasing the transmit power and bandwidth. Well-known diversity combining methods are MRC, SC, and EGC. MRC is one of the easiest and optimal algorithm to improve the SNR. In this technique, the copies of all information-bearing signals are combined at the receiver. Operating with MRC diversity, the performance measures such as Moments, AF, ABER, and Channel Capacity are computed in this Chapter. A tractable and straightforward shadowed fading model, known as Fisher Snedecor ($\mathcal{F}$), is used to obtain these expressions.

5.1 Introduction

The Nakagami-*m* distribution is the multipath fading model. It is a purely statistical and simpler model because the performance matrices are available in closed-form. This model often shows a good match with empirical data obtained in LMS and indoor radio propagation environments [150]. The Nakagami-*m* model can be reduced to Rayleigh and one-sided Gaussian model. The Nakagami-*m* distribution based shadowed fading model includes Nakagami-*m*/lognormal [33], Nakagami-*m*/gamma (Generalized *K*) [18] and Nakagami-*m*/inverse Gaussian (G distribution) [36]. Recently, one more shadowed fading model, namely Fisher Snedecor ($\mathcal{F}$), associated with Nakagami-*m* distribution has been proposed [48]. The work on this tractable model has been provided in many literatures [84-94, 109, 111]. The investigation on the $\mathcal{F}$ model (i.n.i.d. case) was performed by O. S. Badarneh *et al.* [109]. Correspondingly, the author derived the

expressions of PDF, CDF, Outage Probability, and ABER for BPSK signaling. However, the MGF expression of i.i.d. MRC receiver and it's throughout analysis is not given in [109]. Therefore, in this Chapter, performance evaluation of $\mathcal{F}$ shadowed fading model over i.i.d. MRC receiver has been elaborated.

Research hypothesis test: The MRC diversity improves the system performance over $\mathcal{F}$ shadowed fading channels.

5.2 System Model

Assuming user equipment 1 (UE1) sends information to the user equipment 2 (UE2) through a wireless medium. The UE1 consists of a single transmitting antenna and UE2 has multiple receiving antennas followed by maximum ratio combiner, as shown in Figure 5.1. The channel is assumed to be characterized by $\mathcal{F}$ model. It is also assuming that the transmitting signal is represented as $x(t)$. For i^{th} diversity branch in $\mathcal{F}$ channel, the received signal is expressed as

$$y_i(t) = h_i x(t) + c_i(t) \tag{5.1}$$

The instantaneous SNR (γ) at the output of L branch MRC diversity is represented as [8]

$$\gamma = \sum_{i=0}^{L} \gamma_i \tag{5.2}$$

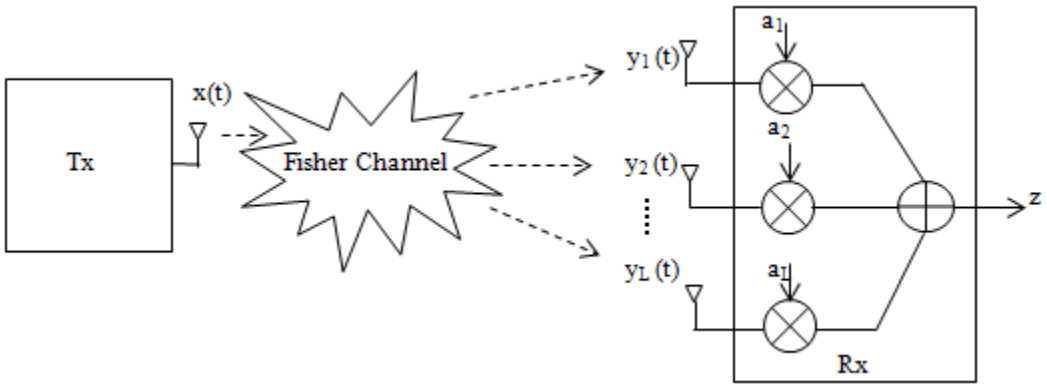

Figure 5.1: MRC diversity in $\mathcal{F}$ channel.

The density function at each receiving diversity branch for $\mathcal{F}$ model is given by [48]

$$f_{\gamma_i}(\gamma) = \frac{m_i^{\,m_i} \cdot (m_{s_i}\bar{\gamma})^{m_{s_i}} \gamma^{m_i - 1}}{B(m_i, m_{s_i})(m_i\gamma + m_{s_i}\bar{\gamma}_i)^{m_i + m_{s_i}}} \tag{5.3}$$

Let us also assume that all branches of MRC receiver have equal average SNR. Therefore, at the output of MRC diversity, the density function for i.i.d. branches is given by [109]

$$f_{MRC}(\gamma) = \frac{1}{\Gamma(mL)}\left(\frac{m}{m_s\bar{\gamma}}\right)^{mL}\left[\frac{\Gamma(m+m_s)}{\Gamma(m_s)}\right]^{L}\gamma^{mL-1}\,{}_2F_1\left(m+m_s, mL; mL; \frac{-m\gamma}{m_s\bar{\gamma}}\right) \tag{5.4}$$

where ${}_2F_1(\cdot)$ is the Gauss hypergeometric function [135, Eq.(9.100)].

5.3 MRC Diversity for $\mathcal{F}$ Model

5.3.1 MGF

The MGF of γ for MRC diversity is represented as [8]

$$M_{MRC}(s) = \int_0^\infty \exp(-s\gamma) f_{MRC}(\gamma) d\gamma \tag{5.5}$$

By plugging (5.4) into (5.5), (5.5) can be expressed as

$$M_{MRC}(s) = \left(\frac{m}{m_s\bar{\gamma}}\right)^{mL}\frac{1}{\Gamma(mL)}\left(\frac{\Gamma(m+m_s)}{\Gamma(m_s)}\right)^{L}\int_0^\infty {}_2F_1\left(m+m_s, mL; mL; \frac{-m\gamma}{m_s\bar{\gamma}}\right)\exp(-s\gamma)\gamma^{mL-1}d\gamma \tag{5.6}$$

The $G_{p,q}^{m,n}[\cdot\,|\,\cdot]$ and ${}_2\mathrm{F}_1(\cdot)$ function is related by following mathematical expression as [135, Eq. (9.34.7)]

$$\frac{m\gamma}{\Gamma(m+m_s)m_s\bar{\gamma}}G_{2,2}^{1,2}\left(\frac{m\gamma}{m_s\bar{\gamma}}\middle|\begin{matrix}-m-m_s, & -mL\\ -1, & -mL\end{matrix}\right) = {}_2F_1\left(m+m_s, mL; mL; \frac{-m\gamma}{m_s\bar{\gamma}}\right) \tag{5.7}$$

By substituting (5.7) into (5.6), (5.6) becomes

$$M_{MRC}(s) = \frac{1}{\Gamma(mL)\Gamma(m+m_s)}\left(\frac{m}{m_s\bar{\gamma}}\right)^{mL+1}\left(\frac{\Gamma(m+m_s)}{\Gamma(m_s)}\right)^{L}\int_0^\infty \gamma^{mL}\exp(-s\gamma)G_{2,2}^{1,2}\left(\frac{m\gamma}{m_s\bar{\gamma}}\middle|\begin{matrix}-m-m_s, & -mL\\ -1, & -mL\end{matrix}\right) \tag{5.8}$$

With the help of [135, Eq. (7.813.1)] and after performing some mathematical steps, the MGF expression can be obtained as

$$M_{MRC}(s)=\frac{1}{\Gamma(mL)\Gamma(m+m_s)}\left(\frac{m}{sm_s\bar{\gamma}}\right)^{mL+1}\left(\frac{\Gamma(m+m_s)}{\Gamma(m_s)}\right)^{L}G_{3,2}^{1,3}\left(\frac{m}{sm_s\bar{\gamma}}\middle|\begin{matrix}-mL, & -m-m_s, & -mL\\ -1, & -mL, & \end{matrix}\right) \tag{5.9}$$

5.3.2 Moments

The Moments of γ operated for MRC receiver is given as

$$E[\gamma^n]=\int_0^{\infty}\gamma^n f_{MRC}(\gamma)d\gamma \tag{5.10}$$

By plugging (5.4) into (5.10), (5.10) becomes

$$E[\gamma^n]=\frac{1}{\Gamma(mL)}\left(\frac{m}{m_s\bar{\gamma}}\right)^{mL}\left(\frac{\Gamma(m+m_s)}{\Gamma(m_s)}\right)^{L}\int_0^{\infty}\gamma^{n+mL-1}\,{}_2F_1\left(m+m_s,mL;mL;\frac{-m\gamma}{m_s\bar{\gamma}}\right)d\gamma \tag{5.11}$$

By substituting (5.7) into (5.11), (5.11) can be written as

$$E[\gamma^n]=\frac{1}{\Gamma(mL)\Gamma(m+m_s)}\left(\frac{m}{m_s\bar{\gamma}}\right)^{mL+1}\left(\frac{\Gamma(m+m_s)}{\Gamma(m_s)}\right)^{L}\int_0^{\infty}\gamma^{n+mL}G_{2,2}^{1,2}\left(\frac{m\gamma}{m_s\bar{\gamma}}\middle|\begin{matrix}-m-m_s, & -mL\\ -1, & -mL\end{matrix}\right)d\gamma \tag{5.12}$$

With the help of [135, Eq. (7.811.4)] and after some algebraic calculation, (5.12) can be solved as

$$E[\gamma^n]=\frac{\Gamma(mL+n)\Gamma(m+m_s-mL-n)}{\Gamma(m+m_s)\Gamma(mL)}\left(\frac{m}{m_s\bar{\gamma}}\right)^{-n}\left(\frac{\Gamma(m+m_s)}{\Gamma(m_s)}\right)^{L} \tag{5.13}$$

5.3.3 Amount of Fading

The definition of AF is given in (3.32). Therefore, by using (5.13) and (3.32), after performing some mathematical steps, the AF becomes

$$AF=\frac{(mL+1)\Gamma(mL)\Gamma(m+m_s)}{(m+m_s-mL-2)\Gamma(m+m_s-mL-1)\Gamma(mL+1)}\cdot\left(\frac{\Gamma(m_s)}{\Gamma(m+m_s)}\right)^{L}-1 \tag{5.14}$$

5.3.4 Average Bit Error Rate

ABER of L branch MRC diversity for $\mathcal{F}$ model is given by

$$P_e(E) = \int_0^{\infty} P_e(E/\gamma) f_{MRC}(\gamma) d\gamma \tag{5.15}$$

(A) NCFSK and BDPSK

The average error probability expression for BDPSK and NCFSK can be obtained with the help of Table 3.2

$$P_e(E) = 0.5 \cdot M_{MRC}(a) \tag{5.16}$$

By putting (5.9) into (5.16), the ABER can be obtained as

$$P_e(E) = \frac{0.5}{\Gamma(mL)\Gamma(m+m_s)} \left(\frac{m}{am_s\bar{\gamma}}\right)^{mL+1} \left(\frac{\Gamma(m+m_s)}{\Gamma(m_s)}\right)^{L} G_{3,2}^{1,3}\left(\frac{m}{am_s\bar{\gamma}}\middle| \begin{matrix} -mL, & -m-m_s, & -mL \\ -1, & -mL, & \end{matrix}\right) \tag{5.17}$$

where $a = 1$ for BDPSK and $a = 0.5$ for NCFSK.

(B) BFSK and BPSK

The average error probability for BPSK and BFSK is given by (Table 3.2)

$$P_e(E) = \frac{1}{\pi} \int_0^{\pi/2} M_{MRC}\left(\frac{a}{\sin^2\theta}\right) d\theta \tag{5.18}$$

By putting (5.9) into (5.18), (5.18) becomes

$$P_e(E) = \frac{1}{\pi\Gamma(mL)\Gamma(m+m_s)} \left(\frac{\Gamma(m+m_s)}{\Gamma(m_s)}\right)^{L} \left(\frac{m}{m_s\bar{\gamma}}\right)^{mL+1} \int_0^{\pi/2} \left(\frac{\sin^2\theta}{a}\right)^{mL+1} G_{3,2}^{1,3}\left(\frac{m\sin^2\theta}{am_s\bar{\gamma}}\middle| \begin{matrix} -mL, & -m-m_s, & -mL \\ -1, & -mL, & \end{matrix}\right) d\theta \tag{5.19}$$

Let $\sin^2\theta = t$ i.e. $2\sin\theta\cos\theta d\theta = dt$, after performing integration by substitution, (5.19) can be written as

$$P_e(E) = \frac{1}{2\pi\Gamma(mL)\Gamma(m+m_s)} \left(\frac{\Gamma(m+m_s)}{\Gamma(m_s)}\right)^{L} \left(\frac{m}{am_s\bar{\gamma}}\right)^{mL+1} \int_0^{1} t^{mL+1/2}(1-t)^{-1/2} G_{3,2}^{1,3}\left(\frac{mt}{am_s\bar{\gamma}}\middle| \begin{matrix} -mL, & -m-m_s, & -mL \\ -1, & -mL, & \end{matrix}\right) dt \tag{5.20}$$

By using [135, Eq. (7.811.2)], (5.20) becomes

$$P_e(E) = \frac{\Gamma(0.5)}{2\pi\Gamma(mL)\Gamma(m+m_s)} \left(\frac{\Gamma(m+m_s)}{\Gamma(m_s)}\right)^{L} \left(\frac{m}{am_s\bar{\gamma}}\right)^{mL+1} G_{4,3}^{1,4}\left(\frac{m}{am_s\bar{\gamma}}\middle| \begin{matrix} -mL-0.5, & -mL, & -m-m_s, & -mL \\ -1, & -mL, & -mL-1, & \end{matrix}\right) \tag{5.21}$$

(C) MAM

The ABER for MAM is given by (Table 3.2)

$$P_e(E) = \frac{2(M-1)}{M\pi \log_2(M)} \int_0^{\pi/2} M_{MRC}\left(\frac{g_{AM}}{\sin^2\theta}\right) d\theta \tag{5.22}$$

By following the similar step from (5.18)-(5.21), the solution of (5.22) can be obtained as

$$P_e(E) = \frac{(M-1)\Gamma(0.5)}{\pi M \log_2(M)\Gamma(mL)\Gamma(m+m_s)} \left(\frac{\Gamma(m+m_s)}{\Gamma(m_s)}\right)^L \left(\frac{m}{g_{AM} m_s \bar{\gamma}}\right)^{mL+1} G_{4,3}^{1,4}\left(\frac{m}{g_{AM} m_s \bar{\gamma}}\middle| \begin{matrix} -mL-0.5, & -mL, & -m-m_s, & -mL \\ -1, & -mL, & -mL-1, & \end{matrix}\right) \tag{5.23}$$

(D) MQAM

Exact analysis: The expression of ABER for square MQAM is defined as [150]

$$P_e(E) = \frac{4}{\pi \log_2(M)} \left\{ \left(1-\frac{1}{\sqrt{M}}\right) \int_0^{\pi/2} M_{MRC}\left(\frac{g_{MQAM}}{\sin^2(\theta)}\right) d\theta - \left(1-\frac{1}{\sqrt{M}}\right)^2 \int_0^{\pi/4} M_{MRC}\left(\frac{g_{MQAM}}{\sin^2(\theta)}\right) d\theta \right\} \tag{5.24}$$

By using [151, Eq. (19)], (5.24) becomes

$$P_e(E) = \frac{4}{\pi \log_2(M)} \left[\left(1-\frac{1}{\sqrt{M}}\right) \left\{ \frac{1}{12} M_{MRC}\left(g_{MQAM}\right) + \frac{1}{4} M_{MRC}\left(\frac{4}{3} g_{MQAM}\right) \right\} - \left(1-\frac{1}{\sqrt{M}}\right)^2 \left\{ \frac{1}{8} M_{MRC}\left(2 g_{MQAM}\right) \right\} \right] \tag{5.25}$$

By putting (5.9) into (5.25) and after performing some mathematical steps, the above expression can be written as

$$\begin{aligned} P_e(E) = \frac{4}{\pi \log_2(M)\Gamma(mL)\Gamma(m+m_s)} \left(\frac{\Gamma(m+m_s)}{\Gamma(m_s)}\right)^L \left(\frac{m}{m_s \bar{\gamma}}\right)^{mL+1} \Bigg[\left(1-\frac{1}{\sqrt{M}}\right) \Bigg\{ \frac{1}{12} \left(\frac{1}{g_{MQAM}}\right)^{mL+1} G_{3,2}^{1,3}\left(\frac{m}{m_s \bar{\gamma} g_{MQAM}}\middle| \begin{matrix} -mL, & -m-m_s, & -mL \\ -1, & -mL, & \end{matrix}\right) \\ + \frac{1}{4} \left(\frac{3}{4 g_{MQAM}}\right)^{mL+1} G_{3,2}^{1,3}\left(\frac{3m}{4 m_s \bar{\gamma} g_{MQAM}}\middle| \begin{matrix} -mL, & -m-m_s, & -mL \\ -1, & -mL & \end{matrix}\right) \Bigg\} \\ - \left(1-\frac{1}{\sqrt{M}}\right)^2 \left\{ \frac{1}{8} \left(\frac{1}{2 g_{MQAM}}\right)^{mL+1} G_{3,2}^{1,3}\left(\frac{m}{2 m_s \bar{\gamma} g_{MQAM}}\middle| \begin{matrix} -mL, & -m-m_s, & -mL \\ -1, & -mL, & \end{matrix}\right) \right\} \Bigg] \end{aligned} \tag{5.26}$$

Tight bound analysis: The conditional BER expression (tight bound) for MQAM over AWGN channels is given by [75]

$$P_e(E/\gamma) \le 0.2\exp\left(\sqrt{\frac{1.5\gamma}{(M-1)}}\right), \quad \gamma \ge 0, M \ge 4 \tag{5.27}$$

By putting (5.27) into (5.15), the ABER for MQAM (tight bound) can be expressed as

$$P_e(E) = 0.2\int_0^\infty f_{MRC}(\gamma)\exp\left(-\frac{1.5\gamma}{(M-1)}\right)d\gamma \tag{5.28}$$

With the help of (3.31), (5.28) becomes

$$P_e(E) = 0.2M_{MRC}\left(\frac{1.5}{(M-1)}\right) \tag{5.29}$$

By putting (5.9) into (5.29), the tight bound ABER expression for MQAM can be obtained as

$$P_e(E) = \frac{0.2}{\Gamma(mL)\Gamma(m+m_s)}\left(\frac{m(M-1)}{1.5m_s\bar{\gamma}}\right)^{mL+1}\left(\frac{\Gamma(m+m_s)}{\Gamma(m_s)}\right)^{L} G_{3,2}^{1,3}\left(\frac{m(M-1)}{1.5m_s\bar{\gamma}}\middle| \begin{matrix} -mL, & -m-m_s, & -mL \\ -1, & -mL, & \end{matrix}\right) \tag{5.30}$$

(E) MPSK

The ASER for MPSK in the term of MGF is defined by [8]

$$P_e(E) = \frac{1}{\pi}\int_0^{\pi-\pi/M} M_{MRC}\left(\frac{g_{MPSK}}{\sin^2(\theta)}\right)d\theta \tag{5.31}$$

where $g_{MPSK} = \sin^2(\pi/M)$

By using [151, Eq. (16)], (5.31) can be written as

$$P_e(E) = \left(\frac{\Theta}{2\pi}-\frac{1}{6}\right)M_{MRC}(g_{MPSK}) + \frac{1}{4}M_{MRC}\left(\frac{4}{3}g_{MPSK}\right) + \left(\frac{\Theta}{2\pi}-\frac{1}{4}\right)M_{MRC}\left(\frac{g_{MPSK}}{\sin^2\Theta}\right) \tag{5.32}$$

where $\Theta = \pi - \pi/M$

By putting (5.9) into (5.32), the ASER for MPSK becomes

$$P_e(E) = \frac{1}{\Gamma(mL)\Gamma(m+m_s)}\left(\frac{m}{m_s\bar{\gamma}}\right)^{mL+1}\left(\frac{\Gamma(m+m_s)}{\Gamma(m_s)}\right)^{L}\left[\left(\frac{\Theta}{2\pi}-\frac{1}{6}\right)\left(\frac{1}{g_{MPSK}}\right)^{mL+1} G_{3,2}^{1,3}\left(\frac{m}{m_s\bar{\gamma}g_{MPSK}}\middle| \begin{matrix} -mL, & -m-m_s, & -mL \\ -1, & -mL, & \end{matrix}\right)\right.$$

$$\left. + \frac{1}{4}\left(\frac{3}{4g_{MPSK}}\right)^{mL+1} G_{3,2}^{1,3}\left(\frac{3m}{4m_s\bar{\gamma}g_{MPSK}}\middle| \begin{matrix} -mL, & -m-m_s, & -mL \\ -1, & -mL, & \end{matrix}\right)\right]$$

$$+\left(\frac{\Theta}{2\pi}-\frac{1}{4}\right)\left(\frac{\sin^2\Theta}{g_{MPSK}}\right)^{mL+1} G_{3,2}^{1,3}\left(\frac{m\sin^2\Theta}{m_s\bar{\gamma}g_{MPSK}}\middle|\begin{matrix}-mL, & -m-m_s, & -mL\\ -1, & -mL, & \end{matrix}\right) \tag{5.33}$$

(F) NCMFSK

The CEP using NCMFSK is represented as (Table 3.1)

$$P_s(E/\gamma)=\frac{1}{M}\sum_{i=2}^{M}(-1)^i\binom{M}{i}\exp\left(-\left(1-\frac{1}{i}\right)\gamma\right) \tag{5.34}$$

By plugging (5.34) into (5.15), the ASER for NCMFSK can be written as

$$P_s(E)=\frac{1}{M}\sum_{i=2}^{M}(-1)^i\binom{M}{i}\int_0^{\infty} f_{MRC}(\gamma)\exp\left(-\left(1-\frac{1}{i}\right)\gamma\right)d\gamma \tag{5.35}$$

By substituting (5.4) into (5.35), therefore (5.35) becomes

$$P_e(E)=\frac{\sum_{i=2}^{M}(-1)^i\binom{M}{i}}{M\Gamma(mL)}\left(\frac{m}{m_s\bar{\gamma}}\right)^{mL}\left[\frac{\Gamma(m+m_s)}{\Gamma(m_s)}\right]^L\int_0^{\infty}\gamma^{mL-1}\exp\left(-\left(1-\frac{1}{i}\right)\gamma\right){}_2F_1\left(m+m_s,mL;mL;\frac{-m\gamma}{m_s\bar{\gamma}}\right)d\gamma \tag{5.36}$$

Using [135, Eq. (7.522.3)], the ASER for NCMFSK can be obtained as

$$P_e(E)=\frac{1}{M}\sum_{i=2}^{M}(-1)^i\binom{M}{i}\left(\left(1-\frac{1}{i}\right)\frac{m_s\bar{\gamma}}{m}\right)^{\frac{m+m_s-mL-1}{2}}\left[\frac{\Gamma(m+m_s)}{\Gamma(m_s)}\right]^L$$
$$\times\exp\left(\left(1-\frac{1}{i}\right)\frac{m_s\bar{\gamma}}{2m}\right)\cdot W_{\frac{1-m-m_s-mL}{2},\frac{m+m_s-mL}{2}}\left(\left(1-\frac{1}{i}\right)\frac{m_s\bar{\gamma}}{m}\right) \tag{5.37}$$

where $W_{a,b}(.)$ denotes the Whittaker function [135, Eq.(9.220)]. It is noted that for $M = 2$, (5.37) reduces to ABER for NCFSK (5.17).

5.3.5 Channel Capacity

For adaptive transmission, the cutoff SNR having optimal power must satisfy the following relationship [150]

$$\int_{\gamma_0}^{\infty}\left(\frac{1}{\gamma_0}-\frac{1}{\gamma}\right)f_{MRC}(\gamma)d\gamma=\int_{\gamma_0}^{\infty}\left(\frac{\gamma-\gamma_0}{\gamma_0\gamma}\right)f_{MRC}(\gamma)d\gamma=1 \tag{5.38}$$

By putting (5.4) into (5.38) and using [146, Eq. (2.21.1.13)], (5.38) can be solved as

$$\frac{1}{\gamma_0\Gamma(mL)}\left[\frac{\Gamma(m+m_s)}{\Gamma(m_s)}\right]^L\left\{{\gamma_0}^{mL}B(2,-mL)\left(\frac{m}{m_s\bar{\gamma}}\right)^{mL}{}_3F_2\left(m+m_s,mL,mL-1;mL,mL+1;\frac{-2m}{m_s\bar{\gamma}}\right)\right.$$

$$\left.+\frac{\Gamma(m+m_s-mL)}{\Gamma(m+m_s)}{}_3F_2\left(-1,m+m_s-mL,0;1-mL,0;\frac{-m\gamma_0}{m_s\bar{\gamma}}\right)\right\}=1 \tag{5.39}$$

(A) ORA

The Channel Capacity for ORA policy (in bit/second/Hz) can be obtained by putting (5.4) into (3.37) as

$$C_{ORA}=\frac{1}{\Gamma(mL)}\left(\frac{m}{m_s\bar{\gamma}}\right)^{mL}\left[\frac{\Gamma(m+m_s)}{\Gamma(m_s)}\right]^L\int_0^\infty\gamma^{mL-1}\log_2(1+\gamma){}_2F_1\left(m+m_s,mL;mL;\frac{-m\gamma}{m_s\bar{\gamma}}\right)d\gamma \tag{5.40}$$

Using (4.51) and (5.7), (5.40) becomes

$$C_{ORA}=\frac{1}{\ln(2)\Gamma(mL)\Gamma(m+m_s)}\left(\frac{m}{m_s\bar{\gamma}}\right)^{mL+1}\left[\frac{\Gamma(m+m_s)}{\Gamma(m_s)}\right]^L\int_0^\infty\gamma^{mL}G_{2,2}^{1,2}\left(\gamma\middle|\begin{matrix}1,&1\\1,&0\end{matrix}\right)G_{2,2}^{1,2}\left(\frac{m\gamma}{m_s\bar{\gamma}}\middle|\begin{matrix}-m-m_s,&-mL\\-1,&-mL\end{matrix}\right)d\gamma \tag{5.41}$$

By using [146, Eq. (2.24.1.1)], C_{ORA} can be obtained as

$$C_{ORA}=\frac{1}{\ln(2)\Gamma(mL)\Gamma(m+m_s)}\left(\frac{m}{m_s\bar{\gamma}}\right)^{mL+1}\left[\frac{\Gamma(m+m_s)}{\Gamma(m_s)}\right]^L G_{4,4}^{3,3}\left(\frac{m}{m_s\bar{\gamma}}\middle|\begin{matrix}-m-m_s,&-mL,&-mL-1,&-mL\\-1,&-mL-1,&-mL-1,&-mL\end{matrix}\right) \tag{5.42}$$

*Low SNR regime***:** By putting (5.4) into (3.39), the C_{ORA} in low SNR is given as

$$C_{ORA}^{LSNR}\cong\frac{1}{\ln(2)\Gamma(mL)}\left[\frac{\Gamma(m+m_s)}{\Gamma(m_s)}\right]^L\left(\frac{m}{m_s\bar{\gamma}}\right)^{mL}\int_0^\infty{}_2F_1\left(m+m_s,mL;mL;\frac{-m\gamma}{m_s\bar{\gamma}}\right)\gamma^{mL}d\gamma \tag{5.43}$$

With the help of (5.7) and [135, Eq. (7.811.4)], C_{ORA} expression for low SNR regime can be obtained as

$$C_{ORA}^{LSNR}\cong\frac{1}{\ln(2)}\frac{\Gamma(mL+1)\Gamma(m+m_s-mL-1)}{\Gamma(mL)\Gamma(m+m_s)}\left(\frac{m}{m_s\bar{\gamma}}\right)^{-1}\left(\frac{\Gamma(m+m_s)}{\Gamma(m_s)}\right)^L \tag{5.44}$$

High SNR regime: The C_{ORA} in high SNR can be obtained by putting (5.4) into (3.40) as follows

$$C_{ORA}^{HSNR}=\frac{1}{\Gamma(mL)}\left(\frac{m}{m_s\bar{\gamma}}\right)^{mL}\left[\frac{\Gamma(m+m_s)}{\Gamma(m_s)}\right]^{L}\int_0^{\infty}\gamma^{mL-1}\log_2(\gamma)\,{}_2F_1\left(m+m_s,mL;mL;\frac{-m\gamma}{m_s\bar{\gamma}}\right)d\gamma \tag{5.45}$$

By using (5.7), and [146, Eq. (8.4.6.11)], the above equation can also be expressed as

$$C_{ORA}^{HSNR}=\frac{1}{\ln(2)\Gamma(mL)}\left(\frac{m}{m_s\bar{\gamma}}\right)^{mL}\left[\frac{\Gamma(m+m_s)}{\Gamma(m_s)}\right]^{L}\int_0^{\infty}\gamma^{mL}(\gamma-1)G_{2,2}^{2,2}\left(\gamma\middle|\begin{matrix}0 & 0\\ 0 & 0\end{matrix}\right)G_{2,2}^{1,2}\left(\frac{m\gamma}{m_s\bar{\gamma}}\middle|\begin{matrix}-m-m_s, & -mL\\ -1, & -mL\end{matrix}\right)d\gamma \tag{5.46}$$

or,

$$C_{ORA}^{HSNR}=\frac{1}{\ln(2)\Gamma(mL)}\left(\frac{m}{m_s\bar{\gamma}}\right)^{mL}\left[\frac{\Gamma(m+m_s)}{\Gamma(m_s)}\right]^{L}\left[\underbrace{\int_0^{\infty}\gamma^{mL+1}G_{2,2}^{2,2}\left(\gamma\middle|\begin{matrix}0, & 0\\ 0, & 0\end{matrix}\right)G_{2,2}^{1,2}\left(\frac{m\gamma}{m_s\bar{\gamma}}\middle|\begin{matrix}-m-m_s, & -mL\\ -1, & -mL\end{matrix}\right)d\gamma}_{I_1}\right.$$

$$\left.-\underbrace{\int_0^{\infty}\gamma^{mL}G_{2,2}^{2,2}\left(\gamma\middle|\begin{matrix}0, & 0\\ 0, & 0\end{matrix}\right)G_{2,2}^{1,2}\left(\frac{m\gamma}{m_s\bar{\gamma}}\middle|\begin{matrix}-m-m_s, & -mL\\ -1, & -mL\end{matrix}\right)d\gamma}_{I_2}\right] \tag{5.47}$$

By using [146, Eq. (2.24.1.1)], (5.47) can be computed as

$$C_{ORA}^{HSNR}=\frac{1}{\log(2)\Gamma(mL)}\left(\frac{m}{m_s\bar{\gamma}}\right)^{mL}\left[\frac{\Gamma(m+m_s)}{\Gamma(m_s)}\right]^{L}\left[G_{4,4}^{3,4}\left(\frac{m}{m_s\bar{\gamma}}\middle|\begin{matrix}-mL-1, & -mL-1, & -m-m_s, & -mL\\ -mL-1, & -mL-1, & -1, & -mL\end{matrix}\right)\right.$$

$$\left.-G_{4,4}^{3,4}\left(\frac{m}{m_s\bar{\gamma}}\middle|\begin{matrix}-mL, & -mL, & -m-m_s, & -mL\\ -mL, & -mL, & -1, & -mL\end{matrix}\right)\right] \tag{5.48}$$

(B) CIFR

The Channel Capacity under CIFR protocol can be obtained by solving the integral term presented in (3.45) and using (5.4), it is given by

$$\int_0^{\infty}\frac{f_{MRC}(\gamma)}{\gamma}d\gamma=\frac{1}{\Gamma(mL)}\left(\frac{\Gamma(m+m_s)}{\Gamma(m_s)}\right)^{L}\left(\frac{m}{m_s\bar{\gamma}}\right)^{mL}\int_0^{\infty}{}_2F_1\left(m+m_s,mL;mL;\frac{-m}{m_s\bar{\gamma}}\right)\gamma^{mL-2}d\gamma \tag{5.49}$$

Using [146, Eq. (2.21.1.1)], (5.49) can be written as

$$\int_0^{\infty} \frac{f_{MRC}(\gamma)}{\gamma} d\gamma = \frac{1}{(mL)} \left(\frac{m}{m_s \bar{\gamma}} \right) \left(\frac{\Gamma(m+m_s)}{\Gamma(m_s)} \right)^L \frac{\Gamma(m+m_s-mL+1)}{\Gamma(m+m_s)} \tag{5.50}$$

By substituting (5.50) into (3.45), C_{CIFR} becomes

$$C_{CIFR} = \log_2 \left(1 + \left(\frac{\Gamma(m_s)}{\Gamma(m+m_s)} \right)^L \frac{m_s \bar{\gamma} \cdot L \cdot \Gamma(m+m_s)}{\Gamma(m+m_s-mL+1)} \right) \tag{5.51}$$

(C) TIFR

The Channel Capacity under TIFR protocol (in bit/sec/Hz) can be obtained by evaluating the integral term presented in (3.47) as

$$\int_{\gamma_0}^{\infty} \frac{f_{MRC}(\gamma)}{\gamma} d\gamma = \int_0^{\infty} \frac{f_{MRC}(\gamma)}{\gamma} d\gamma - \int_0^{\gamma_0} \frac{f_{MRC}(\gamma)}{\gamma} d\gamma \tag{5.52}$$

By putting (5.4) into (5.52), therefore (5.52) becomes

$$\int_{\gamma_0}^{\infty} \frac{f_{MRC}(\gamma)}{\gamma} d\gamma = \frac{1}{\Gamma(mL)} \left(\frac{\Gamma(m+m_s)}{\Gamma(m_s)} \right)^L \left(\frac{m}{m_s \bar{\gamma}} \right)^{mL} \left[\int_0^{\infty} {}_2F_1 \left(m+m_s, mL; mL; \frac{-m}{m_s \bar{\gamma}} \right) \gamma^{mL-2} d\gamma \right.$$
$$\left. - \int_0^{\gamma_0} \gamma^{mL-2} \, {}_2F_1 \left(m+m_s, mL; mL; \frac{-m}{m_s \bar{\gamma}} \right) d\gamma \right] \tag{5.53}$$

By using [146, Eq. (2.21.1.1) and Eq. (2.21.1.4)], (5.53) can be expressed as

$$\int_{\gamma_0}^{\infty} \frac{f_{MRC}(\gamma)}{\gamma} d\gamma = \left(\frac{\Gamma(m+m_s)}{\Gamma(m_s)} \right)^L \left\{ \frac{\Gamma(m+m_s-mL+1)}{\Gamma(m+m_s)} \left(\frac{1}{Lm_s \bar{\gamma}} \right) - \frac{{\gamma_0}^{mL-1}}{\Gamma(mL)} \left(\frac{m}{m_s \bar{\gamma}} \right)^{mL} B(mL-1,1) \right.$$
$$\left. \times \, {}_3F_2 \left(m+m_s, mL, mL-1; mL, mL; \frac{-m\gamma_0}{m_s \bar{\gamma}} \right) \right\} \tag{5.54}$$

By putting (5.54) into (3.47), the Channel Capacity for TIFR policy can be obtained as

$$C_{TIFR} = \log_2 \left(1 + \left(\frac{\Gamma(m_s)}{\Gamma(m+m_s)} \right)^L \frac{1}{A(\bar{\gamma})} \right) (1 - P_{out}) \tag{5.55}$$

where

$$A(\bar{\gamma}) = \left\{ \frac{\Gamma(m+m_s-mL+1)}{\Gamma(m+m_s)Lm_s\bar{\gamma}} - \left(\frac{m}{m_s\bar{\gamma}}\right)^{mL} \frac{\gamma_0{}^{mL-1}B(mL-1,1)}{\Gamma(mL)} {}_3F_2\left(m+m_s, mL, mL-1; mL, mL; \frac{-m\gamma_0}{m_s\bar{\gamma}}\right) \right\} \quad (5.56)$$

5.3.6 Results

The analytical and simulation results of $\mathcal{F}$ model with MRC diversity technique are illustrated in this section. The results are depicted in the term of several performance matrices like Channel Capacities, AF and Error Probability. Several modulation techniques are carried out for presenting the error rate results. Both Monte Carlo simulation results and achieved results show excellent agreement. With $m_s \to \infty$, the results obtained from derived mathematical expressions get closely overlapped with results reported in literature.

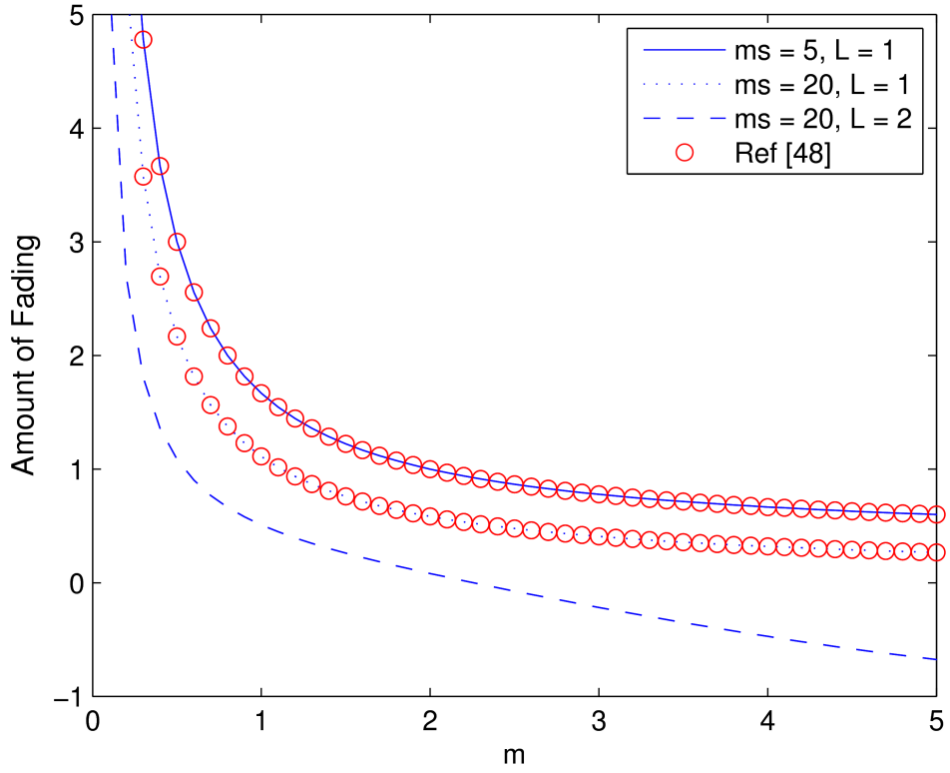

Figure 5.2: Amount of fading with m_s=5,20 and L=1,2.

Figure 5.2 depicts the AF versus m with L=1,2, and m_s=5,20. The AF curve goes down with increasing m. For large value of m, minimum AF is achieved. For MRC with single branch (L=1), the AF curve closely matches with AF results available in [48], as shown in Figure 5.2. In light shadowing environment (m_s=20), the AF has lower value because of lower severity in

shadowing. However, in moderate shadowing environment (m_s=5), the AF becomes high because of higher severity in shadowing. Thus, in Figure 5.2, the AF decreases as m_s varies (5to20) with constant L. The AF becomes almost constant at the higher value of m (m>4). It is the point to notice that, the AF is low for two branch MRC diversity technique.

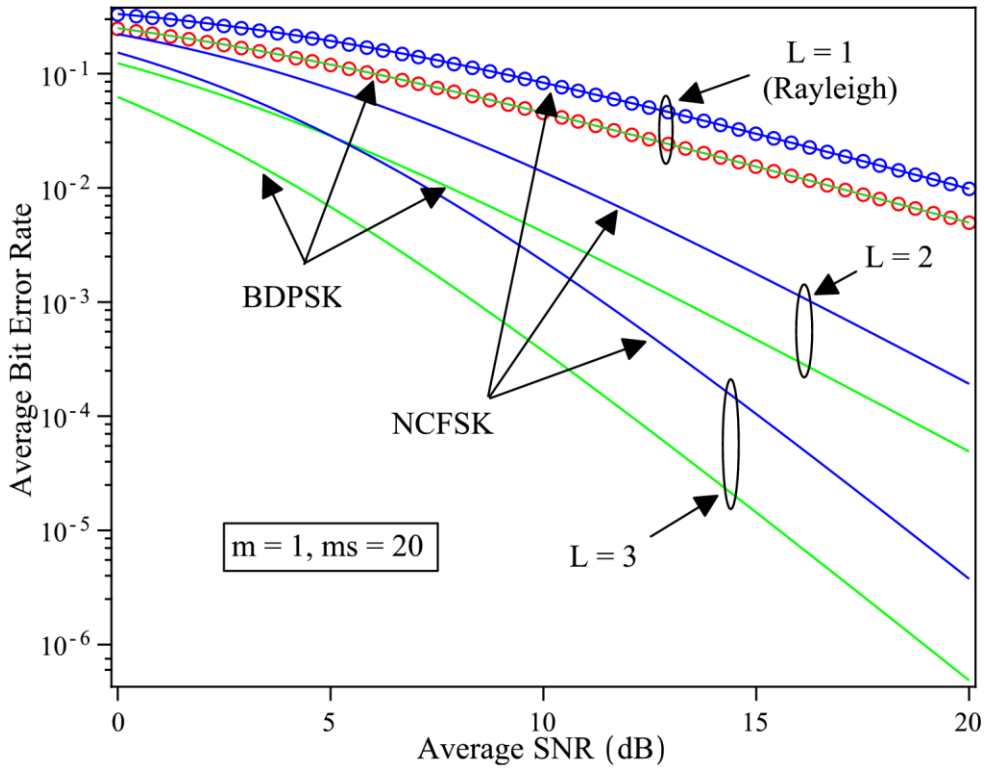

Figure 5.3: Error probability of NCFSK and BDPSK signaling with varying *L*.

Figure 5.3 represents the ABER of BDPSK and NCFSK for m_s=20, m=1 and L=1,2,3. In Figure 5.3, the NCFSK modulation technique has high error probability than BDPSK. Since the curve is plotted for light shadowing; therefore it converges to results of the Rayleigh model [9] for L=1. In Figure 5.3, by varying L (1 to 3), the ABER decreases for BDPSK (or NCFSK).

Figure 5.4 depicts the curve of error rate using BDPSK and NCFSK modulation technique for m_s=0.5,20, and m=1,2 with L=2. For the lower severity parameter (m), the error rate is high for any fixed m_s as shown in Figure 5.4. It is the point to be noted that the error rate curve for BDPSK outperforms the NCFSK. In Figure 5.4, the ABER reduces as m increases with constant m_s and any modulation technique. Also, the error rate graph decreases slightly by increasing m_s (0.5 to 20) with constant m.

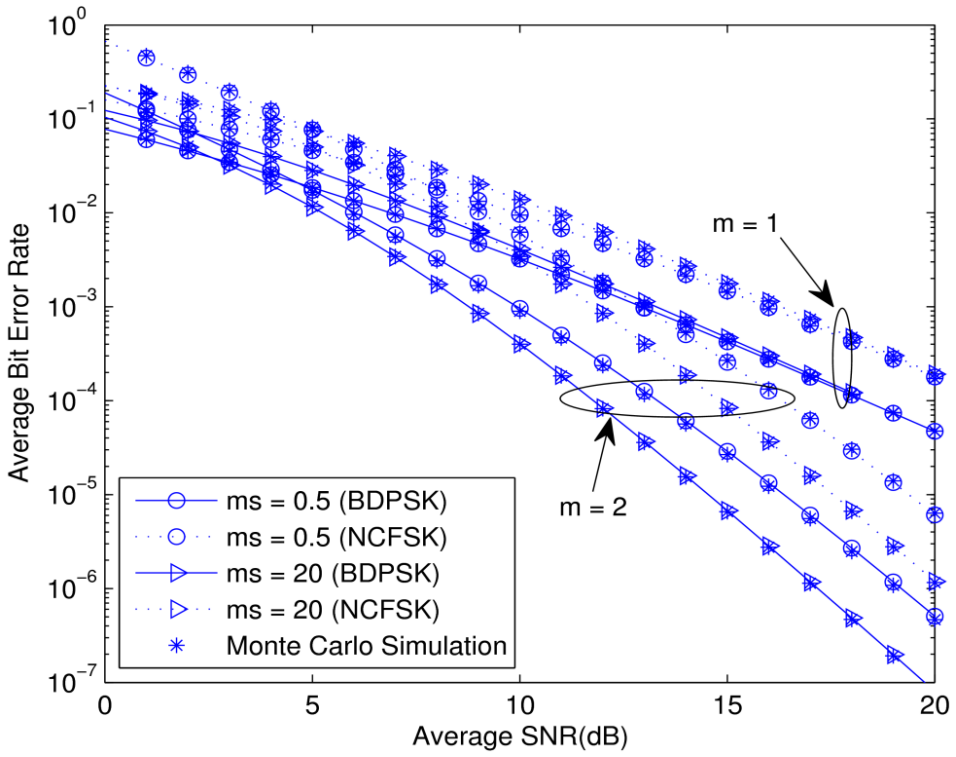

Figure 5.4: Error probability of NCFSK and BDPSK with m_s and m varying.

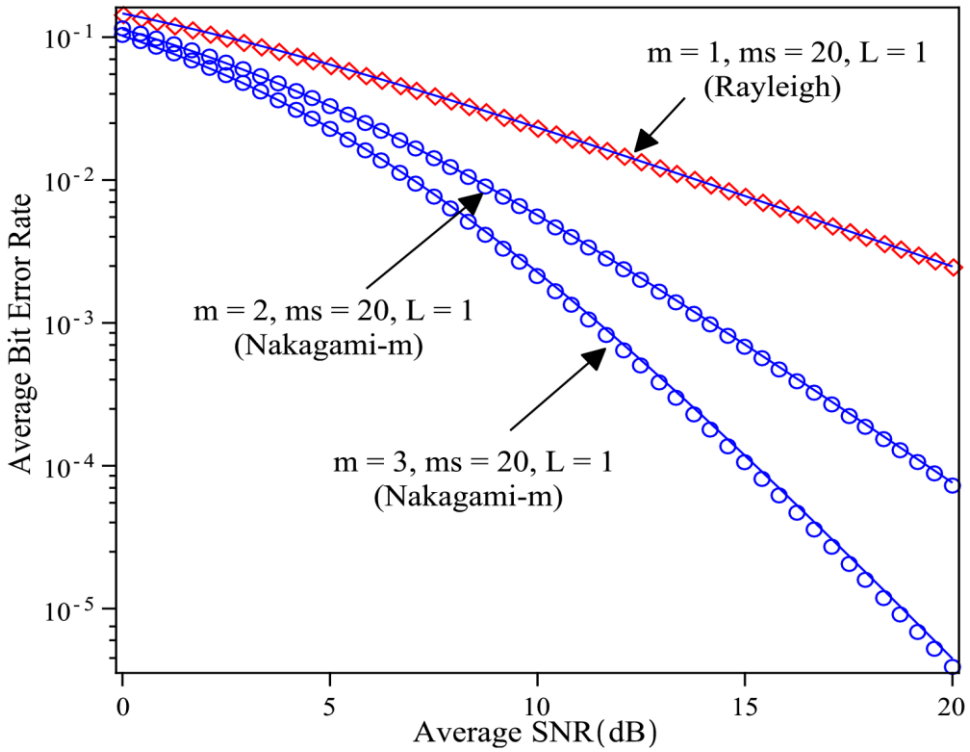

Figure 5.5: ABER comparison using BPSK with several fading distributions for m=1,2,3, m_s=20, and L=1.

Figure 5.5 shows the ABER comparison curve using BPSK technique for m_s=20, m=1,2,3, and L=1 with Rayleigh [9, Eq. (4.134)] and Nakagami-m [9, Eq. (4.138)]. In Figure 5.5, the ABER decreases sharply by increasing m. For higher m, the fading becomes less severe and therefore minimum error rate is achieved as illustrated in Figure 5.5.

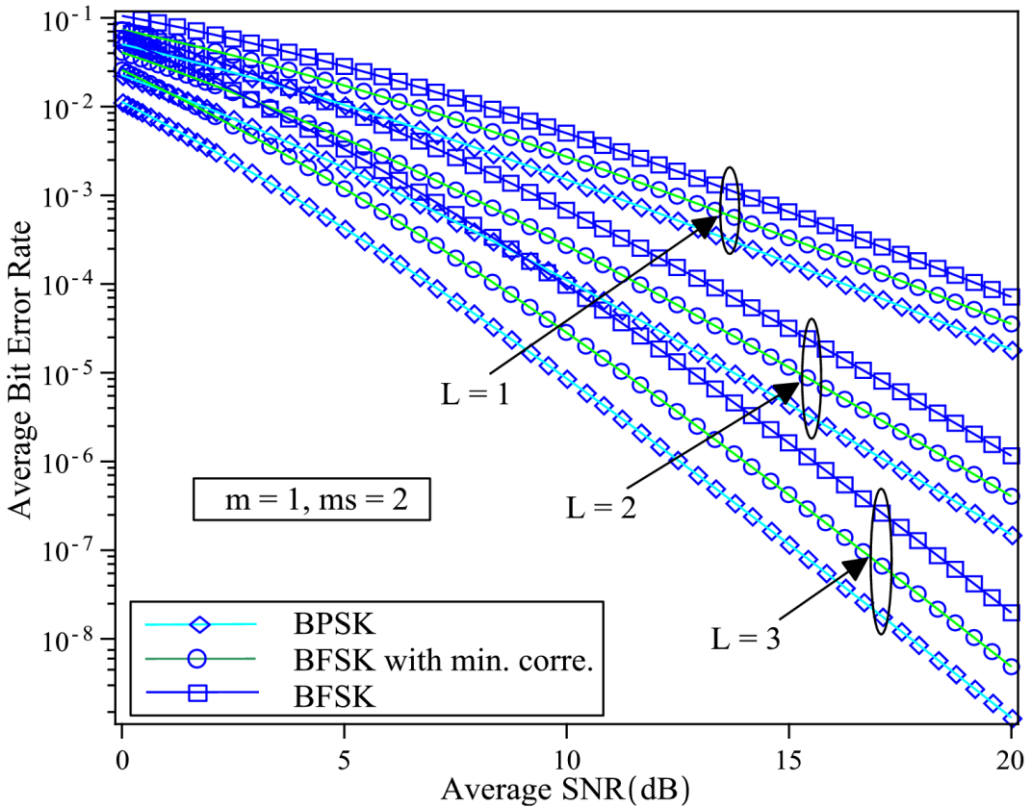

Figure 5.6: ABER using BFSK and BPSK signaling with *L* varying.

Figure 5.6 depicts the error rate comparison curves between BPSK and BFSK technique with m_s=2 and m=1 up to three diversity branches. In Figure 5.6, the ABER decreases as L increases from 1 to 3. More importantly, the BFSK technique shows higher error probability than BPSK for constant m_s, m, and L. Moreover, BFSK with minimum correlation represents minimum ABER in comparison with BFSK modulation scheme.

The error probability for BFSK and BPSK signaling for different diversity branches is tabulated in Table 5.1. It is clear that three branch diversity has achieved minimum error probability for any modulation scheme. Moreover, BPSK signaling has a minimum error rate than the BFSK signaling for fixed L.

Table 5.1: Error rate comparisons of BPSK, BFSK, and BFSK with minimum correlation for m=1 and m_s=2 at 15 dB average SNR.

Modulation Scheme	ABER	Number of Branches (L)
BPSK	1.07×10^{-7}	3
BFSK with min. corre.	3.82×10^{-7}	3
BFSK	1.52×10^{-6}	3
BPSK	3.88×10^{-6}	2
BFSK with min. corre.	1.05×10^{-5}	2
BFSK	2.68×10^{-5}	2
BPSK	1.66×10^{-4}	1
BFSK with min. corre.	3.21×10^{-4}	1
BFSK	5.9×10^{-4}	1

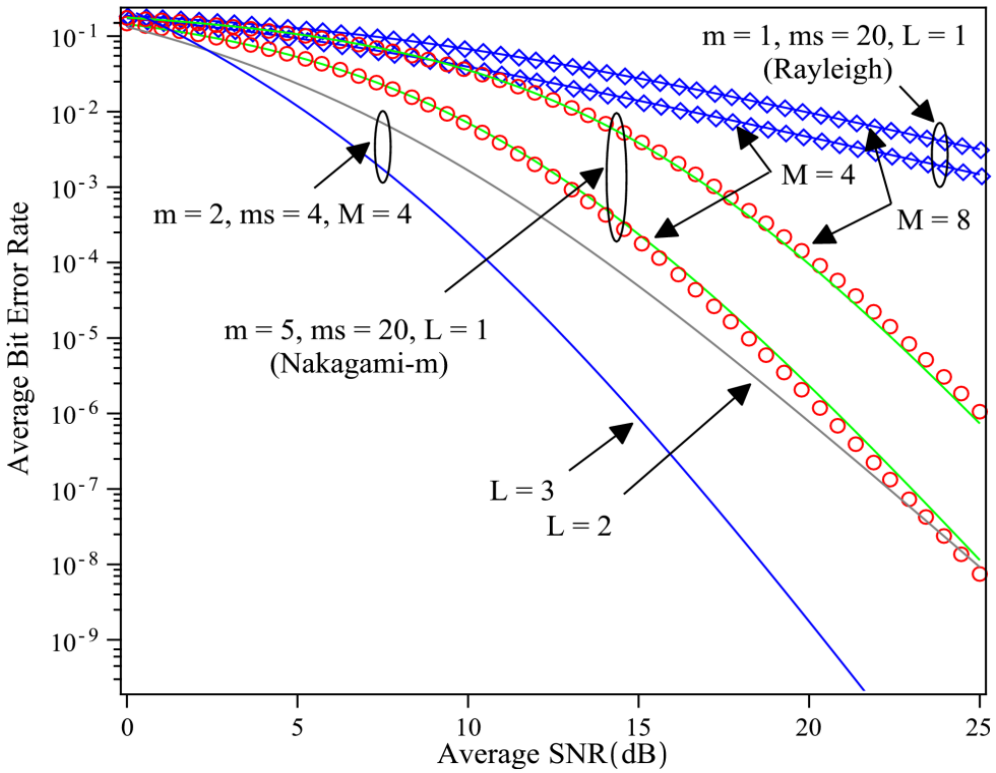

Figure 5.7: Error probability of MAM signaling with M=4,8.

Figure 5.7 depicts the ABER for 4-AM and 8-AM with m=1,2,5 and L=1,2,3 under moderate (m_s = 4) and light shadowing environment (m_s=20). The error rate comparisons are carried out with the relevant results of Nakagami-m [8, Eq. (8.106)] and Rayleigh model [8, Eq. (8.103)]. The BER (MAM) result is obtained from the derived expression given in (5.23). In Figure 5.7, the BER (using 4-AM) becomes minimum by varying the L between 2 and 3 with m_s=4, and m=2. For the case of no shadowing (m_s=20), the error rate of 4-AM technique outperforms the 8-AM technique with m_s=20, m=5 (or 1), and no diversity (L=1). In Figure 5.7, by varying m (1to5) in light shadowing environment (m_s=20) with L=1, a sharp improvement in ABER performance is observed.

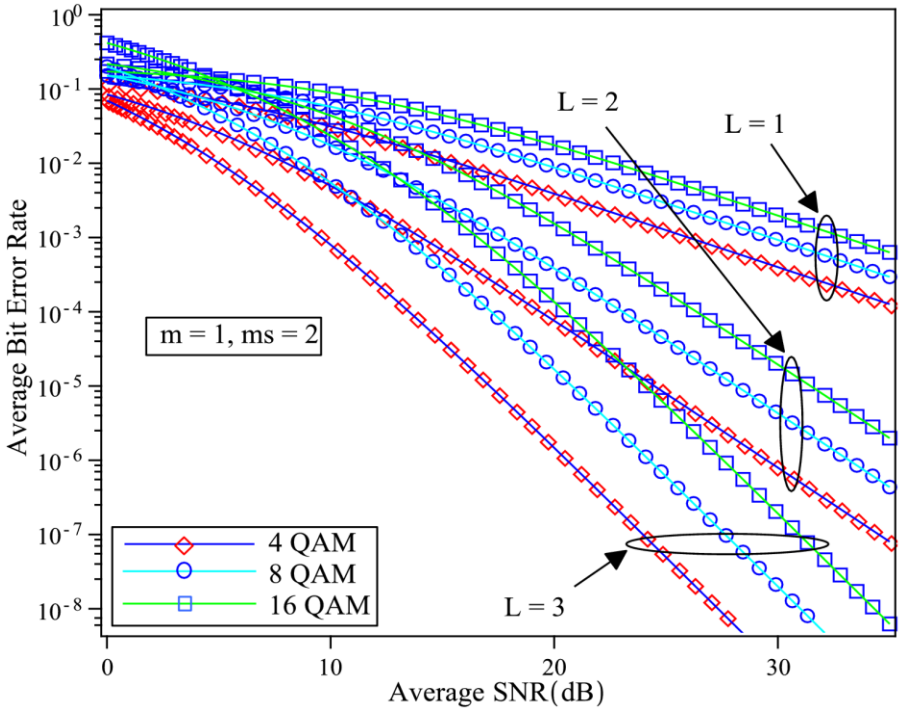

Figure 5.8: ABER using 4-QAM, 8-QAM and 16-QAM for m=1, m_s=2 with L=1,2,3.

Figure 5.8 depicts the ABER for MQAM (M=4,8,16) with m=1, m_s=2 and L=1,2,3. In Figure 5.8, on increasing the modulation index (M=4to16) for any value of L, the BER performance degrades as expected. Also, on increasing L (1to3) for any value of M, the BER decreases.

Figure 5.9 illustrates the ABER of MPSK for m=1,5, M=4,8, and L=1,2 in light shadowing environment. The BER comparisons are performed with Nakagami-m [8, Eq. (8.115)] and Rayleigh [8, Eq. (8.113)] for no diversity. In Figure 5.9, the error probability decreases as L

increases with constant m_s, M, m. From the curves, it clear that the ABER performance improves as m increases with constant m_s, M, L.

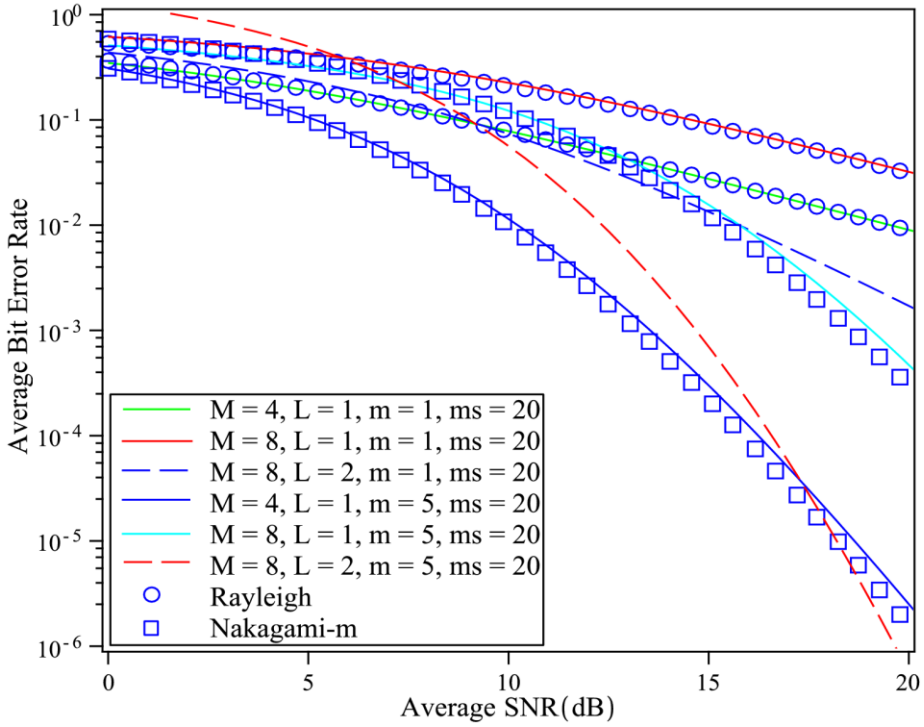

Figure 5.9: ABER using 4-PSK and 8-PSK for m=1, 5, m_s=20 and L=1,2.

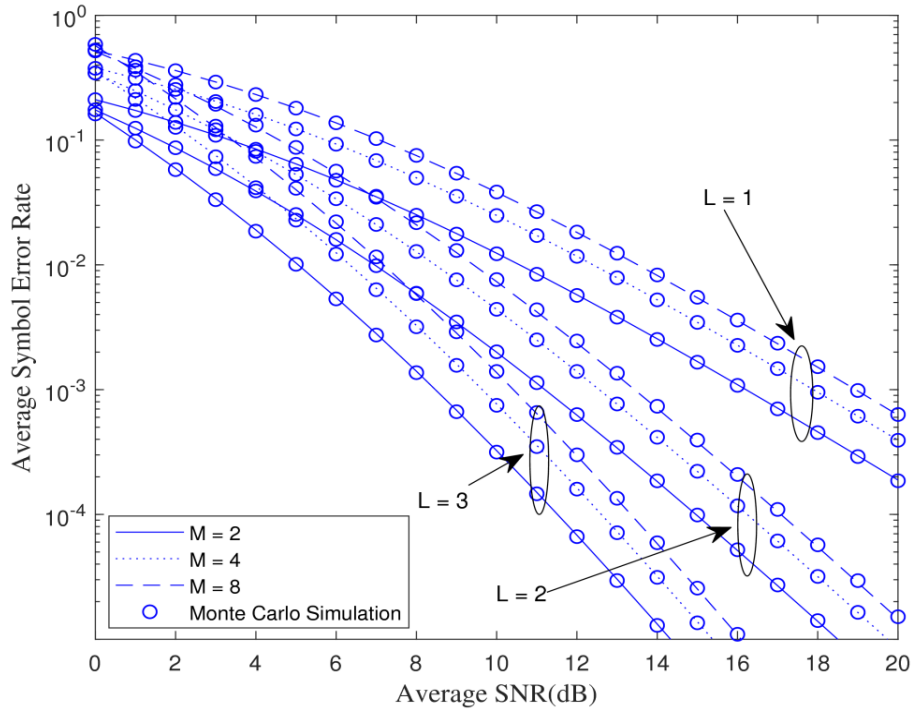

Figure 5.10: ASER using NCMFSK technique with varying L.

Figure 5.10 depicts the plot of ASER for NCMFSK with m=1, m_s=2, M=2,4,8 and L=1,2,3. The result is obtained from the derived expression presented in (5.37). In Figure 5.10, the lowest error rate is obtained for larger diversity branch with constant modulation index. Also, on increasing M (2 to 8) with fixed L, the BER performance degrades.

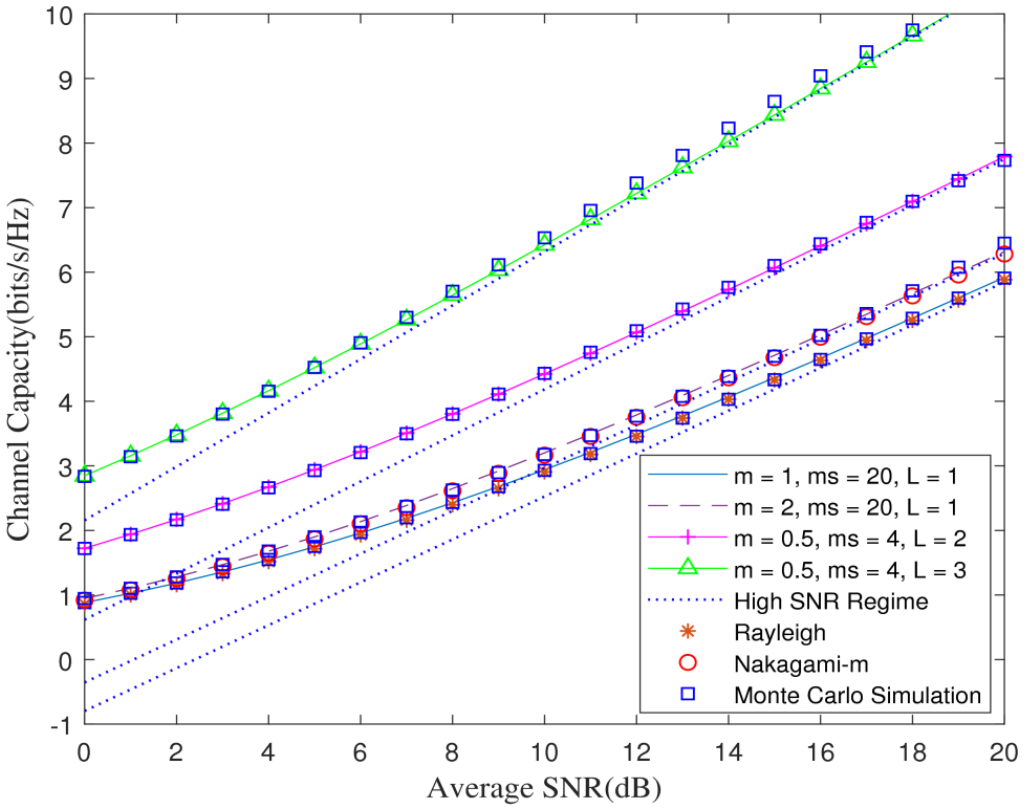

Figure 5.11: Capacity with ORA method for m=0.5,1,2, m_s=4,20 and L=1,2,3.

Figure 5.11 depicts the capacities comparison curve of ORA scheme with up to 3-branch diversity. The C_{ORA} of $\mathcal{F}$ model (5.42) converges to C_{ORA} of Nakagami-m [9, Eq. (4.207)], and Rayleigh [51, Eq. (36)] with no diversity (L=1). In Figure 5.11, higher capacity is achieved for higher diversity branch (L=3). At high SNR regime, both exact and asymptotic C_{ORA} show excellent agreement. The capacity improvement is seen as m increases between 1 and 2 with m_s=20, L=1 as illustrated in Figure 5.11. The channel capacity increases as the average SNR increases.

The capacity curve of CIFR technique for several diversity branches is shown in Figure 5.12. In Figure 5.12, C_{CIFR} increases as the diversity branch varies (L=1 to 3) with constant m_s and m. The capacity performance also improves by increasing the average SNR as expected.

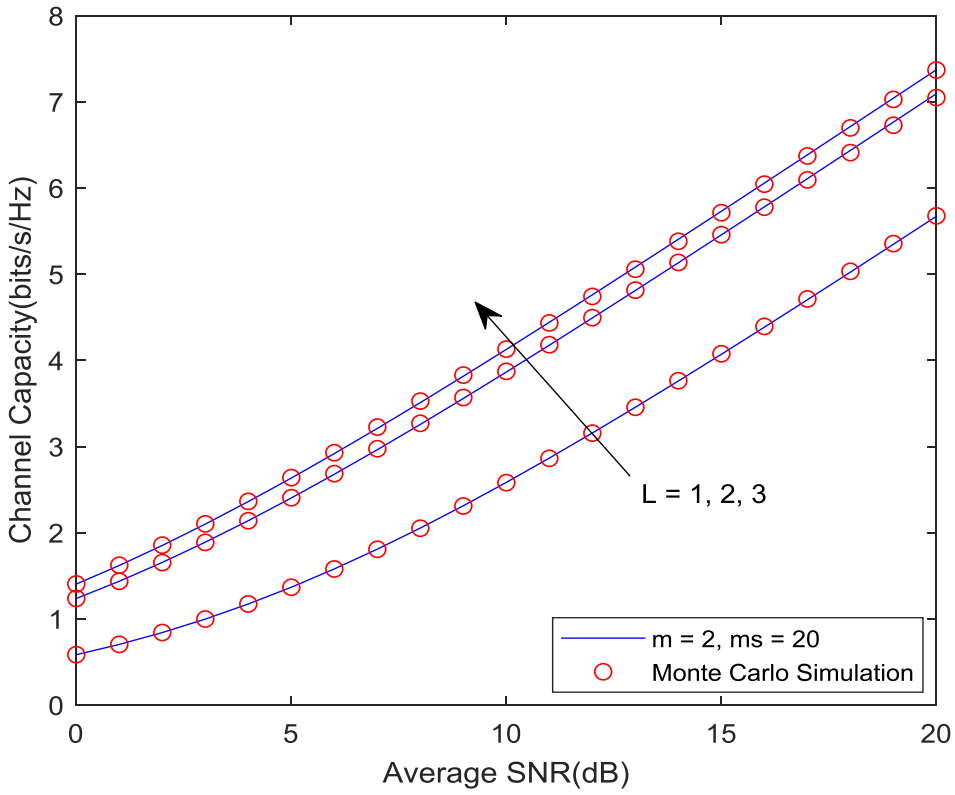

Figure 5.12: Capacity with CIFR method for m_s=20, m=2 and L=1,2,3.

The comparison between C_{CIFR} and C_{TIFR} technique is presented in Figure 5.13. The results of C_{CIFR} and C_{TIFR} are plotted using derived expression shown in (5.51) and (5.55), respectively. The effects of shadowing can be observed in the amount of data transmission using Figure 5.13. In the case of no shadowing (m_s=40), the capacity has high value, and however, for the case of moderate shadowing (m_s=10), a low capacity value is achieved. The C_{CIFR} has a lower value than C_{TIFR} because this technique sends a high amount of power to the R_X. However, C_{TIFR} sends the power to R_X only above the cutoff SNR level.

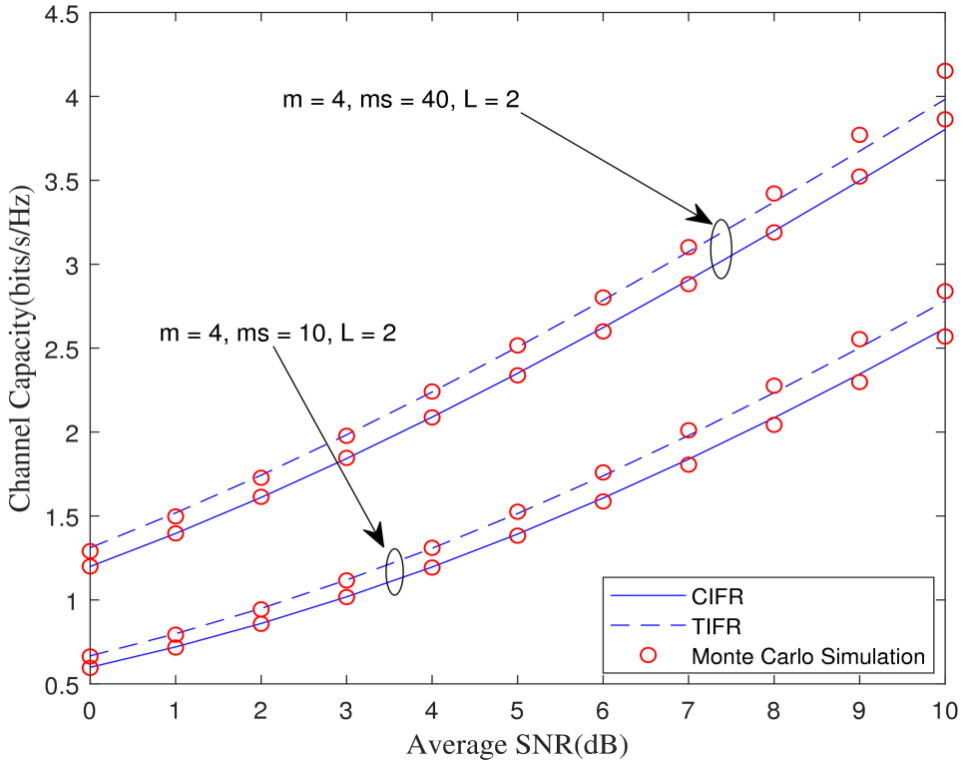

Figure 5.13: Capacities comparison between TIFR and CIFR method.

5.4 Contribution

The analysis of $\mathcal{F}$ model for i.i.d. MRC receiver has been presented. Correspondingly, the expressions of Moments, AF, Capacities, and Error Probabilities using several signaling techniques have been computed. The performance improvement at the output of the MRC receiver for $\mathcal{F}$ shadowed fading model depends on m, m_s, and L. The numerical results have been presented for different values of m under light shadowing ($m_s \to \infty$) and deeply shadowing environment ($m_s \to 0$). For the case of no diversity and $m_s \to \infty$, the achieved results converge to several fading distributions results. In the case of higher m, the Error Probabilities and AF become lower. Moreover, on increasing L at the output of MRC diversity, the overall performance improved as expected. Thus, it can be concluded that the MRC diversity has a significant role to enhance the quality and reliability of the signal at the receiver output.

The contributions of this Chapter are as below:

- The expressions of Moments, MGF, and AF are derived mathematically.

- The Average Error Probability expressions for several modulation schemes are computed.
- The Capacity for ORA method is computed.
- To go more insight, the Asymptotic Capacity for ORA protocol in low and high SNR region are computed mathematically.
- The Capacity expressions for CIFR and TIFR methods are derived.
- The results converge to special cases that show the generality of $\mathcal{F}$ model.

Based on the research outcomes reported in this Chapter, it is concluded that performance of $\mathcal{F}$ shadowed fading model using MRC diversity has been improved. Therefore, the research hypothesis statement is absolutely correct.

Published papers related to this Chapter:

(1) Hari Shankar, Ankush Kansal, "MGF-based Analysis of Maximum Ratio Combining Receiver over Fisher-Snedecor Composite Fading Channel", International Journal of Innovative Technology and Exploring Engineering (IJITEE), vol-8(9S), pp. 1-8, 2019.

(2) Hari Shankar, Ankush Kansal, "Performance Analysis of MRC Receiver over Fisher Snedecor (F) Composite Fading Channels". Wireless Personal Communications, Springer, 2020.

Chapter 6

Shadowed Fading Model using OFDM and FrFT OFDM System

The spreading of the signal occurs in time domain (time taken by the signal between Tx and Rx) when it propagates through the multiple paths, which causes ISI. Additionally, the signal may undergo frequency-selective fading which distorts the shape of the signal and also challenging to detect the signal. This ISI impairment can be overcome by enhancing the OFDM technique at Tx and Rx. Also, because of movements of Tx and/or Rx (and surrounding objects also), the signal may spread in the frequency domain (Doppler spread) which causes ICI. The conventional OFDM systems suffer from CFO and do not cooperate with ICI. The FrFT based OFDM technique can efficiently deal with ICI (or effects of Doppler spread). Moreover, SFBC-OFDM provides high reliability, high data rate, high spectral efficiency in the wireless system.

In this Chapter, the performance of uncoded OFDM and SFBC-OFDM is analyzed in the term of ABER for two shadowed fading channels. Mainly, MPSK and MQAM modulation techniques are used to obtain BER expressions. The results are demonstrated for various shadowed fading parameters.

6.1 Introduction

In a real indoor radio environment, both phenomena i.e. delay spread (that causes ISI) and Doppler spread (that causes ICI) may happen simultaneously. The common methods to overcome the ICI effect are to use the ICI self-cancellation and receiver windowing [152-154]. The use of OFDM with FrFT is also the best method to overcome the ICI impairments. The performance analysis of the conventional OFDM and FrFT-OFDM systems has been provided in many literatures [113-134]. Generally, Nakagami-*N*/gamma, κ-μ, Rayleigh, Nakagami-*m*, and TWDP fading distribution were employed to evaluate the performance over conventional OFDM and FrFT-OFDM systems.

SFBC-OFDM system provides a high data rate, high spectral efficiency, and reliability improvement. Performances of SFBC encoded OFDM over various multipath fading (Nakagami-

m, Rayleigh, κ-μ, TWDP) and shadowed fading (*K*, Generalized K) channels have been elaborated in many literatures [113, 120-124].

In this Chapter, the performance of uncoded OFDM and SFBC-OFDM systems for two recently proposed shadowed fading models (κ-μ/gamma and $\mathcal{F}$) are evaluated.

Research hypothesis test: The error probability performance of FrFT based OFDM is better in comparison with FFT based OFDM.

6.2 System Model

Considering the transmitting and receiving OFDM system with SFBC encoder that contains V number of subchannels and each subchannels is divided into V_a number of subbands, $V_a = V/t$, where t is symbol duration. As given in Figure 6.1, at the starting, the serial data sequence is converted into parallel data sequence which is mapped onto carrier signal using MQAM/MPSK modulator. The modulated data signal $A = \{a[0], a[1].....a[V_q\text{-}1]$ is passes through the SFBC encoder having R_c coded rate, where $V_q = V \times R_c$. The output of the SFBC encoder passes through the OFDM multicarrier modulator (operated in Fourier and Fractional domain) which covert the discrete-frequency signal component into the discrete-time signal component. After adding CP, the signals are transmitted through the M_T number of transmitting antennas.

At the receiving section, the received signals are denoted by $Y_1, Y_2,...Y_{M_R}$. At the receiver, the CP becomes removed from the received signal, and the remaining received signal component passes towards the FrFT/FFT block that outputs the discrete frequency signal components $b_1, b_2,...b_{M_R}$. These frequency signal components pass through the SFBC decoder and demodulator. After go through the parallel to serial converter, the received serial sequence is represented as

$$B_j = \sum_{i=1}^{M_T} H_{j,i} A_i + C_j \quad , 1 \le j \le M_R \tag{6.1}$$

where $(C_j = c_j[0], c_j[1],..... c_j[V\text{-}1])^T$ represents the AWGN, $(A_i = a_i[0], a_i[1],..... a_i[V/t\text{-}1])^T$ denotes the transmitting signals at i^{th} transmit antennas and $(B_j = b_j[0], b_j[1],..... b_j[V\text{-}1])^T$ is receiving signal at j^{th} receive antennas. $H_{j,i} = diag\{H_{j,i}[\lambda]\}_{\lambda=0}^{V-1}$ denotes the channel frequency response.

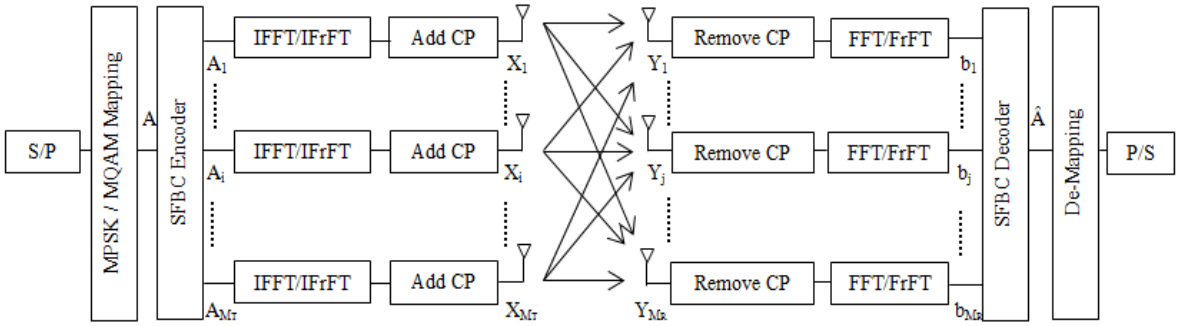

Figure 6.1: Structure of SFBC encoded OFDM Model.

6.3 Error Probability of OFDM with FFT

The basic formula to obtain the BER is given in (3.33) which will be used here to derive such expressions.

6.3.1 Error Probability of Uncoded OFDM with FFT

At the receiving OFDM section, the received signal (b) at FFT output is represented as

$$b[\lambda] = H[\lambda]a[\lambda] + c[\lambda] \tag{6.2}$$

where $\lambda = 0,.....,V\text{-}1$

Its matrix representation is

$$\mathrm{B} = \mathrm{H} \cdot \mathrm{A} + \mathrm{C} \tag{6.3}$$

where $\mathrm{A} = (a[0],....a[V\text{-}1])^T$ represents the transmitting signal, $\mathrm{B} = (b[0],....b[V\text{-}1])^T$ denotes the receiving signal, $H = diag\{H[k]\}_{\lambda=0}^{V-1}$ is diagonal matrix having size $V \times V$, and $\mathrm{C} = (c[0],....c[V\text{-}1])^T$ is the AWGN.

At the output of receiving OFDM section, the Conditional BER is given as [113, Eq. (16)]

$$P_e(E/\gamma) = \frac{1}{V}\sum_{\lambda=0}^{V-1} P_{e[\lambda]}(E/\gamma) \tag{6.4}$$

where $P_{e[\lambda]}(E/\gamma)$ denotes the CEP of λ^{th} subchannel. The expression of CEP for OFDM technique is [113, Eq. (17)]

$$P_{e[\lambda]}(E/\gamma) = \xi_1 erfc\left(\sqrt{\xi_2 \gamma}\right) \tag{6.5}$$

where, for MPSK $\xi_1 = 1/\log_2(M)$, $\xi_2 = \sin^2(\pi/M)$, and for MQAM $\xi_1 = (2/\log_2(M)) \cdot (1 - 1/\sqrt{M})$, $\xi_2 = 1.5/(M-1)$. $\gamma = |H[\lambda]|^2 E_a / N_0$ denotes the instantaneous SNR. Let us consider, each sub-channels has same CEP. So, net CEP becomes

$$P_e(E/\gamma) = \xi_1 erfc\left(\sqrt{\xi_2 \gamma}\right) \tag{6.6}$$

By putting (6.6) into (3.33), the exact error rate of conventional OFDM in shadowed channels is given by

$$P_e(E) = \xi_1 \int_0^\infty erfc\left(\sqrt{\xi_2 \gamma}\right) f_\gamma(\gamma) d\gamma \tag{6.7}$$

An approximate CEP expression is [113]

$$P_{e[\lambda]}(E/\gamma) = \xi_3 \exp(-\xi_4 \gamma) \tag{6.8}$$

where for MPSK $\xi_3 = 0.2$, $\xi_4 = 7/(2^{1.9\log_2 M} + 1)$, and for MQAM $\xi_3 = 0.2$, $\xi_4 = 1.6/(M\text{-}1)$.

Now, the expression of conditional BER by letting V identical sub-channels can be given as

$$P_e(E/\gamma) = \xi_3 \exp(-\xi_4 \gamma) \tag{6.9}$$

On substituting (6.9) into (3.33), the approximate ABER expression over shadowed fading channels is given by

$$P_e(E) = \xi_3 \int_0^\infty f_\gamma(\gamma) \exp(-\xi_4 \gamma) d\gamma \tag{6.10}$$

With the help of (3.31), the above equation can be written as

$$P_e(E) = \xi_3 M_\gamma(\xi_4) \tag{6.11}$$

(A) $\mathcal{F}$ Model

By substituting (3.16) into (6.7), the Error Probability expression of $\mathcal{F}$ model is obtained as

$$P_e(E) = \xi_1 \int_0^{\infty} erfc\left(\sqrt{\xi_2 \gamma}\right) \frac{m^m \cdot (m_s \bar{\gamma})^{m_s} \gamma^{m-1}}{B(m, m_s)(m\gamma + m_s \bar{\gamma})^{m+m_s}} d\gamma \tag{6.12}$$

or

$$P_e(E) = \frac{\xi_1}{B(m, m_s)} \left(\frac{m_s \bar{\gamma}}{m}\right)^{m_s} \int_0^{\infty} erfc\left(\sqrt{\xi_2 \gamma}\right) \frac{\gamma^{m-1}}{(\gamma + m_s \bar{\gamma}/m)^{m+m_s}} d\gamma \tag{6.13}$$

Let $\gamma = x^2$ i.e. $d\gamma = 2xdx$. With the help of integral by substitution property and after performing some mathematical steps, (6.13) becomes

$$P_e(E) = \frac{\xi_1}{B(m, m_s)} \left(\frac{m_s \bar{\gamma}}{m}\right)^{m_s} \int_0^{\infty} erfc\left(\sqrt{\xi_2 x^2}\right) \frac{x^{2m-1}}{(x^2 + m_s \bar{\gamma}/m)^{m+m_s}} dx \tag{6.14}$$

By using [155, Eq. (2.8.3.4)] and after performing some mathematical steps, (6.14) can be obtained as

$$P_e(E) = \frac{\xi_1 \Gamma(m + 0.5)}{B(m, m_s)\sqrt{\pi} m \xi_2^{\,m}} {}_3F_1\left(m + m_s, m, m + 0.5; m + 1; \frac{-m}{\xi_2 m_s \bar{\gamma}}\right) \left(\frac{m_s \bar{\gamma}}{m}\right)^{-m} \tag{6.15}$$

where, ${}_3F_1(\cdot,\cdot,\cdot;\cdot;\cdot)$ denotes the Gauss hypergeometric function [146].

The expression of approximate Error Rate can be obtained by putting (3.17) into (6.11)

$$P_e(E) = \frac{\xi_3}{\Gamma(m)\Gamma(m_s)} G_{2,1}^{1,2}\left(\frac{m}{m_s \bar{\gamma} \xi_4} \middle| \begin{matrix} 1 - m_s, & 1 \\ m, & 0 \end{matrix}\right) \tag{6.16}$$

(B) κ-μ/gamma Model

By putting (4.14) into (6.7), the expression of Error Probability for OFDM becomes

$$P_e(E) = \sum_{j=0}^{\infty} \frac{2\mu^{\frac{\alpha+\mu+3j}{2}} \kappa^j (1+\kappa)^{\frac{\alpha+\mu+j}{2}} \xi_1}{j! \exp(\mu\kappa)\Gamma(\alpha)\Gamma(\mu + j)\beta^{\frac{\alpha+\mu+j}{2}}} \left(\frac{\Omega}{\bar{\gamma}}\right)^{\frac{\alpha+\mu+j}{2}} \int_0^{\infty} erfc\left(\sqrt{\xi_2 \gamma}\right) \gamma^{\frac{\alpha+\mu+j-2}{2}} K_{\alpha-\mu-j}\left(2\sqrt{\frac{\mu(1+\kappa)\Omega\gamma}{\beta\bar{\gamma}}}\right) d\gamma \tag{6.17}$$

The erfc(·) and $G_{p,q}^{m,n}[\cdot|\cdot]$ functions are related by following mathematical formula [146, Eq. (8.4.14.2)]

$$erfc\left(\sqrt{\xi_2\gamma}\right)=G_{1,2}^{2,0}\left(\xi_2\gamma\left|\begin{matrix}1\\0,0.5\end{matrix}\right.\right) \tag{6.18}$$

By putting (4.17) and (6.18) into (6.17), the ABER becomes

$$P_e(E)=\frac{\xi_1}{\sqrt{\pi}}\sum_{j=0}^{\infty}\frac{(\mu\kappa)^j}{j!\Gamma(\mu+j)\exp(\mu\kappa)\Gamma(\alpha)}\left(\frac{\mu(1+\kappa)\Omega}{\beta\bar{\gamma}}\right)^j\int_0^{\infty}G_{1,2}^{2,0}\left(\xi_2\gamma\left|\begin{matrix}1\\0,0.5\end{matrix}\right.\right)G_{0,2}^{2,0}\left(\frac{\mu(1+\kappa)\Omega}{\beta\bar{\gamma}}\gamma\left|\begin{matrix}\\\alpha-1,\mu+j-1\end{matrix}\right.\right)d\gamma \tag{6.19}$$

With the help of [135, Eq. (7.811.1)], (6.19) becomes

$$P_e(E)=\sum_{j=0}^{\infty}\frac{(\mu\kappa)^j\xi_1}{j!\Gamma(\mu+j)\exp(\mu\kappa)\sqrt{\pi}\Gamma(\alpha)}\left(\frac{\mu(1+\kappa)\Omega}{\xi_2\beta\bar{\gamma}}\right)^j G_{2,3}^{2,2}\left(\frac{\mu(1+\kappa)\Omega}{\xi_2\beta\bar{\gamma}}\left|\begin{matrix}0, & -0.5\\\alpha-1, & \mu+j-1, \quad -1\end{matrix}\right.\right) \tag{6.20}$$

The ABER expression (approximate) is computed by putting (4.19) into (6.11) as

$$P_e(E)=\sum_{j=0}^{\infty}\frac{\xi_3\mu^j\kappa^j}{j!\Gamma(\mu+j)\Gamma(\alpha)\exp(\mu\kappa)}\left(\frac{\mu(1+\kappa)\Omega}{\xi_4\beta\bar{\gamma}}\right)^j G_{1,2}^{2,1}\left(\frac{\mu(1+\kappa)\Omega}{\xi_4\beta\bar{\gamma}}\left|\begin{matrix}0\\\alpha-1,\mu+j-1\end{matrix}\right.\right) \tag{6.21}$$

6.3.2 Error Probability of SFBC-OFDM with FFT

The SNR is represented as [113, Eq. (30)]

$$\gamma=\frac{1}{M_T R_c}\sum_{j=1}^{M_R}\sum_{i=1}^{M_T}\left|H_{j,i}[\lambda]\right|^2 E_a/N_0=\frac{1}{M_T R_c}\sum_{j=1}^{M_R}\sum_{i=1}^{M_T}\gamma_{j,i} \tag{6.22}$$

where $H_{j,i}[\lambda]$ denotes λ^{th} subchannel having j^{th} receiving and i^{th} transmitting antenna.

The CEP can be calculated by substituting (6.22) into (6.6) as

$$P_e(E/\gamma)=\xi_1 erfc\left(\sqrt{\frac{\xi_2\sum_{j=1}^{M_R}\sum_{i=1}^{M_T}\gamma_{j,i}}{R_c M_T}}\right) \tag{6.23}$$

The ABER is given as [113, Eq. (33)]

$$P_e(E) = \int_0^{\infty} \ldots \int_0^{\infty} P_e(E/\gamma) f_{\gamma_{1,1}}(\gamma_{1,1}) \cdots f_{\gamma_{M_R,M_T}}(\gamma_{M_R,M_T}) d\gamma_{1,1} \cdots d\gamma_{M_R,M_T} \tag{6.24}$$

By putting (6.23) into (6.24), (6.24) can be expressed as

$$P_e(E) = \xi_1 \int_0^{\infty} \ldots \int_0^{\infty} erfc\left(\sqrt{\frac{\xi_2 \sum_{j=1}^{M_R} \sum_{i=1}^{M_T} \gamma_{j,i}}{R_c M_T}}\right) f_{\gamma_{1,1}}(\gamma_{1,1}) \cdots f_{\gamma_{M_R,M_T}}(\gamma_{M_R,M_T}) d\gamma_{1,1} \cdots d\gamma_{M_R,M_T} \tag{6.25}$$

The complementary error function is defined as [8, Eq. (4A.6)]

$$erfc(x) = \frac{2}{\pi} \int_0^{\frac{\pi}{2}} \exp\left(-\frac{x^2}{2\sin^2\theta}\right) d\theta \tag{6.26}$$

By putting (6.26) into (6.25), (6.25) can be written as

$$P_e(E) = \frac{2\xi_1}{\pi} \int_0^{\infty} \ldots \int_0^{\infty} \int_0^{\frac{\pi}{2}} \exp\left(-\frac{\xi_2 \sum_{j=1}^{M_R} \sum_{i=1}^{M_T} \gamma_{j,i}}{2R_c M_T \sin^2\theta}\right) f_{\gamma_{1,1}}(\gamma_{1,1}) \cdots f_{\gamma_{M_R,M_T}}(\gamma_{M_R,M_T}) d\gamma_{1,1} \cdots d\gamma_{M_R,M_T} \tag{6.27}$$

Using the property of exponential function, (6.27) becomes

$$P_e(E) = \frac{2\xi_1}{\pi} \int_0^{\frac{\pi}{2}} \left[\int_0^{\infty} \exp\left(-\frac{\xi_2 \gamma_{1,1}}{2R_c M_T \sin^2\theta}\right) f_{\gamma_{1,1}}(\gamma_{1,1}) d\gamma_{1,1} \cdots \cdots \int_0^{\infty} \exp\left(-\frac{\xi_2 \gamma_{M_R,M_T}}{2R_c M_T \sin^2\theta}\right) f_{\gamma_{M_R,M_T}}(\gamma_{M_R,M_T}) d\gamma_{M_R,M_T} \right] d\theta \tag{6.28}$$

By the definition of MGF as given in (3.31), the above equation can be obtained as

$$P_e(E) = \frac{2\xi_1}{\pi} \int_0^{\frac{\pi}{2}} M_{\gamma_{1,1}}\left(\frac{\xi_2}{2R_c M_T \sin^2\theta}\right) \cdots M_{\gamma_{M_R,M_T}}\left(\frac{\xi_2}{2R_c M_T \sin^2\theta}\right) d\theta \tag{6.29}$$

In a simplified form, (6.29) becomes

$$P_e(E) = \frac{2\xi_1}{\pi} \int_0^{\frac{\pi}{2}} \prod_{j=1}^{M_R} \prod_{j=1}^{M_T} M_{\gamma_{j,i}}\left(-\frac{\xi_2}{2R_c M_T \sin^2\theta}\right) d\theta \tag{6.30}$$

For the i.i.d. fading channels, (6.30) becomes

$$P_e(E) = \frac{2\xi_1}{\pi}\int_0^{\frac{\pi}{2}}\left(M_\gamma\left(-\frac{\xi_2}{2R_cM_T\sin^2\theta}\right)\right)^{M_RM_T} d\theta \tag{6.31}$$

By putting (6.22) into (6.9), the approximate expression of CEP is

$$P_e(E/\gamma) = \xi_3 \exp\left(-\frac{\xi_4\sum_{j=1}^{M_R}\sum_{i=1}^{M_T}\gamma_{j,i}}{R_cM_T}\right) \tag{6.32}$$

Thus, an approximate ABER expression can be obtained by substituting (6.32) into (6.24)

$$P_e(E) = \xi_3\int_0^{\infty}.....\int_0^{\infty}\exp\left(-\frac{\xi_4\sum_{j=1}^{M_R}\sum_{i=1}^{M_T}\gamma_{j,i}}{R_cM_T}\right) f_{\gamma_{1,1}}(\gamma_{1,1})\cdots f_{\gamma_{M_R,M_T}}(\gamma_{M_R,M_T})d\gamma_{1,1}\cdots d\gamma_{M_R,M_T} \tag{6.33}$$

Considering same steps between (6.27) and (6.30), (6.33) becomes

$$P_e(E) = \xi_3\prod_{j=1}^{M_R}\prod_{i=1}^{M_T}M_{\gamma_{j,i}}\left(\frac{\xi_4}{M_TR_c}\right) \tag{6.34}$$

With i.i.d. channels, (6.34) becomes

$$P_e(E) = \xi_3\left[M_\gamma\left(\frac{\xi_4}{M_TR_c}\right)\right]^{M_RM_T} \tag{6.35}$$

(A) $\mathcal{F}$ Model

By putting (3.17) into (6.31), exact Average Error Probability expression (finite integral term) can be obtained as

$$P_e(E) = \frac{2\xi_1}{\pi}\int_0^{\frac{\pi}{2}}\left(\frac{1}{\Gamma(m)\Gamma(m_s)}G_{2,1}^{1,2}\left(\frac{2R_cM_Tm\sin^2\theta}{m_s\bar{\gamma}\xi_2}\middle|\begin{matrix}1-m_s, & 1\\ m & \end{matrix}\right)\right)^{M_RM_T} d\theta \tag{6.36}$$

By plugging (3.17) into (6.35), the expression of approximate Average Error Probability is computed as

$$P_e(E) = \xi_3 \left[\frac{1}{\Gamma(m_s)\Gamma(m)} G_{2,1}^{1,2}\left(\frac{R_c M_T}{m_s \bar{\gamma} \xi_4} \middle| \begin{matrix} 1-m_s, & 1 \\ m & \end{matrix} \right) \right]^{M_R M_T} \tag{6.37}$$

(B) κ-μ/gamma Model

The Average Probability of Error (exact) can be computed by putting (4.19) into (6.31) as

$$P_e(E) = \frac{2\xi_1}{\pi} \int_0^{\frac{\pi}{2}} \left(\sum_{j=0}^{\infty} \frac{\mu^j \kappa^j}{j! \exp(\mu\kappa)\Gamma(\alpha)\Gamma(\mu+j)} \left(\frac{2R_c M_T \sin^2\theta \mu(1+\kappa)\Omega}{\xi_2 \beta \bar{\gamma}} \right) G_{1,2}^{2,1}\left(\frac{2R_c M_T \sin^2\theta \mu(1+\kappa)\Omega}{\xi_2 \beta \bar{\gamma}} \middle| \begin{matrix} 0 \\ \alpha-1, \mu+j-1 \end{matrix} \right) \right)^{M_R M_T} d\theta \tag{6.38}$$

By putting (4.19) into (6.35), an approximate ABER expression can be obtained as

$$P_e(E) = \xi_3 \left[\sum_{j=0}^{\infty} \frac{\mu^j \kappa^j}{j! \exp(\mu\kappa)\Gamma(\alpha)\Gamma(\mu+j)} \left(\frac{R_c M_T \mu(1+\kappa)\Omega}{\xi_4 \beta \bar{\gamma}} \right) G_{1,2}^{2,1}\left(\frac{R_c M_T \mu(1+\kappa)\Omega}{\xi_4 \beta \bar{\gamma}} \middle| \begin{matrix} 0 \\ \alpha-1, \mu+j-1 \end{matrix} \right) \right]^{M_R M_T} \tag{6.39}$$

6.4 Error Probability of OFDM with FrFT

The received signal (b_ϕ) at the output of receiving OFDM with FrFT operation can be represented as

$$b_\phi[\lambda] = H_\phi[\lambda] a[\lambda] + c[\lambda] \tag{6.40}$$

where λ = 0,.....,V-1

Its matrix representation is

$$\mathrm{B}_\phi = \mathrm{H}_\phi \cdot \mathrm{A} + \mathrm{C} \tag{6.41}$$

where A = $(a[0],....a[V\text{-}1])^{\mathrm{T}}$ represents the transmitting signals, B_ϕ = $(b_\phi[0],....b_\phi[V\text{-}1])^{\mathrm{T}}$ denotes the receiving signals, $H_\phi = diag\{H_\phi[\lambda]\}_{\lambda=0}^{V-1}$ denotes diagonal matrix, and C = $(c[0],....c[V\text{-}1])^{\mathrm{T}}$ is the AWGN.

The channel response at the order of p is given by [133]

$$H_\phi(\lambda) = \sqrt{\frac{1 - j\cot(\phi)}{V}} \sum_{z=0}^{V-1} \exp(-j\Delta t^2 \cot(\phi) - j\Delta u^2 \cot(\phi) - 2\pi z\lambda) h(n) \tag{6.42}$$

The instantaneous received SNR in fraction domain can be given by

$$\gamma_\phi = \left|H_\phi(\lambda)\right|^2 E_a / N_0 \tag{6.43}$$

Applying expectation in (6.43), average SNR in fractional domain becomes

$$\bar{\gamma}_\phi = E\left[\left|H_\phi(\lambda)\right|^2\right] E_a / N_0 \tag{6.44}$$

Considering ρ is the ratio of fractional channel to Fourier channel [133]

$$\rho = \frac{E[\left|H_\phi(\lambda)\right|^2]}{E[\left|H(\lambda)\right|^2]} \tag{6.45}$$

By maximizing the ratio given in (6.45), the optimal angle (ϕ) can be obtained and therefore it can be represented as [133]

$$\rho_\phi = \left| \frac{E[\left|H_\phi(\lambda)\right|^2]}{E[\left|H(\lambda)\right|^2]} \right|_{\max} \tag{6.46}$$

With the help of (6.44) and (6.45), the mean SNR in FrFT is represented by

$$\bar{\gamma}_\phi = E[\gamma_\phi] = \rho\bar{\gamma} \tag{6.47}$$

6.5 Results

The analytical results of Error Probability for uncoded and SFBC coded OFDM using M-ary signaling techniques with FrFT and FFT are presented in this Section. Mainly, κ-μ/gamma and $\mathcal{F}$ models are selected to achieve such results. The Error Rate performance depends on the shadowed fading parameters, type of modulation scheme, M_R, M_T, mean SNR, modulation index, and code rate (R_c). The results are reduced to corresponding existing results of special cases for the higher value of shadowing factors. The Monte Carlo simulations are provided to validate the derived expressions presented in the last section.

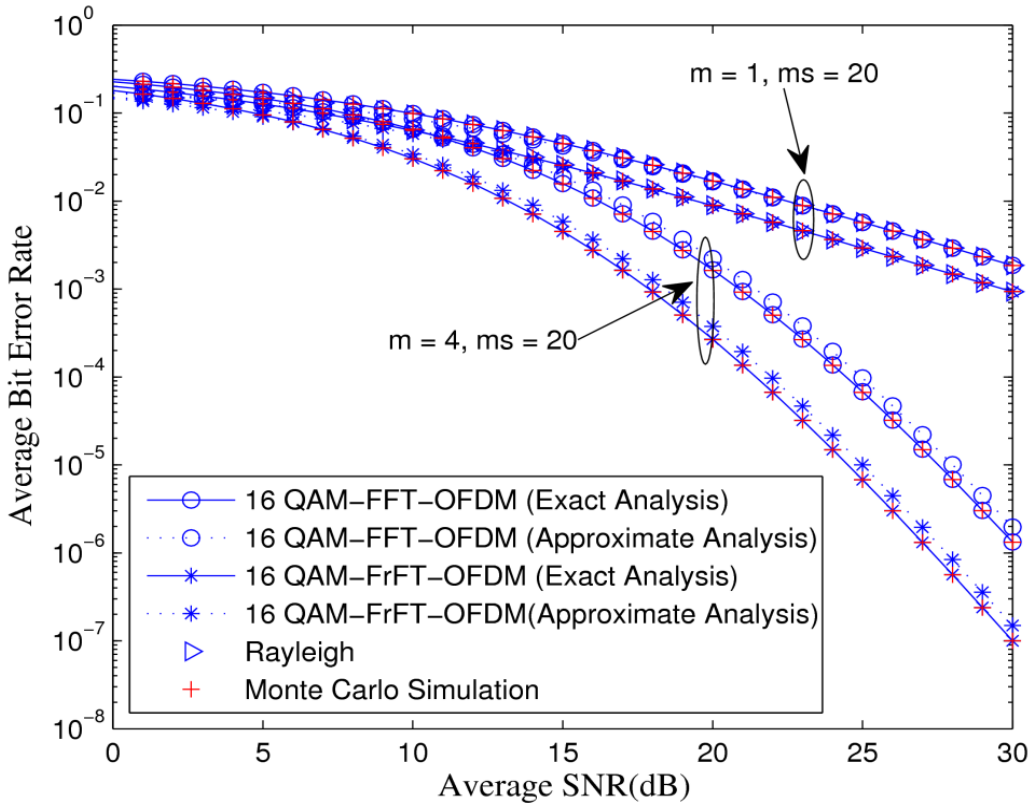

Figure 6.2: Error probability of OFDM using 16-QAM signaling scheme with FrFT/FFT for $\mathcal{F}$ fading distribution.

Figure 6.2 illustrates the Error Probability of OFDM system using 16-QAM modulation technique with FFT/FrFT for $\mathcal{F}$ model. For the case of no shadowing (m_s=20) with m=1, the error rate curve reduces to corresponding results of Rayleigh model in FFT [113, Eq. (22)] and FrFT [133, Eq. (12)] domain. In Figure 6.2, the exact result closely overlapped with approximated results. Also, for m=1 (or 4) under the light shadowing environment (m_s=20), the FrFT based OFDM outperforms the FFT based OFDM. In Figure 6.2, the error rate is minimum for higher m. The error rate reduces as the average SNR increases for both FrFT and FFT cases.

The error rate comparison curves between FrFT and FFT of OFDM system using MPSK signaling with m_s=2, m=4 for $\mathcal{F}$ model is presented in Figure 6.3. The reduction in error rate is seen in the case of FrFT based OFDM. In Figure 6.3, 8-PSK gives better BER performance than 16-PSK.

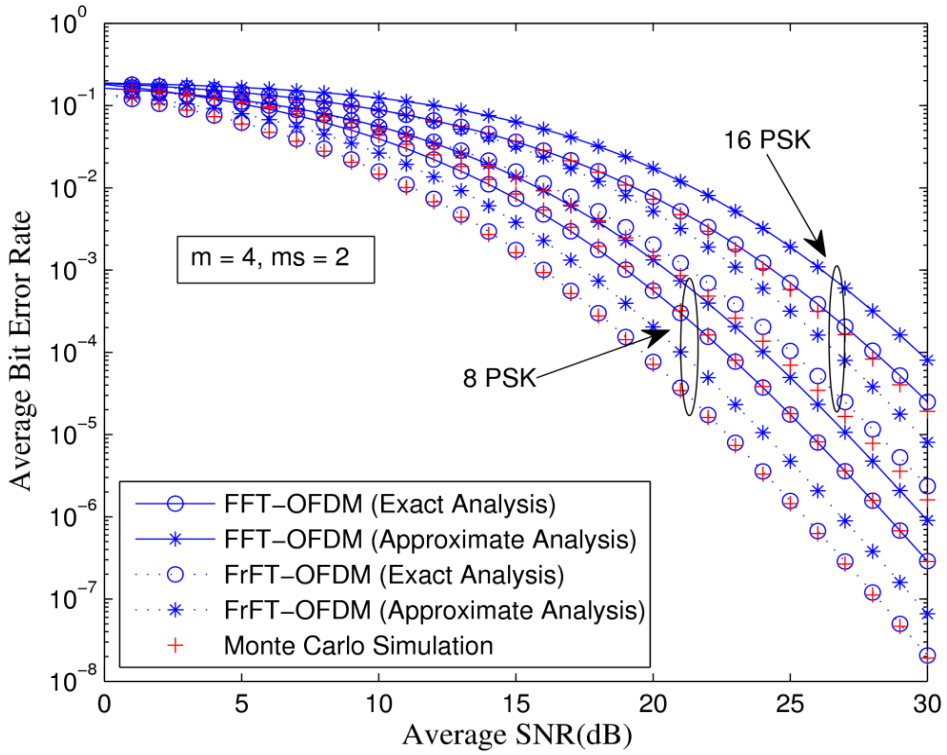

Figure 6.3: Error probability of OFDM using MPSK signaling scheme with FrFT/FFT for $\mathcal{F}$ fading distribution.

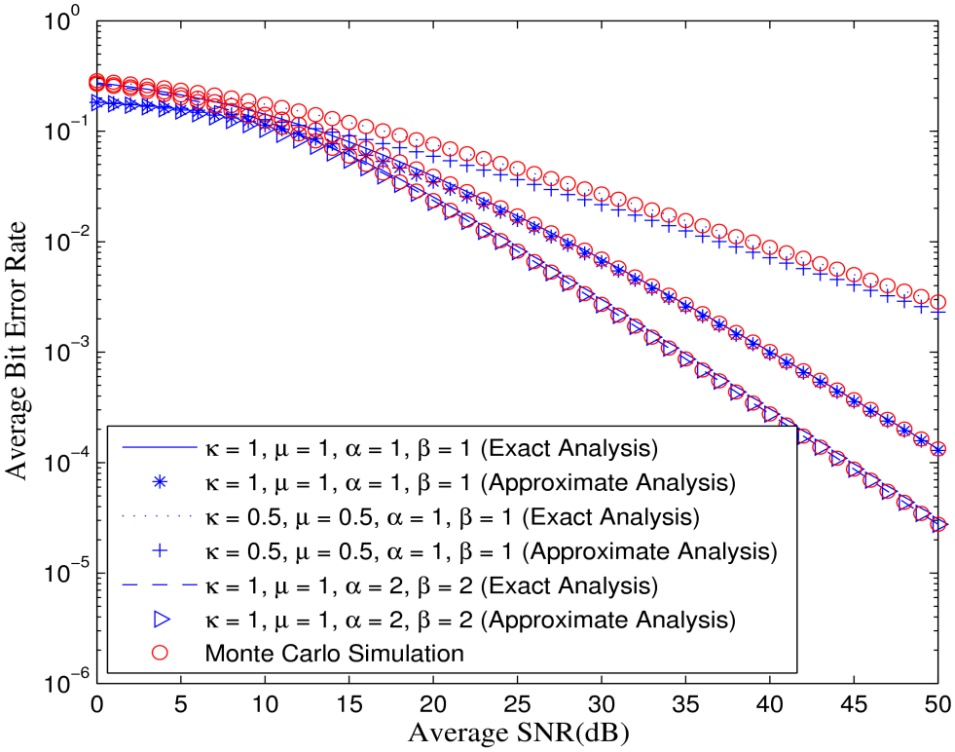

Figure 6.4: Error probability of OFDM using 16-QAM signaling technique with FFT for κ-μ/gamma fading distribution.

Figure 6.4 depicts the error probability of OFDM using 16-QAM signaling with FFT for κ-μ/gamma model. The largest decrement in error rate is seen as μ,κ varies between 0.5 and 1 with shadowing factors kept constant. However, a slight improvement in ABER performance is observed as β, α varies between 1 and 2 with constant μ,κ. The approximate and exact 16-QAM signaling based BER curve showing tightly closer with each other.

Table 6.1: Required number of terms in (6.21) to achieve an error probability less than 10^{-6}

Parameters (κ, μ, α, β)	Number of Terms in (6.21)
κ=1,μ=1,α=1,β=1	8
κ=0.5,μ=0.5,α=1,β=1	5
κ=1,μ=1,α=2,β=2	6

Table 6.1 depicts the required number of terms in exact ABER expression (6.21) to achieve the error probability less than 10^{-6} for several κ,μ,α,β values. To obtain the desired accuracy, only few terms are required as clearly depicted in Table 6.1.

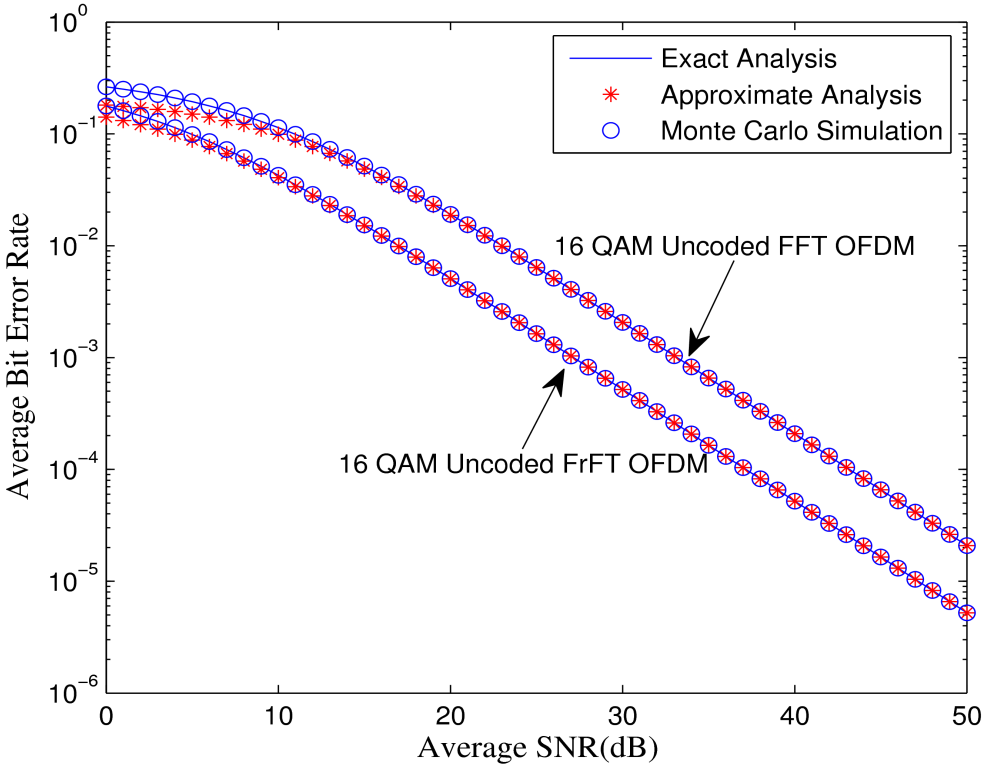

Figure 6.5: Error probability of OFDM using 16-QAM signaling scheme with FrFT and FFT for κ-μ/gamma fading distribution.

Figure 6.5 represents the error probabilities comparison plot between FrFT and FFT of 16-QAM signaling based uncoded OFDM in κ-μ/gamma channel. It is the point to notice that the OFDM technique using FrFT achieved higher reduction in error rates.

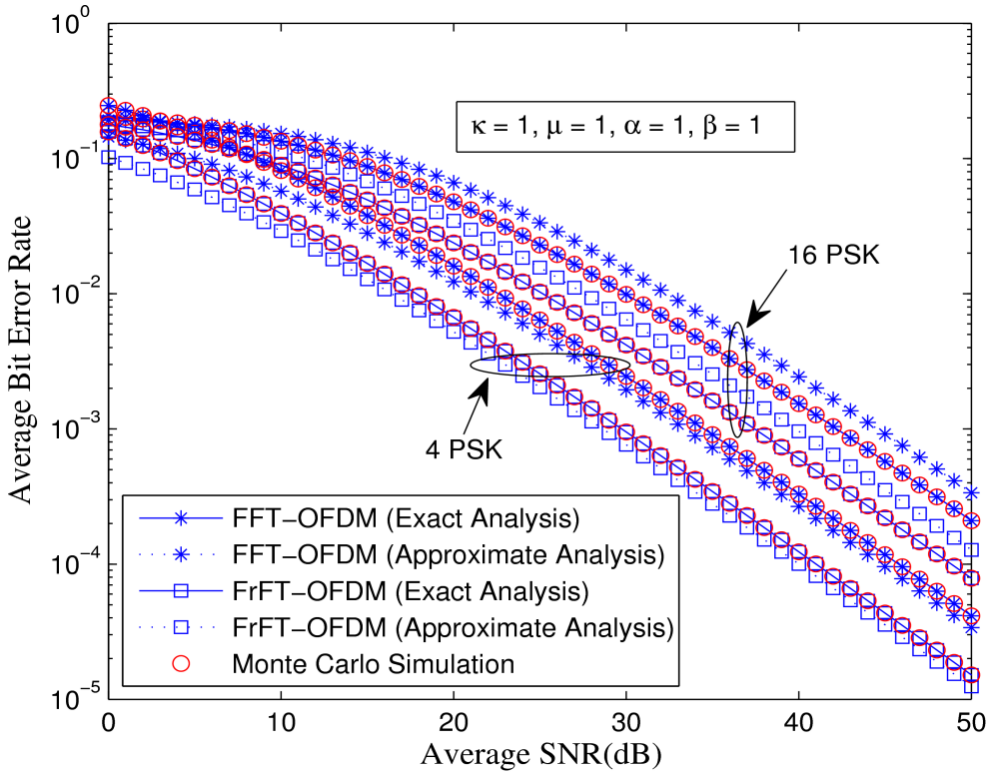

Figure 6.6: Error probability of OFDM technique using MPSK signaling scheme with FrFT and FFT for κ-μ/gamma fading distribution.

Figure 6.6 illustrates the error probabilities of OFDM using MPSK signaling in κ-μ/gamma channel. As can be observed in Figure 6.6, FrFT based OFDM outperforms the FFT based OFDM system. More importantly, 4-PSK has lowest BER as compared to 16-PSK for any type of Fourier transform algorithm based OFDM.

Table 6.2: ABER using MPSK signaling of uncoded OFDM system for κ-μ/gamma model with $\kappa=\mu=\alpha=\beta=1$ at 40 dB average SNR

Modulation Schemes	With FFT	With FrFT
Exact analysis (4-PSK)	7.755×10^{-3}	3.121×10^{-3}
Approximate analysis (4-PSK)	6.055×10^{-3}	2.475×10^{-3}
Exact analysis (16-PSK)	3.8957×10^{-2}	1.8526×10^{-2}
Approximate analysis (16-PSK)	2.475×10^{-2}	1.2309×10^{-2}

The error probability for 4-PSK and 16-PSK signaling of uncoded OFDM at 40 dB average SNR is tabulated in Table 6.2. Both approximate and exact error rate has almost similar value for 4-PSK (or 16-PSK). Moreover, the error rate of FrFT-OFDM is minimum in comparison with FFT-OFDM.

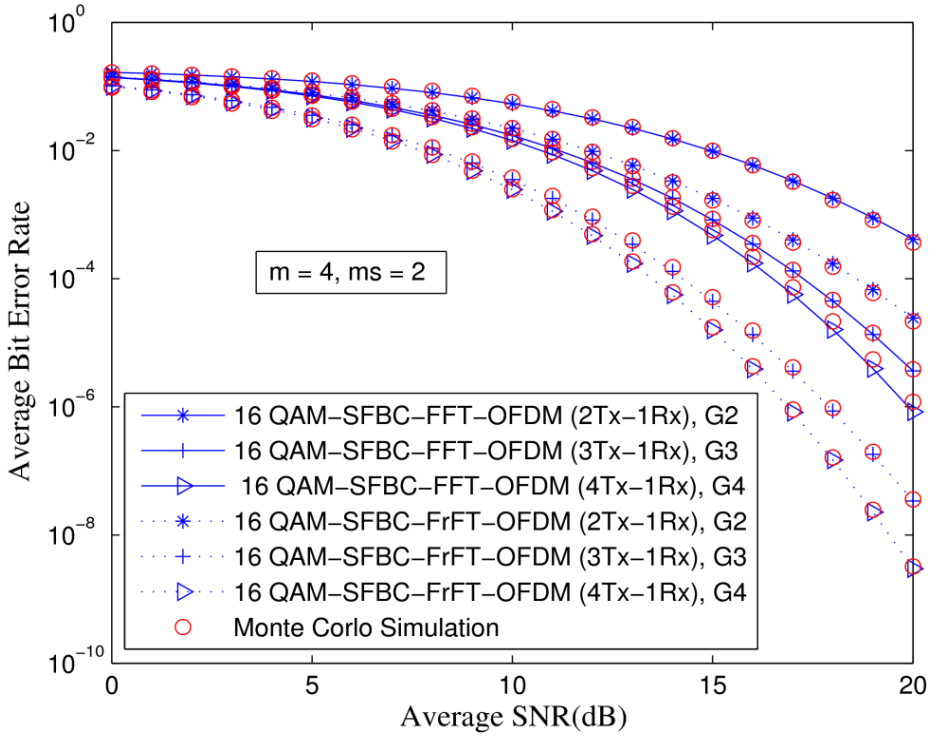

Figure 6.7: Error probability of SFBC coded OFDM using 16-QAM signaling for several M_R and M_T with m_s=2 and m=4 for $\mathcal{F}$ fading distribution.

Figure 6.7 depicts the error probabilities of SFBC-OFDM using 16-QAM signaling for $\mathcal{F}$ model. Particularly, M_T=2, M_R=1 (G2=1), M_T=3, M_R=1 (G3=0.5), and M_T=4, M_R=1(G4=0.5) are used to plot the BER curve. As can be observed that, the SFBC-OFDM using FrFT showing the lowest probability of error than FFT based SFBC-OFDM for any number of M_R and M_T. Also, on increasing M_T (2 to 4) with M_R=1, the ABER decreases. Thus, it is the point to conclude that the largest number of M_T provides a huge reduction in error probabilities.

Figure 6.8 depicts the probability of error comparison curves between 16-PSK and 8-PSK signaling scheme of coded OFDM for $\mathcal{F}$ model with m=4,8, m_s=2, M_T=2, M_R=1. In Figure 6.8, the error rate reduces as m increases (4 to 8) with constant m_s and M. Moreover, for FFT (or FrFT) domain with fixed m and m_s, 8-PSK-SFBC-OFDM has the lowest ABER than 16-PSK-SFBC-OFDM.

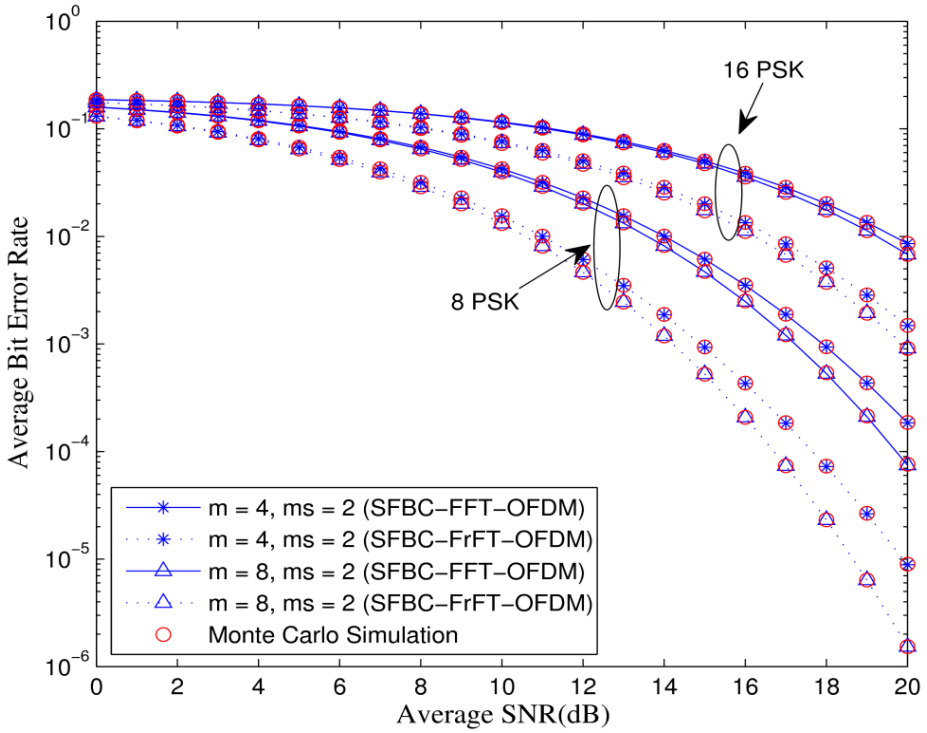

Figure 6.8: Error probability of SFBC coded OFDM using MPSK signaling technique with FrFT/FFT for $\mathcal{F}$ fading distribution.

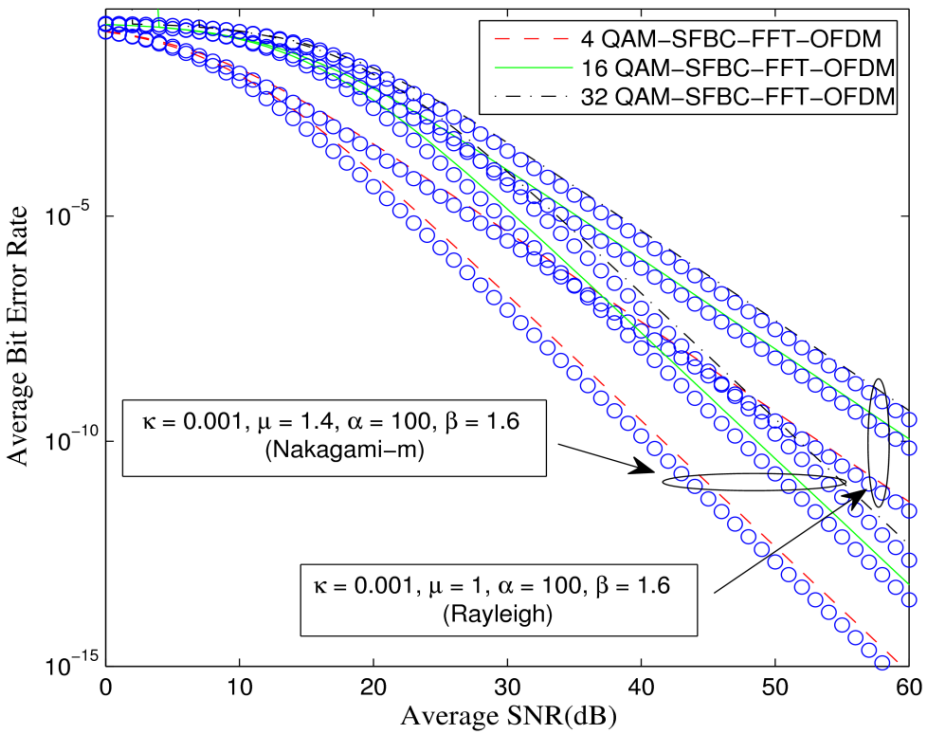

Figure 6.9: Error probability of SFBC coded OFDM using MQAM signaling technique for κ-μ/gamma fading distribution.

Figure 6.9 illustrates the error rate plot of SFBC coded OFDM using 16-QAM modulation technique for κ-μ/gamma model and its comparison with corresponding results of Nakagami-m [123, Eq. (33)] and Rayleigh fading [113, Eq. (35)]. Particularly, M_T=2, M_R=1 with M=4,16 and 32 is chosen to plot the error rate curve. The error probability reduces as μ varies between 1 and 1.4 for any value of M, and constant κ,α,β. Moreover, the higher value of modulation index M has higher BER and it reduces as M decreases.

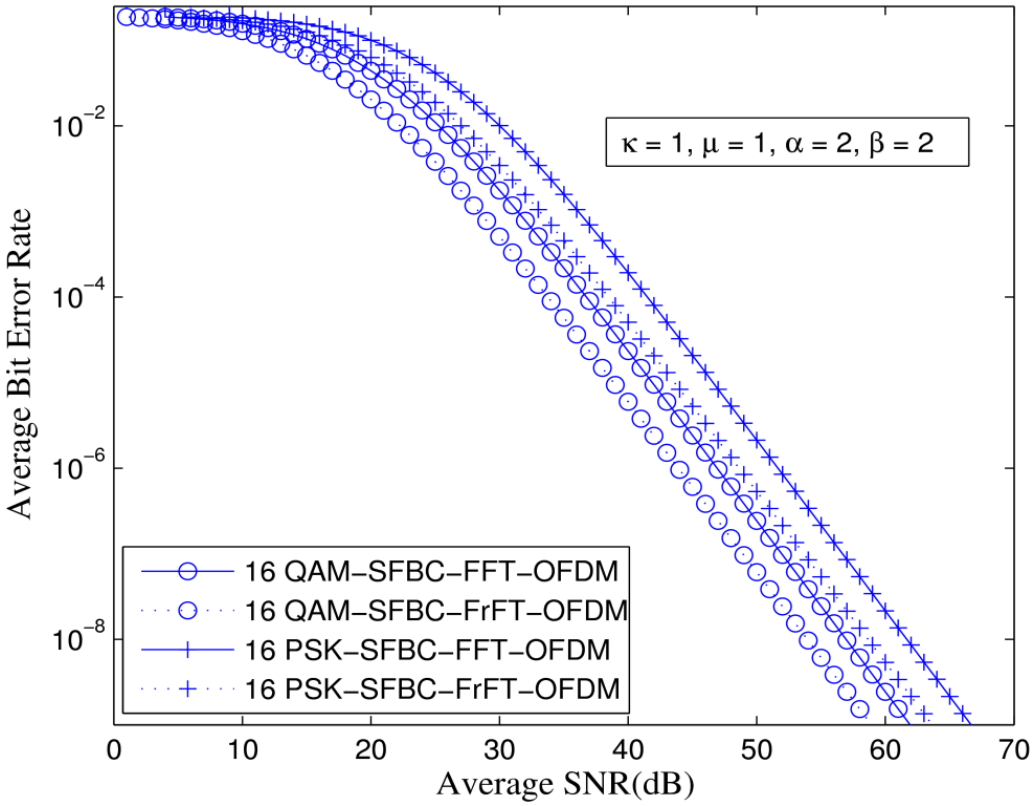

Figure 6.10: Error probability of SFBC coded OFDM using 16 QAM and 16 PSK signaling technique with FrFT/FFT for κ-μ/gamma fading distribution.

Figure 6.10 illustrates the error rate plot of SFBC coded OFDM using 16 QAM and 16 PSK signaling for κ-μ/gamma distribution. The curves are obtained for M_T=2, M_R=1 with κ=1, μ=1, α=2 and β=2. In Figure 6.10, 16 QAM signaling technique has lower BER in comparison with 16 PSK. Also, for any signaling technique (16 QAM or 16 PSK), the FrFT based SFBC-OFDM represents better BER performance in comparison with FFT based SFBC-OFDM.

6.6 Contribution

The OFDM (SFBC coded and uncoded) based error probabilities performance of κ-μ/gamma and $\mathcal{F}$ model have been analyzed in this Chapter. Correspondingly, the error probabilities expressions of M-ary signaling schemes have been computed mathematically. The error rate variation depends on the means SNR, fading factor, modulation index, M_R, M_T, and shadowing factor. In light shadowing environment, the new generalized results have been reduced to corresponding existing results of small-scale fading models. The best reductions in BER have been seen for higher value of M_T. The error rates have also become lower by selecting FrFT algorithm in OFDM system. The simulation and mathematical results show tight closer with each other. The study shows that the error rate performance of the FrFT-OFDM is much better than FFT-OFDM. Moreover, MQAM has the highest BER as compared to MPSK. Also, on increasing M_T and M_R in the SFBC-OFDM system, the error rate performance improved.

The main contributions of this Chapter are as follows:

- The mathematical expressions of Error Probability of MPSK/MQAM signaling technique for uncoded and SFBC encoded OFDM are derived.
- Approximate as well as exact analyses are presented to compute the BER.
- By setting the value of several shadowed factors, the generalized proposed results converge to special cases.
- The simulation results are carried out for validation purposes.

Based on the research outcomes reported in this Chapter, it is concluded that the FrFT based OFDM has achieved better error probability performance as compared to FFT based OFDM. Therefore, the research hypothesis has been tested successfully.

Published paper related to this Chapter:

(1) Hari Shankar, Ankush Kansal, "Performance Analysis of uncoded and SFBC OFDM system over composite fading channels". Physical Communication, Elsevier, vol. 40, pp. 1-10, 2020.

Chapter 7

Conclusions and Future Work

This Chapter presents the summary of the research work and Future scope. Some significant findings of research works are also pointed here. Section 7.1 introduces the conclusion of the research work and Section 7.2 discusses the Future scope.

7.1 Conclusions

The performance for several shadowed fading models over indoor wireless communication channels has been presented in this thesis. In this context, the performance for single-channel, diversity system and OFDM system using FFT and FrFT have been analyzed. Three shadowed fading models i.e., κ-μ/gamma, $\mathcal{F}$, and Rayleigh/TWDP are considered for mathematical analysis. The numerical results have been presented for several shadowing/multipath fading parameter values and verified with Monte Carlo simulation and reported existing results.

The analytical expressions of statistical parameters such as Density Function, MGF, and Distribution Function in the term of SNR over κ-μ/gamma shadowed fading channels have been derived. By using these statistical parameters, the expressions of Error Probability for several signaling techniques, Outage Probability, and Capacities for different adaptive transmissions protocols have been derived. The numerical results have been presented for four parameters (κ, μ, α, and β) which shows excellent agreement with existing results. It is pointed that, the improvement in performances have been obtained as the fading factor (μ,κ) increases with constant shadowing factors (β,α) and vice versa.

The analytical expressions of PDF, CDF, MGF, Outage Probability, and Error Probability for Rayleigh/TWDP shadowed fading distribution have been computed. The performance improvement has been presented by increasing the shadowing parameter (S_h) with a fixed shape parameter (Δ).

The diversity combining technique improves the quality of the signal at receiver output by utilizing the multiple receiving antennas. Therefore, the expressions of MGF, Moments, AF,

ABER, and Capacities for i.i.d. $\mathcal{F}$ distribution with MRC diversity have been computed. The reductions in error rates for several signaling techniques have been presented as L, m_s, and m varies. Further, the Error Probability expressions of the OFDM technique with FrFT/FFT using M-ary signaling scheme (including uncoded and SFBC coded) for two shadowed fading channels have been derived. The Error Rate performances depend on the type of signaling technique, modulation index, mean SNR, M_R, M_T, code rate, shadowing, and fading factors. The FrFT-OFDM shows minimum Error Probability in comparison to FFT-OFDM. By varying the number of transmitting antennas (M_T) with a constant receiving antenna (M_R), the BER performances have been improved. Moreover, both exact and approximate results have shown excellent agreement. Also, Monte Carlo simulations have been carried out to cross verify the derived expressions. The derived expressions are available in the term of special function such as hypergeometric, Bessel, Meijer G, beta, and gamma.

7.2 Future Work

The performance improvement techniques of the shadowed fading model over indoor communication channels have been presented in this thesis. The research works have been carried out by considering three shadowed fading models i.e. $\mathcal{F}$, κ-μ/gamma, and Rayleigh/TWDP. However, there are lots of works that still need to be done in the future, these include

(1) Performance of energy detection and physical layer security: Energy detection method is used to measure the energy level of an unknown received signal and compares it with a specific threshold in order to determine its presence or absence within a given bandwidth. Energy detection is considered as most practical spectrum sensing method for cognitive radio because the unlicensed user can detect unknown signals of licensed user. The performance of energy detection is influenced by fading channels between wireless nodes. To analyze the energy detection performance, the expressions of probability of detection and probability of false alarm can be derived. The performance of energy detection can also be analyzed using different diversity combining schemes such as MRC, SC, EGC, SSC, and square law combining.

Security is the major concern in indoor wireless communication because the data transmission occurs in open space. The implementation of physical layer security at lower layer is a best

method for designer to achieve secure transmission. The performance of physical layer security can be analyzed by computing the secrecy capacity.

(2) Performance of space-time block coding (STBC) system: The MIMO system can use multiple antennas at both transmitter and receiver sections in order to improve data rates and quality (reliability) of the signal. The space-time block coding system provides full diversity gain with low computational complexity. The STBC system is also used to combat the effects of fading channels. The expressions of ABER and Channel Capacity for STBC system over different shadowed fading channels can be derived.

(3) Performance over interference-limited scenarios: Interference degrades the wireless system performance. The interference can occur in multiuser and multicellular environment. In the interference-limited environment, the received signal quality is represented by signal to interference ratio (SIR) and noise is assumed to be negligible. If both noise and interference are present in the wireless environment, the received signal quality is represented as signal to interference plus noise ratio (SINR). Both SIR and SINR have an important role in wireless system performance. The statistical parameter such as PDF, CDF, and MGF can be derived. Using these statistical parameters, several performance measures such as ABER, OP and channel capacity can be derived for interference-limited system. Moreover, different diversity reception techniques with multiple antennas can be used to combat fading effects in interference limited scenarios.

References

[1] S. Kumar, "Wireless communication: the fundamental and advanced concepts, River publishers, 2015.

[2] T. K. Sarkar, Z. Ji, K. Kim, A. Medouri, and M.S. Palma, "A survey of various propagation models for mobile communication," *IEEE Antennas Propag. Mag*., vol. 45, no. 3, pp. 51-82, 2003.

[3] W. Fu, J. Hu, and S. Zhang, "Frequency-domain measurement of 60 GHz indoor channels: a measurement setup, literature data, and analysis," *IEEE Instrum. Meas. Mag*., vol. 16, no. 2, pp. 34-40, 2013.

[4] I. Dey, G. G. Messier, and S. Magierowski, "Joint fading and shadowing model for large office indoor WLAN environments," *IEEE Trans. Antennas Propag*., vol. 62, no. 4, pp. 2209-2222, 2014.

[5] J. S. Kalsi, and J. S. Ubhi, "A study of conventional protocols applicable to the emerging IoT systems and devices," *In Proc. IEEE Int. Conf. Auto. Comp. Technol. Management (ICACTM)*, pp. 395-399, 2019.

[6] D. B. Smith, D. Miniutti, T. A. Lamahewa, and L. W. Hanlen, "Propagation models for body-area networks: A survey and new outlook," *IEEE Antennas Propag. Mag*., vol. 55, no. 5, pp. 97-117, 2013.

[7] J. A. Fraile, J. Bajo, J. M. Corchado, and A. Abraham, "Applying wearable solutions in dependent environments," *IEEE Trans. Inf. Technol. Bio*., vol. 14, no. 6, pp. 1459-1467, 2010.

[8] M. K. Simon, and M. S. Alouini, Digital communication over fading channels, 2nd ed. New Jersey: John Wiley & Sons, 2005.

[9] P. M. Shankar, Fading and shadowing for wireless system, New York: Springer; 2012.

[10] C. Loo, "A statistical model for a land mobile satellite link," *IEEE Trans. Veh. Technol.*, vol. 34, no. 3, pp. 122-127, 1985.

[11] A. Abdi, W. C. Lau, M. S. Alouini, and M. Kaveh, "A new simple model for land mobile satellite channels: First- and second-order statistics," *IEEE Trans. Wirel. Commun*., vol. 2, no. 3, pp. 519-528, 2003.

[12] J. F. Paris, "Statistical characterization of κ-μ shadowed fading," *IEEE Trans. Veh. Technol*., vol. 63, no. 2, pp. 518-526, 2014.

[13] S. L. Cotton, "A statistical model for shadowed body-centric communications channels: Theory and validation," *IEEE Trans. Antennas Propag*., vol. 62, no. 3, pp. 1416-1424, 2014.

[14] S. L. Cotton, "Human body shadowing in cellular device-to-device communications: Channel modeling using the shadowed κ–μ fading model," *IEEE J. Sel. Areas Commun*., vol. 33, no. 1, pp. 111-119, 2015.

[15] G. E. Corazza, and F. Vatalaro, "A statistical model for land mobile satellite channels and its application to nongeostationary orbit systems," *IEEE Trans. Veh. Technol*., vol. 43, no. 3, pp. 738-742, 1994.

[16] H. Suzuki, "A statistical model for urban radio propagation," *IEEE Trans. Commun*., vol. 25, no. 7, pp. 673-680, 1977.

[17] A. Abdi, and M. Kaveh, "K distribution: An appropriate substitute for Rayleigh-lognormal distribution in fading-shadowing wireless channels," *Electron. Lett*., vol. 34, no. 9, pp. 851-852, 1998.

[18] P. M. Shankar, "Error rates in generalized shadowed fading channels," *Wirel. Pers. Commun*., vol. 28, pp. 233-238, 2004.

[19] S. K. Yoo, S. L. Cotton, P. C. Sofotasios, and S. Freear, "Shadowed fading in indoor off-body communication channels: A statistical characterization using the κ-μ/gamma composite fading model," *IEEE Trans. Wirel. Commun*., vol. 15, no. 8, pp. 5231-5244, 2016.

[20] T. K. Bhatia, R. K. Ramachandran, R. Doss, and L. Pan, "A comprehensive review on the vehicular ad-hoc networks," *In Proc. IEEE Int. Conf. Reliab. Infocom Technol. Optimization (ICRITO)*, pp. 515-520, 2020.

[21] A. A. M. Saleh, and R. Valenzuela, "A statistical model for indoor multipath propagation," *IEEE J. Sel. Areas Commun*., vol. 5, no. 2, pp. 128-137, 1987.

[22] Q. H. Spencer, B. D. Jeffs, M. A. Jensen, and A. L. Swindlehurst, "Modeling the statistical time and angle of arrival characteristics of an indoor multipath channel," *IEEE J. Sel. Areas Commun.*, vol. 18, no. 3, pp. 347-360, 2000.

[23] “Further advancements for E-UTRA physical layer aspects,” 3rd Gen. Partnership Project, Sophia Antipolis, France, Rep. 36.814, 2010. http://www.3gpp.org/DynaReport/36814.htm.

[24] M. F. Iskander, and Z. Yun, “Propagation prediction models for wireless communication systems,” *IEEE Trans. Micro. Theory Tech*., vol. 50, no. 3, 2002.

[25] X. Wu, C. X. Wang, J. Sun, J. Huang, R. Feng, Y. Yang, and X. Ge, “60-GHz millimeter-wave channel measurements and modeling for indoor office environments” *IEEE Trans. Antennas Propag*., vol. 65, no. 4, pp.1912-1924, 2017.

[26] J. Senic, C. Gentile, P. B. Papazian, K. A. Remley, and J. K. Choi, “Analysis of E-band path loss and propagation mechanisms in the indoor environment,” *IEEE Trans. Antennas Propag*., vol. 65, no. 12, pp. 6562-6573, 2017.

[27] K. Turbic, S. J. Ambroziak, and L. M. Correia, “A body-shadowing model for off-body and body-to-body communications,” *In Proc. IEEE Baltic URSI Sym.*, pp. 53-54, 2018.

[28] L. Petrillo, T. Mavridis, J. Sarrazin, A. B. Delai, and P. D. Doncker, “Wideband off-body measurements and channel modeling at 60 GHz,” *IEEE Antennas Wirel. Propag. Lett*., vol. 16, pp.1088-1091, 2017.

[29] T. Mapayi, and J. R. Tapamo, “Performance comparison of supervised learning methods for retinal vessel tortuosity characterization,” *In Proc. IEEE Conf. Info. Commun. Technol. Society*, pp. 1-7, 2018.

[30] D. Dash, V. Abrol, A. K. Sao, and B. Biswal, “Spatial sparsification and low rank projection for fast analysis of multi-subject resting state fMRI data,” *In Proc. IEEE Int. Sym. Bio. Imag.*, pp. 1280-1283, 2018.

[31] F. Vatalaro, “Generalized Rice-lognormal channel model for wireless communications,” *Electron. Lett*., vol. 31, no. 22, pp. 1899-1900, 1995.

[32] S. H. Hwang, K. J. Kim, J. Y. Ahn, and K. C. Whang, “A channel model for non-geostationary orbiting satellite system,” *In Proc. IEEE Veh. Technol. Conf*., Phoenix, AZ, USA, pp. 41-45, 1997.

[33] T. T. Tjhung, and C. C. Chai, “Fade statistics in Nakagami-lognormal channels,” *IEEE Trans. Commun*., vol. 47, no. 12, pp. 1769-1772, 1999.

[34] T. Eltoft, “The Rician inverse Gaussian distribution: a new model for non-Rayleigh signal amplitude statistics,” *IEEE Trans. Image Process*., vol. 14, no. 11, pp. 1722-1735, 2005.

[35] Karmeshu, and R. Agrawal, "On efficacy of Rayleigh-inverse Gaussian distribution over K-distribution for wireless fading channels," *Wirel. Commun. Mob. Comput*., vol. 7, no.1, pp.1-7, 2007.

[36] A. Laourine, M. S. Alouini, S. Affes, and A. Stephenne, "On the performance analysis of composite multipath/shadowing channels using the G-distribution," *IEEE Trans. Commun*., vol. 57, no. 4, pp. 1162-1170, 2009.

[37] P. S. Bithas, "Weibull-gamma composite distribution: alternative multipath/shadowing fading model," *Electron. Lett*., vol. 45, no. 14, pp.749-751, 2009.

[38] F. Yilmaz, and M. S. Alouini, "Extended generalized-K (EGK): A new simple and general model for composite fading channels," *IEEE Trans. Commun*., vol. x, no. xx, 2010.

[39] P. C. Sofotasios, and S. Freear, "The η-μ/gamma composite fading model," In *Proc. IEEE Int. Conf. Wirel. Inform. Technol. Syst.*, pp. 1-4, 2010.

[40] P. C. Sofotasios, T. A. Tsiftsis, K. H. Van, S. Freear, L. R. Wilhelmsson, and M. Valkama, "The κ-μ/IG composite statistical distribution in RF and FSO wireless channels," *In Proc. IEEE Veh. Technol. Conf.*, pp. 1-5, 2013

[41] P. C. Sofotasios, T. A. Tsiftsis, M. Ghogho, L. R. Wilhelmsson, and M. Valkama, "The η-μ/IG distribution: A novel physical multipath/shadowing fading model," *In Proc. IEEE Int. Conf. Commun.*, pp. 5715-5719, 2013.

[42] P. C. Sofotasios, and S. Freear, "On the κ-μ/gamma composite distribution: A generalized multipath/shadowing fading model," *In Proc. IEEE Int. Microw. Optoelectron. Conf.*, pp. 390-394, 2011.

[43] H. Shankar, and A. Kansal, "CDF and MGF based analysis over Rayleigh TWDP shadowed fading channel for indoor communication". *Int. J. Electron*., vol. 105, no. 12, pp. 2099-2113, 2018.

[44] H. Shankar, and S. P. Singh, "A Novel POCA-TWDP based joint fading model for indoor wireless system," *In Proc. IEEE Int. Conf. Signal Process. Integrated Net.*, pp. 290-295, 2016.

[45] S. K. Yoo, N. Bhargav, S. L. Cotton, P. C. Sofotasios, M. Matthaiou, M. Valkama, and G. K. Karagiannidis, "The κ-μ/inverse gamma and η-μ/inverse gamma composite fading models: Fundamental statistics and empirical validation," *IEEE Trans. Commun*., 2017.

[46] S. K. Yoo, S. L. Cotton, P. C. Sofotasios, M. Matthaiou, M. Valkama, and G. K. Karagiannidis, "The κ-μ/inverse gamma fading model," *In Proc. IEEE PIMRC*, pp. 425-429, 2015.

[47] S. K. Yoo, P. C. Sofotasios, S. L. Cotton, M. Matthaiou, M. Valkama, and G. K. Karagiannidis, "The η-μ/inverse gamma composite fading model," *In Proc. IEEE PIMRC*, pp. 166-170, 2015.

[48] S. K. Yoo, S. L. Cotton, P. C. Sofotasios, M. Matthaiou, M. Valkama, and G. K. Karagiannidis, "The Fisher-Snedecor F distribution: A simple and accurate composite fading model," *IEEE Commun. Lett.*, vol. 21, no. 7, pp. 1661-1664, 2017.

[49] O. S. Badarneh, S. Muhaidat, P. C. Sofotasios, S. L. Cotton, K. Rabie, and D. B. da Costa, "The N∗ Fisher-Snedecor F cascaded fading model," *In Proc. IEEE Int. Conf. Wirel. Mob. Comput. Net. Commun.*, pp. 1-7, 2018.

[50] N. Bhargav, C. R. N. da Silva, Y. J. Chun, E. J. Leonardo, S. L. Cotton, and M. D. Yacoub, "On the product of two κ-μ random variables and its application to double and composite fading channels," *IEEE Trans. Wirel. Commun*., vol. 17, no. 4, pp. 2457-2470, 2018.

[51] M. S. Alouini, and A. Goldsmith, "Capacity of Rayleigh fading channels under different adaptive transmission and diversity combining techniques," *IEEE Trans. Veh. Technol*., vol. 48, no. 4, pp. 1165-1181, 1999.

[52] J. Sun, and I. S. Reed, "Performance of MDPSK, MPSK, and Noncoherent MFSK in wireless Rician fading channels," *IEEE Trans. Commun*., vol. 47, no. 6, pp. 813-816, 1999.

[53] A. Abdi, and K. Mostafa, "Comparison of DPSK and MSK bit error rates for K and Rayleigh-lognormal fading distributions," *IEEE Commun. Lett*., vol. 4, no. 4, pp. 122-124, 2000.

[54] H. Shin, and J. H. Lee, "On the error probability of binary and M-ary signals in Nakagami-m fading channels," *IEEE Trans. Commun*., vol. 52, no. 4, pp. 536-539, 2004.

[55] P. S. Bithas, N. C. Sagias, P. T. Mathiopoulos, G. K. Karagiannidis, and A. A. Rontogiannis, "On the performance analysis of digital communications over generalized-K fading channels," *IEEE Commun. Lett*., vol. 10, no. 5, pp. 353-355, 2006.

[56] D. B. Da Costa, and M. D. Yacoub, "Average channel capacity for generalized fading scenarios," *IEEE Commun. Lett*., vol. 11, no. 12, pp. 949-951, 2007.

[57] D. B. Da Costa, and M. D. Yacoub, "Moment generating functions of generalized fading distributions and applications," *IEEE Commun. Lett*., vol. 12, no. 2, pp. 112-114, 2008.

[58] A. Laourine, M. S. Alouini, S. Affes, and A. Stephenne, "On the capacity of generalized-K fading channels. *IEEE Trans. Wirel. Commun*., vol. 7, no.7, pp. 2441-2445, 2008.

[59] K. P. Peppas, "Capacity of η-μ fading channels under different adaptive transmission techniques," *IET Commun*., vol. 4, no. 5, pp. 532-539, 2010.

[60] G. P. Efthymoglou, N. Y. Ermolova, and V. A. Aalo, "Channel capacity and average error rates in generalized-K fading channels," *IET Commun*., vol. 4, no. 11, pp. 1364-1372, 2010.

[61] A. M. Magableh, and M. M. Matalgah, "Moment generating function of the generalized α-μ distribution with applications," *IEEE Commun. Lett*., vol. 13, no. 6, pp. 411-413, 2009.

[62] M. D. Renzo, F. Graziosi, and F. Santucci, "Channel capacity over generalized fading channels: A novel MGF-based approach for performance analysis and design of wireless communication systems," *IEEE Trans. Veh. Technol*., vol. 59, no. 1, pp. 127-149, 2010.

[63] F. Yilmaz, and M. S. Alouini, "A novel unified expression for the capacity and bit error probability of wireless communication systems over generalized fading channels," *IEEE Trans. Commun*., vol. 60, no. 7, pp. 1862-1876, 2012.

[64] G. P. Efthymoglou, "On the performance analysis of digital modulations in generalized-K fading channels," *Wirel. Pers. Commun*., vol. 65, no. 3, pp. 643-651, 2012.

[65] I. Dey, G. G. Messier, and S. Magierowski, "Fading statistics for the joint fading and two path shadowing channel," *IEEE Wirel. Commun. Lett*., vol. 3, no. 3, pp. 301-304, 2014.

[66] I. Dey, G. G. Messier, and S. Magierowski, "Performance analysis of BPSK over joint fading and two-path shadowing channels," *In Proc. IEEE Veh. Technol. Conf.*, pp. 1-5, 2014.

[67] I. Dey, G. G. Messier, and S. Magierowski, "The cumulative distribution function for the joint fading and two path shadowing channel: Expression and application," *In Proc. IEEE Veh. Technol. Conf.*, pp. 1-5, 2014.

[68] I. Dey, G. G. Messier, and S. Magierowski, "Pairwise error probability of turbo codes over joint fading and two-path shadowing channels," *In Proc. IEEE Global Commun. Conf.*, pp. 3995-4000, 2014.

[69] I. Dey, G. G. Messier, and S. Magierowski, "On the capacity of joint fading and two-path shadowing channels," *IEEE Trans. Veh. Technol*., vol. 65, no. 1, pp. 403-408, 2016.

[70] I. Dey, T. A. Tsiftsis, and C. Rowell, "Achievable channel cutoff rate and bandwidth efficiency in indoor wireless environments," *IEEE Trans. Veh. Technol*., vol. 65, no. 12, pp.10074-10079, 2016.

[71] I. Dey, G. G. Messier, and S. Magierowski, "Average error rates and achievable capacity in large office indoor wireless environments," *IEEE Trans. Commun*., vol. 65, no. 11, pp. 4955-4965, 2017.

[72] I. Dey, and P. S. Rossi, "Probability of outage due to self-interference in indoor wireless environments," *IEEE Commun. Lett*., vol. 21, no. 1, pp. 8-11, 2017.

[73] Y. Xi, A. Burr, J. Wei, and D. Grace, "A general upper bound to evaluate packet error rate over quasi-static fading channels," *IEEE Trans. Wirel. Commun*., vol. 10, no. 5, pp. 1373-1377, 2011.

[74] M**.** Rao, F. J. L. Martinez, M. S. Alouini, and A. Goldsmith, "MGF approach to the analysis of generalized two-ray fading models," *IEEE Trans. Wirel. Commun*., vol. 14, no. 5, pp. 2548-2561, 2015**.**

[75] A. Hamed, M. Alsharef, and R. K. Rao, "MGF based performance analysis of digital wireless system in urban shadowing environment," *In Proc. World Congress Engg. Comput. Sci.*, 2015.

[76] D. Das, P. K. Bora, and R. Bhattacharjee, "Cumulant based automatic modulation classification of QPSK, OQPSK, 8-PSK and 16-PSK," *In Proc. IEEE Int. Conf. Commun. Sys. Net.*, pp. 1-5, 2016.

[77] X. Li, X. Chen, J. Zhang, Y. Liang, and Y. Liu, "Capacity analysis of α-η-κ-μ fading channels," *IEEE Commun. Lett*., vol. 21, pp. 1449-1452, 2017.

[78] T. Aldalgamouni, A. M. Magableh, S. Mater, and O. S. Badarneh, "Capacity analysis of α-η-μ channels over different adaptive transmission protocols," *IET Commn*., vol. 11, no. pp. 1114-1122, 2017.

[79] S. P. Singh, and S. Kumar, "Closed form expressions for ABER and capacity over EGK fading channel in presence of CCI," *Int. J. Electron.*, vol. 104, no. 3, pp. 513-527, 2017.

[80] E. Salahat, A. Hakam, N. Ali, and A. Kulaib, "Moment generating functions of generalized wireless fading channels and applications in wireless communication theory," *In Proc. IEEE Veh. Tech. Conf.*, pp. 1-4, 2017.

[81] F. J. L. Martinez, J. M. R. Jerez, and J. F. Paris, "On the calculation of the incomplete MGF with applications to wireless communications," *IEEE Trans. Commun*., vol. 65, no. 1, pp. 458-469, 2017.

[82] J. Gong, H. Lee, M. Park, J. W. Choi, and J. Kang, "Generalized MGF of the κ-μ extreme distribution and its applications to performance analysis," *Electron. Lett*., vol. 54, no. 25, pp.1458-1460, 2018.

[83] J. P. P. Martín, J. M. R. Jerez, and F. J. L. Martínez, "Generalized MGF of the two-wave with diffuse power fading model with applications," *IEEE Trans. Veh. Technol*., vol. 67, no. 6, pp. 5525-5529, 2018.

[84] T. Aldalgamouni, M. C. Ilter, O. S. Badarneh, and H. Yanikomeroglu, "Performance analysis of Fisher-Snedecor F composite fading channels," *In Proc. IEEE Middle East North Africa Commun. Conf.*, 2018.

[85] J. Gong, H. Lee, and J. Kang, "Generalized moment generating function-based secrecy performance analysis over Fisher-Snedecor composite fading channels," *Electron. Lett*., vol. 54, no. 24, pp. 1381-1383, 2018.

[86] S. Chen, J. Zhang, G. K. Karagiannidis, and B. Ai, "Effective rate of MISO systems over Fisher-Snedecor F Fading Channels," *IEEE Commun. Lett*., vol. 22, no. 12, pp. 2619-2622, 2018.

[87] L. Kong, and G. Kaddoum, "On physical layer security over the Fisher-Snedecor F wiretap fading channels," *IEEE Access*, vol. 7, pp. 39466-39472, 2018.

[88] H. Al-Hmood, "Performance of cognitive radio systems over κ-μ shadowed with integer μ and Fisher-Snedecor F fading channels," *In Proc. IEEE Int. Conf. Engg. Technol. Appl.*, pp. 130-135, 2018.

[89] F. S. Almehmadi, and O. S. Badarneh, "On the effective capacity of Fisher-Snedecor F fading channels," *Electon. Lett*., vol. 54, no. 18, pp. 1068-1070, 2018.

[90] O. S. Badarneh, P. C. Sofotasios, S. Muhaidat, S. L. Cotton, K. Rabie, and N. Al-Dhahir, "On the secrecy capacity of Fisher-Snedecor F fading channels," *In Proc. IEEE Int. Conf. Wirel. Mob. Comput. Net. Commun.*, pp. 102-107, 2018.

[91] S. K. Yoo, P. C. Sofotasios, S. L. Cotton, S. Muhaidat, F. J. L. Martinez, J. M. R. Jerez, and G. K. Karagiannidis, "A comprehensive analysis of the achievable channel capacity in F composite fading channels," *IEEE Access*, vol. 7, pp. 34078-34094, 2019.

[92] H. Zhao, L. Yang, A. S. Salem, and M. S. Alouini, "Ergodic capacity under power adaption over Fisher-Snedecor F fading channels," *IEEE Commun. Lett*., vol. 23, no. 3, pp. 546-549, 2019.

[93] N. Kapucu, and M. Bilim, "Analysis of analytical capacity for Fisher-Snedecor F fading channels with different transmission schemes," *Electron. Lett*., vol. 55, no. 5, pp. 283-285, 2019.

[94] S. K. Yoo, S. L. Cotton, P. C. Sofotasios, S. Muhaidat, O. S. Badarneh, and G. K. Karagiannidis, "Entropy and energy detection-based spectrum sensing over F composite fading channels," *IEEE Trans. Commun*., vol. 67, no. 7, pp. 4641-4653, 2019.

[95] P. M. Shankar, "Performance analysis of diversity combining algorithms in shadowed fading channels," *Wirel. Pers. Commun*., vol. 37, no. 1-2, pp. 61-72, 2006.

[96] P. S. Bithas, P. T. Mathiopoulos, and S. A. Kotsopoulos, "Diversity reception over Generalized-K fading channels," *IEEE Trans. Wirel. Commun*., vol. 6, no. 12, pp. 4238-4243, 2007.

[97] P. Theofilakos, A. G. Kanatas, and G. P. Efthymoglou, "Performance of generalized selection combining receivers in *K* fading channels," *IEEE Commun. Lett*., vol. 12, no. 11, pp. 816-818, 2008.

[98] I. Khan, P. S. Hall, A. A. Serra, A. R. Guraliuc, and P. Nepa, "Diversity performance analysis for on-body communication channels at 2.45 GHz," *IEEE Trans. Antennas Propag*., vol. 57, no. 4, pp. 956-963, 2009.

[99] P. S. Bithas, G. P. Efthymoglou, and N. C. Sagias, "Spectral efficiency of adaptive transmission and selection diversity on generalized fading channels," *IET Commun*., vol. 4, no. 17, pp. 2058-2064, 2010.

[100] V. K Dwivedi, and G. Singh, "Analysis of channel capacity of Generalized -K fading with maximal-ratio combining diversity receiver," *In Proc. IEEE Int. Conf. Commun. Syst. Net. Technol*., 2011.

[101] F. Yilmaz, and M. S. Alouini, "A unified MGF-based capacity analysis of diversity combiners over Generalized fading channels," *IEEE Trans. Commun*., vol. 60, no. 3, pp. 862-875, 2012.

[102] P. M. Shankar, "Maximal ratio combining (MRC) in shadowed fading channels in presence of shadowed fading Co channel Interference (CCI)," *Wirel. Pers. Commun*., vol. 68, pp. 15-25, 2013.

[103] V. K. Dwivedi, and G. Singh, "Moment generating function based performance analysis of maximal ratio combining diversity receivers in the Generalized-K fading channels," *Wirel. Pers. Commun*., vol. 77, no. 3, pp. 1959-1975, 2014.

[104] M. R. Bhatnagar, and M. K. Arti, "On the closed-form performance analysis of maximal ratio combining in shadowed-Rician fading LMS channels," *IEEE Commun. Lett*., vol. 18, no. 1, pp. 54-57, 2014.

[105] E. Salahat, and A. Hakam, "Maximal ratio combining diversity analysis of underwater acoustic communications subject to κ-μ shadowed fading channels," *In Pro. IEEE Conf. Indust. Electron. Society*, pp. 7185-7189, 2016.

[106] H. Al-Hmood, and H. S. Al-Raweshidy, "On the sum and the maximum of non-identically distributed composite η-μ/gamma variates using a mixture gamma distribution with applications to diversity receivers," *IEEE Trans. Veh. Technol.*, vol. 65, no. 12, pp. 10048-10052, 2016.

[107] S. K. Yoo, S. L. Cotton, and W. G. Scanlon, "Switched diversity techniques for indoor off-body communication channels: an experimental analysis and modeling," *IEEE Trans. Antennas Propag*., vol. 64, no. 7, pp. 3202-3207, 2016.

[108] J. P. P. Martín, J. M. R. Jerez, and F. J. L. Martinez, "Generalized MGF of Beckmann fading with applications to wireless communications performance analysis," *IEEE Trans. Commun.*, vol. 65, no. 9, pp. 3933-3943, 2017.

[109] O. S. Badarneh, D. B. da Costa, P. C. Sofotasios, S. Muhaidat, and S. L. Cotton, "On the sum of Fisher-Snedecor F variates and its application to maximal-ratio combining," *IEEE Wirel. Commun. Lett*., vol. 7, no. 6, pp. 966-969, 2018.

[110] Y. A. Rahama, M. H. Ismail, and M. S. Hassan, "On the sum of independent Fox's H-function variates with applications," *IEEE Trans. Veh. Technol.*, vol. 67, no. 8, pp. 6752-6760, 2018.

[111] H. Al-Hmood, and H. S. Al-Raweshidy, "Selection combining scheme over non-identically distributed Fisher-Snedecor (F) fading channels," *IEEE Wirel. Commun. Lett*., 2019.

[112] S. Kumar, S. K. Soni, and P. Jain, "Performance of MRC receiver over Hoyt/lognormal composite fading channel," *Int. J. Electron.*, vol. 105, no. 9, pp. 1433-1450, 2018.

[113] M. Torabi, S. Aissa, M. R. Soleymani, "On the BER performance of space-frequency block coded OFDM systems in fading MIMO channels," *IEEE Trans. Wirel. Commun*., vol. 6, no. 4, pp. 1366-1373, 2007.

[114] T. Aldalgamouni, and A. Elhakeem, "On the performance of down link SFBC-MIMO-CDMA systems," *In Proc. IEEE Canadian Conf. Elec. Comp. Engg.*, pp. 129-134, 2008.

[115] P. Dharmawansa, N. Rajatheva, and H. Minn, "An exact error probability analysis of OFDM systems with frequency offset," *IEEE Trans. Commun*., vol. 57, no. 1, pp. 26-31, 2009.

[116] F. J. L. Martínez, E. M. Naya, J. F. Paris, and A. J. Goldsmith, "BER analysis for MIMO-OFDM beamforming with MRC under channel prediction and interpolation errors," *In Pro. IEEE Global Telecommun. Conf.*, pp. 1-7, 2009.

[117] R. U. Mahesh, and A. K. Chaturvedi, "Closed form BER expressions for BPSK OFDM systems with frequency offset," *IEEE Commun. Lett.*, vol.14, no. 8, pp.731-733, 2010.

[118] S. P. Majumder, and M. A. Jumana, "Performance analysis of a space-frequency block coded OFDM wireless communication system with MSK and GMSK modulation," *In Pro. IEEE Int. Conf. Elec. Engg. Inf. Commun. Technol*., pp. 1-5, 2014.

[119] V. Bhaskar, and K. N. Reddy, "Adaptive transmission in a MIMO-OFDM system in Nakagami-m fading channels," *Int. J. Wirel. Inf. Net.*, vol. 22, pp. 285-293, 2015.

[120] U. Raj, and V. Bhaskar, "Performance analysis of SNR based scheduling scheme for MIMO OSFBC-OFDM systems in η–μ fading channels," *Int. J. Wirel. Inf. Net.*, vol. 22, pp. 147-156, 2015.

[121] D. Singh, H. D. Joshi, "BER performance of SFBC OFDM system over TWDP fading channel," *IEEE Commun. Lett*., vol. 20, pp. 2426-2429, 2016.

[122] D. Singh, and H. D. Joshi, "BER analysis of SFBC-OFDM system with different detection schemes over fading channels," *In Pro. IEEE Int. Symposium Wirel. Commun. Systems*, 2018.

[123] D. Singh, and H. D. Joshi, "Performance analysis of SFBC-OFDM system with channel estimation error over generalized fading channels," *Trans. Emerg. Tele. Technol*, vol. 29, 2018.

[124] D. Singh, and H. D. Joshi, "Generalized MGF based analysis of line-of-sight plus scatter fading model and its applications to MIMO-OFDM systems," *Int. J. Electron. Commun. (AEU)*, vol. 91, pp. 110-117, 2018.

[125] D. Singh, and H. D. Joshi, "Error probability analysis of STBC-OFDM systems with CFO and imperfect CSI over generalized fading channels," *Int. J. Electron. Commun. (AEU)*, vol. 98, pp. 156-163, 2019.

[126] S. Kumari, S. K. Rai, A. Kumar, H. D. Joshi, A. K. Singh, and R. Saxena, "Exact BER analysis of FRFT-OFDM system over frequency selective Rayleigh fading channel with CFO," *Electron. Lett*., vol. 49, no. 20, pp. 1299-1301, 2013.

[127] A. Kansal, K. Singh, and R. Saxena, "Bit error rate analysis of FrFT appended OFDM system," *Optik*, vol. 126, pp. 715-718, 2015.

[128] M. R. Mousavi, and A. Shahzadi, "Hyperbolic FRFT-OFDM system BER analysis over high Doppler Rician fading channels," *Electron. Lett*., vol. 51, no. 24, pp. 2003-2005, 2015.

[129] R. M. Ashri, H. A. Shaban, and M. A. El-Nasr, "BER of FRFT-based OFDM system for underwater wireless communication," *In Pro. National Radio Science Conference, Egypt*, pp. 266-273, 2016.

[130] Z. Mokhtari, and M. Sabbaghian, "Near-optimal angle of transform in FRFT-OFDM systems based on ICI analysis," *IEEE Trans. Veh. Technol*., vol. 65, no. 7, pp. 5777-5783, 2016.

[131] A. Kumar, M. Magarini, H. D. Joshi, and R. Saxena, "Exact SER analysis of DFrFT-based QPSK OFDM system over frequency selective Rayleigh fading channel with CFO," *J. Comp. Net. Commun*., 2016.

[132] V. K. Trivedi, S. Kumari, and P. Kumar, "Generalized error analysis of FRFT-OFDM over Nakagami-m fading channel with arbitrary m," *IET Commun.*, vol. 11, no. 9, pp. 1497-1502, 2017.

[133] T. Chawla, and A. Kansal, "Performance evaluation of SFBC MIMO-OFDM using FrFT under TWDP fading channel," *Wirel. Pers. Commun*., vol. 104, pp. 1121-1131, 2019.

[134] A. Kumar, and M. Magarini, "Symbol error probability analysis of DFrFT-based OFDM systems with CFO and STO in frequency selective Rayleigh fading channels," *IEEE Trans. Veh. Technol*., vol. 68, no. 1, pp. 64-81, 2019.

[135] I. S. Gradshteyn, I. M. Ryzhik. Table of Integrals, Series, and Products. Academic Press, New York, 2007.

[136] G. D. Durgin, T. S. Rappaport, and D. A. de Wolf, "New analytical models and probability density functions for fading in wireless communications," *IEEE Trans. Commun.,* vol. 50, no. 6, pp. 1005-1015, 2002.

[137] M. D. Yacoub, "The κ-μ distribution and the η-μ distribution," *IEEE Antennas Propag. Mag*., vol. 49, no.1, pp. 68-81, 2007.

[138] A. Abdi, and M. Kaveh, "On the utility of gamma PDF in modeling shadow fading (slow fading)," In Proc. *IEEE Veh. Technol. Conf.*, vol. 3, pp. 2308-2312, 1999.

[139] J. D. Cook, "Inverse gamma distribution," Tech. Rep., 2008.

[140] J. L. Folks, and R. S. Chhikara, "The inverse Gaussian distribution and its application-A review," *J. Roy. Statist. Soc. B*, vol. 40, no. 3, pp. 263-289, 1978.

[141] F. Louzada, P. L. Ramos, and D. Nascimento, "The inverse nakagami-m distribution: A novel approach in reliability," *IEEE Trans. Reliability*, vol. 67, no. 3, pp.1030-1042, 2018.

[142] V. Namias, "Fractional order Fourier transform and its applications to quantum mechanics," *IMA J. Appl. Math.*, vol. 25, no. 3, pp. 241-265, 1980.

[143] T. Ran, D. Bing, W. Yue, "Research progress of the fractional Fourier transform in signal processing," *Sci. China Series*, vol. 49, no. 1, pp. 1-25, 2006.

[144] P. Singh, B. Raman, and M. Misra, "A secure image sharing scheme based on SVD and Fractional Fourier Transform" *Signal Process. Image Commun*., vol. 57, pp.46-59, 2017.

[145] M. R. McKay, A. Zanella, I. B. Collings, and M. Chiani, "Error probability and SINR analysis of optimum combining in Rician fading," *IEEE Trans. Commun*., vol. 57, no. 3, pp. 676-687, 2009.

[146] A. P. Prudnikov, Y. A. Brychkov, and O. I. Marichev, "Integrals and Series," vol. 3: more special functions, Gordon and Breach science publishers, 1986.

[147] C. K. Pauw, and D. L. Schilling, "Probability of error of M-ary PSK and DPSK on a Rayleigh fading channel," *IEEE Trans. Commun*., vol. 36, no. 6, pp. 755-756, 1988.

[148] F. Vatalaro, G. E. Corazza, "Probability of error and outage in a Rice-lognormal channel for terrestrial and satellite personal communications," *IEEE Trans. Commun*., vol. 44, no. 8, pp. 921-924, 1996.

[149] A. Erdelyi et al., "Higher Transcendental Functions," vol. II, McGraw Hill, 1953.

[150] M. Khatib, K. P. Peppas, H. E. Nistazakis, and G. S. Tombras, "An overview of the physical insight and the various performance metrics of fading channels in wireless communication

systems: Advanced trends in wireless communications," ISBN: 978-953-307-183-1, In Tech., 2011.

[151] S. P. Singh, and S. Kumar, "A MGF based closed form expressions for error probability and capacity over EGK fading for interference limited system," *Wirel. Pers. Commun*., vol. 91, no. 2, pp. 577-816, 2016.

[152] N. C. Beaulieu, and P. Tan, "Receiver windowing for reduction of ICI in OFDM systems with carrier frequency offset," *In Proc. IEEE Global Telecom. Conf.*, pp. 2680-2684, 2005.

[153] A. Seyedi, and G. J. Saulnier, "General ICI self-cancellation scheme for OFDM systems," *IEEE Trans. Veh. Technol*., vol. 54, pp.198–210, 2005.

[154] Q. Shi, Y. Fang, and M. Wang, "A novel ICI self-cancellation scheme for OFDM systems," *In Proc. IEEE Int. Conf. Wirel. Commun. Net. Mob. Comput*., 2009, pp. 1-4.

[155] A. P. Prudnikov, Y. A. Brychkov, and I. Mariche, "Integrals and Series," vol. 2, Gordon and Breach Science Publishers, 1986.

List of Publications

[P1] Hari Shankar, Ankush Kansal, "CDF and MGF based analysis over Rayleigh TWDP shadowed fading channel for indoor communication". International Journal of Electronics, Taylor & Francis, vol. 105 (12), pp. 2099-2113, 2018. (**IF = 1.004**)

[P2] Hari Shankar, Ankush Kansal, "Performance analysis of κ-μ/gamma shadowed fading model over indoor off body communication channel. International Journal of Electronics and Communication (AEU), Elsevier, vol. 93, pp. 283-288, 2018. (**IF = 3.183**)

[P3] Hari Shankar, Ankush Kansal, "MGF-based analysis of κ-μ/gamma composite fading model for indoor off body communication". Transactions on Emerging Telecommunications Technologies, Wiley, e3566, pp. 1-17, 2019. (**IF = 2.638**)

[P4] Hari Shankar, Ankush Kansal, "Performance Analysis of uncoded and SFBC OFDM system over composite fading channels". Physical Communication, Elsevier, vol. 40, pp. 1-10, 2020. (**IF = 1.81**)

[P5] Hari Shankar, Ankush Kansal, "Performance Analysis of MRC Receiver over Fisher Snedecor (F) Composite Fading Channels". Wireless Personal Communications, Springer, vol. 117(2), pp. 1337-1359, 2021. (**IF = 1.671**).

[P6] Hari Shankar, Ankush Kansal, "MGF-based Analysis of Maximum Ratio Combining Receiver over Fisher-Snedecor Composite Fading Channel", International Journal of Innovative Technology and Exploring Engineering (IJITEE), vol-8(9S), pp. 1-8, 2019.**(Scopus)**

[P7] Hari Shankar, Ankush Kansal, "Performance analysis of switch and stay combining system over Fisher Snedecor ($\mathcal{F}$) fading channels". Wireless Personal Communications, Springer, 2021. (**IF = 1.671**)